NASA CONTRACTOR REPORT

NASA CR-2158

NASA CR-2158

STUDY OF LOAD ALLEVIATION AND MODE SUPPRESSION (LAMS) ON THE YF-12A AIRPLANE

by Lester D. Edinger, Frederick L. Schenk, and Alan R. Curtis

Prepared by
LOCKHEED ADP
Burbank, Calif.
and
HONEYWELL INC.
Minneapolis, Minn.
for Flight Research Center

NATIONAL AERONAUTICS AND SPACE ADMINISTRATION • WASHINGTON, D. C. • DECEMBER 1972

1. Report No.	2. Government Accession No.	3. Recipient's Catalog No.
NASA CR-2158		

4. Title and Subtitle	5. Report Date
STUDY OF LOAD ALLEVIATION AND MODE SUPPRESSION (LAMS) ON THE YF-12 AIRPLANE	December 1972
	6. Performing Organization Code
7. Author(s)	8. Performing Organization Report No.
Lester D. Edinger, Frederick L. Schenk, and Alan R. Curtis	
	10. Work Unit No.
9. Performing Organization Name and Address	
Lockheed ADP, Burbank, California, and Honneywell Inc., Government and Aeronautical Products Division, Minneapolis, Minnesota	11. Contract or Grant No.
	F33657-71-C-0021
	13. Type of Report and Period Covered
12. Sponsoring Agency Name and Address	Contractor Report
National Aeronautics and Space Administration Washington, D. C. 20546	14. Sponsoring Agency Code

15. Supplementary Notes

16. Abstract

The intent of the study was to evaluate the potentials and capability for implementing a LAMS (load alleviation and mode suppression) system on the YF-12A for the purpose of flight research. This research would be a continuation of work performed in LAMS technology on previous programs such as the NASA/Air Force XB-70 and the Air Force B-52 flight test programs. The nature of the research is to minimize the design risk in application of LAMS to future aircraft.

The results of the study show that the YF-12A would be a suitable test bed for continuing development of LAMS technology. This was demonstrated by defining five candidate LAMS systems and analytically evaluating them with regard to performance and mechanization. Each of the five systems used a different combination of force producers. A small canard vane or a mass-reaction device mounted near the cockpit was considered as a possible LAMS force producer, together with the existing inboard and outboard elevons. It was concluded that a combination of canard vane and outboard elevons would provide the most effective system for the YF-12A.

17. Key Words (Suggested by Author(s))	18. Distribution Statement
Control systems, dynamic response, loads alleviation, modal suppression	Unclassified - Unlimited

19. Security Classif. (of this report)	20. Security Classif. (of this page)	21. No. of Pages	22. Price*
Unclassified	Unclassified	133	$3.00

* For sale by the National Technical Information Service, Springfield, Virginia 22151

CONTENTS

ILLUSTRATIONS

ILLUSTRATIONS (Concluded)

TABLES

TABLES (Concluded)

STUDY OF LOAD ALLEVIATION AND MODE SUPPRESSION (LAMS) ON THE YF-12A AIRPLANE

By Lester D. Edinger, Frederick L. Schenk, and Alan R. Curtis

Lockheed ADP, Burbank, California, and
Honeywell GAPD, Minneapolis, Minnesota

SUMMARY

The intent of the study was to evaluate the potentials and capability for implementing a LAMS (load alleviation and mode suppression) system on the YF-12A for the purpose of flight research. This research would be a continuation of work performed in LAMS technology on previous programs such as the NASA/Air Force XB-70 and the Air Force B-52 flight test programs (refs. 1 and 2). The nature of the research is to minimize the design risk in application of LAMS to future aircraft.

The results of the study show that the YF-12A would be a suitable test bed for continuing development of LAMS technology. This was demonstrated by defining five candidate LAMS systems and analytically evaluating them with regard to performance and mechanization. Each of the five systems used a different combination of force producers. A small canard vane or a mass-reaction device mounted near the cockpit were considered as possible LAMS force producers, together with the existing inboard and outboard elevons. It was concluded that a combination of canard vane and outboard elevons would provide the most effective system for the YF-12A.

INTRODUCTION

LAMS (load alleviation and mode suppression) is a flight control technology directed toward improving the efficiency of flight. It uses the principles of feedback control to regulate the loads on the flexible aircraft induced by either flight through turbulent air or by abrupt pilot command inputs. It extends the techniques used in conventional flight controls to include stability augmentation of the aircraft's significant aeroelastic modes.

Most of what is considered today as LAMS technology has evolved from a NASA/Air Force XB-70 program and an Air Force B-52 program. These programs are described in refs. 3 and 4, respectively. Prior to these programs, several smaller studies on airplanes were performed, but most of the prior work in load alleviation and structural mode control was confined to large flexible boosters such as the Saturn 5. Although the potential of this technology had been established for boosters, the benefits possible for the airplane had not been determined. However, experience with structural

flexibility on existing aircraft such as the B-47, B-52, and XB-70, together with extrapolation to potentially more serious problems on vehicles such as the SST, C-5A, 747, and the B-1A, pointed out a need for development of LAMS technology.

The objective of the XB-70 program was to evaluate the use of feedback control techniques to suppress the aircraft's aeroelastic contribution to local accelerations. This comprehensive study led to the design and flight test evaluation on the XB-70 of a system referred to as ILAF (identical location of accelerometer and force). Results of the flight test are described in ref. 2. Although the XB-70 was retired before the tests could be completed, limited results obtained at two flight conditions indicated the feasibility of active structural mode control. During the flight tests, a small canard vane (approximately four sq ft in area) was used as a means for exciting the structural modes to test the system. The demonstrated effectiveness of the vane for exciting the modes led to the conclusion it could also be used as an excellent force producer for controlling the modes. However, termination of the XB-70 program precluded investigation of such a system.

The B-52 program, which ran almost concurrently with the XB-70 program, was established to demonstrate through flight test the use of LAMS techniques to reduce aircraft fatigue damage rates in air turbulence. This represented a formidable problem, as it was necessary to evaluate stress at several vehicle stations and to use several force producers to achieve the desired control. This compounded the synthesis task; hence, the use of modern control theory was introduced as a design tool. The B-52 LAMS system was designed primarily at one flight condition but its performance was evaluated at three discrete conditions. The test results (ref. 1) substantiated the performance predicted by the analytical studies. Although the XB-70 and the B-52 programs served to establish the potential of LAMS technology, additional development is required before LAMS can be applied without significant design risk. Examples of areas requiring further development include evaluation of the effects of LAMS on flutter margins, effective use of auxiliary force producers, and improvements in LAMS sensing techniques. Continued development is also expected to lead to new applications for LAMS, such as augmentation of flutter margins and maneuver load control.

The intent of the LAMS study on the YF-12 is to continue the development of LAMS technology. With the retirement of the XB-70 as a test aircraft, the YF-12A is the most promising candidate available to NASA for a LAMS design base. The YF-12A, like the XB-70, is a low-load-factor, low-aspect-ratio, supersonic aircraft; hence, it exhibits aeroelastic properties characteristic of contemporary transport aircraft. The YF-12A itself does not require LAMS technology, and it is not well suited for evaluating rigid-body load alleviation techniques such as direct lift control. However, because of its aeroelastic properties, it is well suited for evaluating structural mode suppression techniques. With the present state of the art of load alleviation and mode suppression, use of the latter techniques constitutes most of the design risk. Hence, evaluation of mode suppression techniques on the YF-12A could result in eliminating most of the design risk associated with LAMS technology and, thus, lead to acceptance by the airframe manufacturers.

SYMBOLS

A/C	aircraft
BL	butt line
dB	decibel
F/C	flight condition
ft/sec	feet per second
FS	fuselage station
WS	wing station
h	altitude
i	$\sqrt{-1}$
$K_c G(s)$	transfer function
LAMS	load alleviation and mode suppression
M	Mach number
n_z	load factor
PSD	power spectral density
q	dynamic pressure, lb/ft^2
q'_c	pitot differential pressure, lb/ft^2
rms	root mean square
s	Laplace operator
SAS	stability augmentation system
w	vertical velocity, in./sec
w_g	wind state
Γ	desired attenuation
z	vertical displacement, in.
δ_1	inboard elevon deflection, rad

SYMBOLS (concluded)

δ_2	outboard elevon deflection, rad
δ_c, δ_3	canard deflection, rad
δ_M	reaction mass-actuator command, in.
x	mass displacement, in.
ζ	damping ratio
θ	pitch angle, rad
$\dot{\theta}$	rigid-body pitch rate, rad/sec
σ	standard deviation
ω	frequency, rad/sec

STUDY APPROACH

The objective of the study was to establish the effectiveness of using feedback control techniques to suppress the aircraft's structural modes. To meet this objective, it was necessary to synthesize LAMS controllers and analytically demonstrate their potential mode suppression performance. The mode suppression performance was evaluated in terms of the percentage reduction in root-mean-square (rms) normal acceleration at selected stations on the aircraft. The acceleration response was evaluated for both a gust input disturbance and input disturbances introduced through excitation of a control surface.

The analysis was restricted to the longitudinal axis of the airplane. Vehicle data were provided for four flight conditions. Detailed system syntheses were performed at one condition, but performance and stability were evaluated at all four flight conditions.

Several combinations of force producers were evaluated in the study to determine the most effective set for mode suppression. These combinations included not only the existing force producers but an auxiliary force producer as well. The existing force producers consist of inboard and outboard elevons. The candidates considered for the auxiliary force producer were a small canard vane or a mass-reaction device, either one being located near the nose of the aircraft. Since neither one of these auxiliary force producers presently exist on the YF-12A aircraft, feasibility of implementation had to be considered.

Since up to three force producers could be used in a system and since performance was to be evaluated at several aircraft stations, the synthesis

was a multiple-input/multiple-output control problem. Quadratic optimization techniques from modern control theory are especially suited for control problems of this type. Hence, both conventional frequency response analysis techniques and quadratic optimization techniques were used in the study to define the control systems.

Once analytical block diagrams of candidate controllers were defined, studies were made to determine system mechanizations. Mechanization studies included primarily determination of potential feedback sensor location problems and required aircraft modifications

AIRCRAFT DESCRIPTION AND ANALYTICAL REPRESENTATION

Aircraft Description

The YF-12 aircraft is an advanced two-engine, supersonic interceptor with a maximum gross weight of approximately 124 000 lb. The aircraft configuration is shown in Figure 1. As Figure 1 indicates, the aircraft has a delta wing with a chine construction on the forebody. The chine gives the vehicle aerodynamic properties similar to those of a double delta configuration. The two engines are located at about mid-wing on each side, dividing the wing into inboard and outboard sections. Each of the four sections has an elevon surface which is used for pitch and roll control. The inboard elevons are driven by a mechanical linkage commanded by the sum of pilot stick motion and the SAS (stability augmentation system) servo motion. The outboard elevon actuators are each slaved to the inboard elevon actuators by means of a mechanical linkage across the engine nacelles.

The pitch-axis SAS used in the YF-12A is required full time and uses triple redundancy for reliability. A block diagram of this SAS is shown in Figure 2. The pitch SAS uses a pitch rate feedback for normal short-period stability augmentation and, at high altitude, also uses a lagged pitch rate for static stability augmentation. The gain of the SAS is scheduled with dynamic pressure as shown in Figure 2.

The structural and aerodynamic data used in the study were provided for the longitudinal axis at the following flight conditions:

Flight condition	Mach	Altitude, ft	Weight, lb
1	0.95	25 000	124 271
1A	0.95	25 000	68 693
2	Supersonic	Cruise	90 703
3	0.68	22 000	68 693

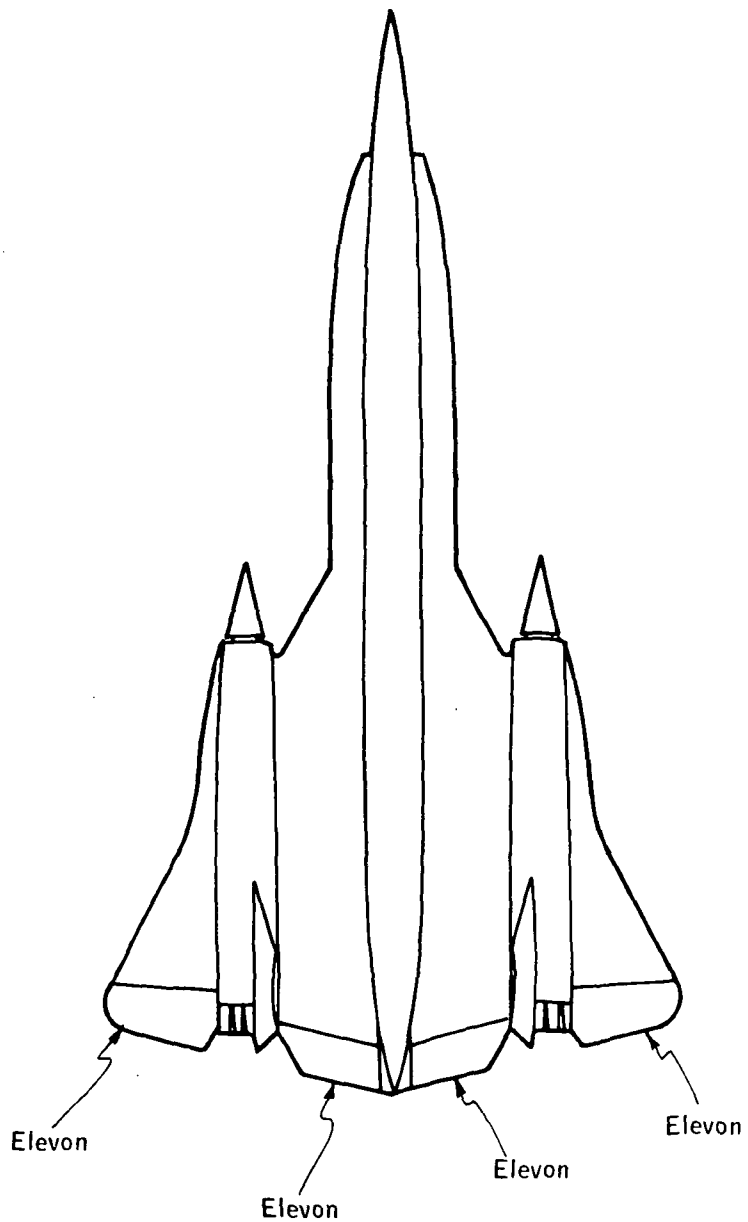

Figure 1. The YF-12A Aircraft

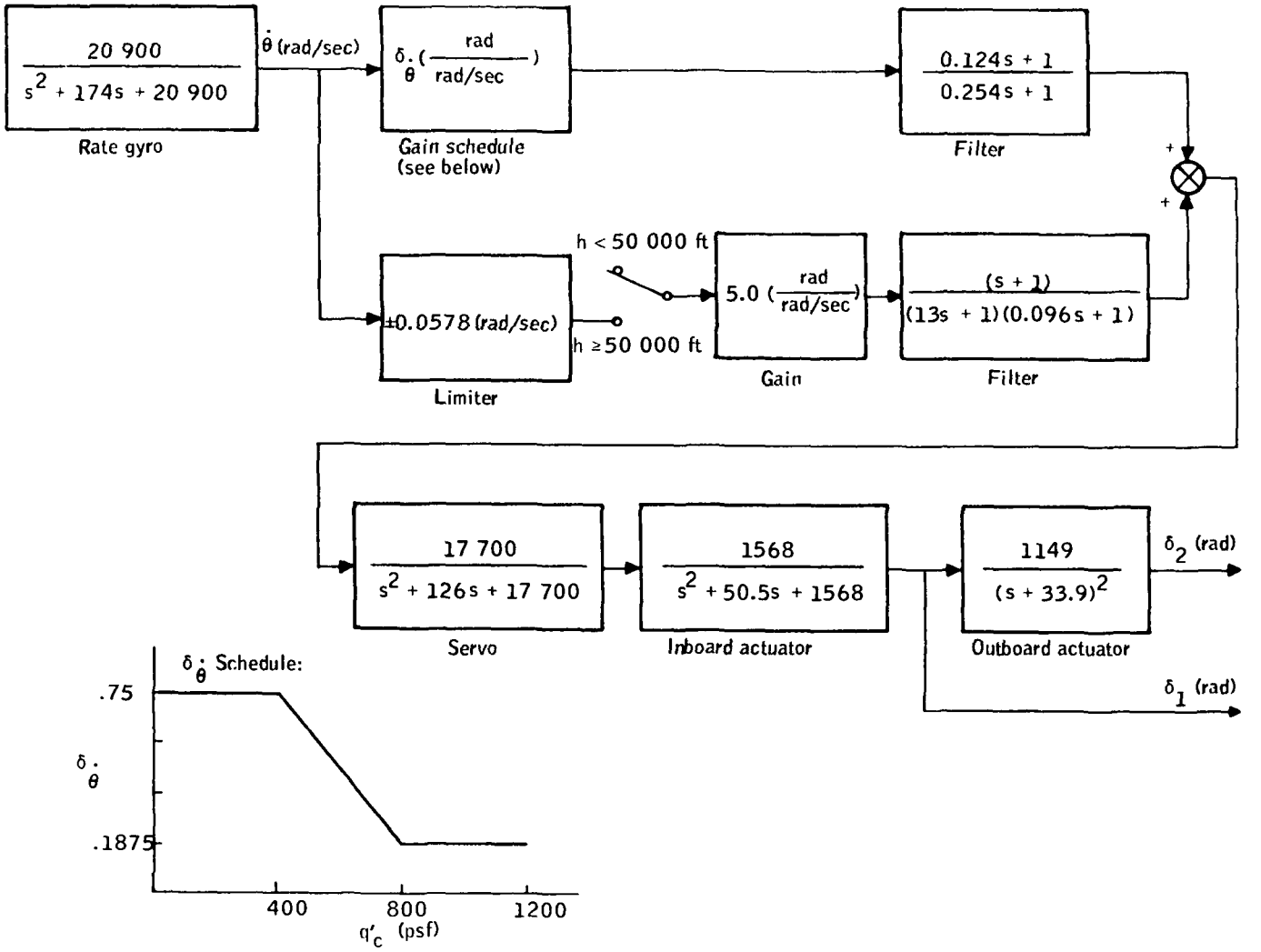

Figure 2. YF-12A Baseline SAS Block Diagram

Analytical Representation

The basic model used to analytically represent the YF-12A in the study did not provide a rigorous description of the vehicle. However, the data used were readily available and were considered adequate for meeting the study objective. The basic model of the aircraft was comprised of a structural model and an aerodynamic and gust model.

Structural model. - The structural model included two-degree-of-freedom rigid body dynamics and 16 symmetric structural modes. The model was capable of approximating the vehicle dynamics up to approximately 150 rad/sec. Figure 3 shows typical mode shapes for the lower-frequency symmetric structural modes. The model is further described in Appendix A.

Aerodynamic and gust model. - The indicial aerodynamic formulation was used in this study to represent the unsteady aerodynamics in the time domain for use in the optimal control study. The aerodynamics are described in Appendix A.

The atmospheric turbulence or gust model chosen for this study was the Press-Meadows model described in ref. 7. The effects of streamwise penetration into the gust were not included in the gust aerodynamic load formulation. This effect was considered minor due to the high velocity of the vehicle. The gust model is described in more detail in Appendix A.

Data Modification. - The basic 18th-order model was modified by a change in variables to remove the zero roots. This was necessary to assure convergence of the computer program which computes the rms of a given aircraft parameter for a disturbance input. This change of variables is described in Appendix A. In the following text, the model resulting from the change of variables is called the "transformed 18th-order model."

The final step in the data modification consisted of generating a simplified vehicle model for preliminary analysis studies. A simplified model was desired primarily to reduce the computation time required on the digital computer. The resulting simplified model was derived from the transformed 18-degree-of-freedom model by neglecting structural modes 9 through 16. These higher-frequency modes had natural frequencies in excess of 100 rad/sec and made a negligible contribution to the aircraft acceleration responses to a gust input. Although the simplified model was used in the preliminary analysis, the transformed 18th-order model was used to obtain a final performance and stability check.

Hence, as a consequence of the data modification, three analytical representations of the aircraft were used in the study. These representations are referred to as follows:

- Basic 18th-order model
- Transformed 18th-order model
- Simplified model.

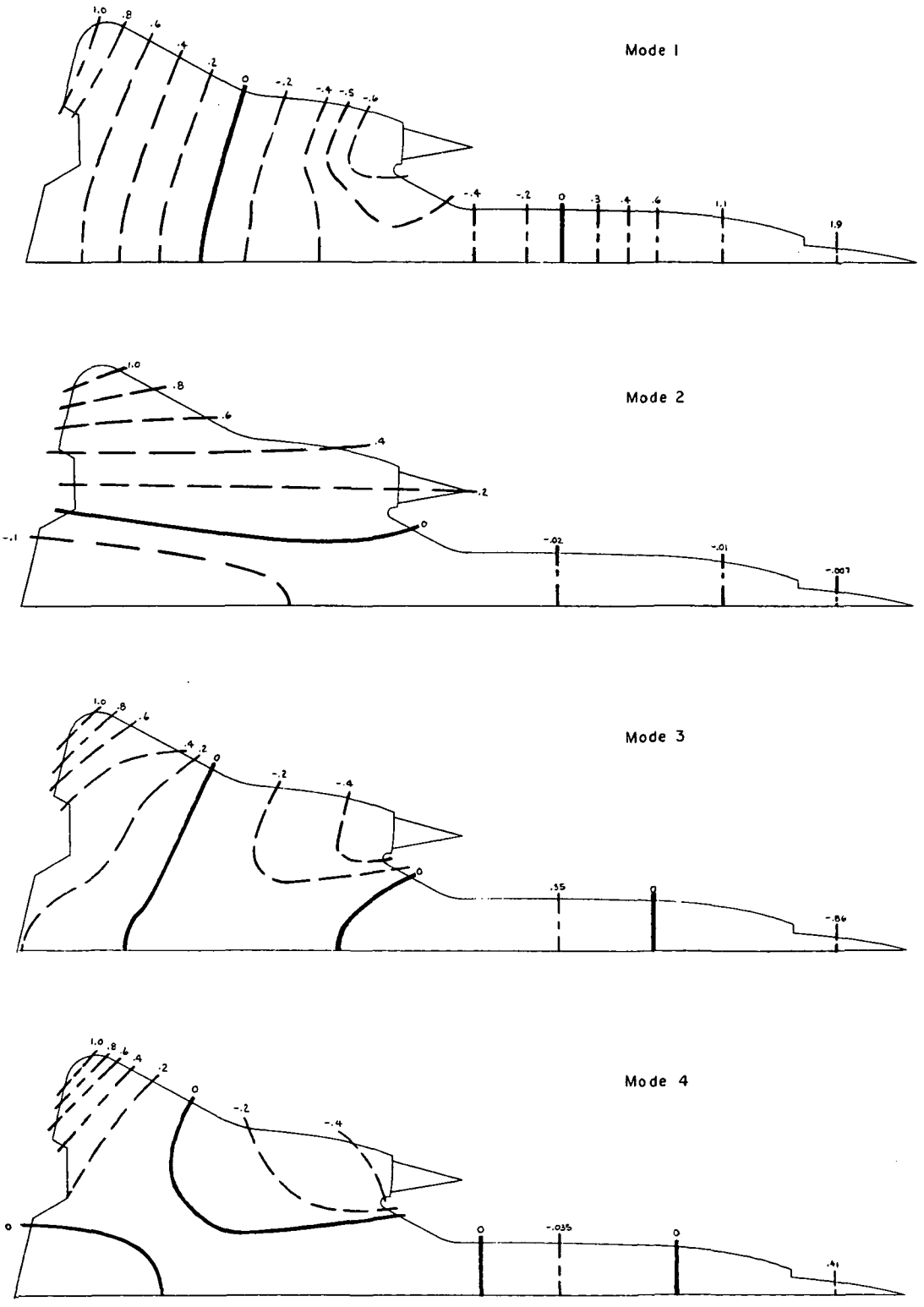

Figure 3. Vehicle Mode Shapes

YF-12A response characteristics. - The basic response characteristics of the YF-12A were examined prior to the synthesis of LAMS control systems. The purpose of this task was threefold, namely:

- To verify the transformed 18-degree-of-freedom aircraft model derived from the basic model
- To verify the simplified model which was extracted from the transformed 18-degree-of-freedom model
- To establish the nominal aircraft response characteristics.

The transformed 18th-order model and the simplified model were verified by comparison of eigenvalues and frequency responses, computed with these models, with similar data furnished for the basic model. Eigenvalues are compared in Table I for F/C 1, the high subsonic, heavyweight flight condition, with the baseline SAS loop opened. The data in Table I shows that the only differences in the eigenvalues of any significance are in the short-period mode. The differences shown were considered acceptable for the purposes of the study.

Frequency responses computed with the transformed 18th-order model and the simplified model are compared with the basic 18th-order model responses in Figure 4. These comparisons show a normal acceleration response at FS 248 to a combined inboard/outboard elevon input disturbance for F/C 1. The response comparisons in Figure 4 show that above 1 rad/sec the responses are in good agreement. The differences at low frequency between the basic model and the transformed model are attributed to the absence of poles at the origin in the transformed model. The differences shown in Figure 4 were considered acceptable. The true test of the simplified model was made when the systems designed using the simplified model were evaluated using the transformed model. These results are discussed later in the text, under SYSTEM PERFORMANCE.

Power spectral density (PSD) plots of normal acceleration for a 1-ft/sec gust input are shown in Figure 5 for the transformed 18th-order model. Plots are shown for acceleration responses at FS 248, 738, and 1236 for both F/C 1 and F/C 2. These data illustrate the performance characteristics of the nominal aircraft with the baseline SAS loop closed. The plots show the relative contribution of each of the aircraft modes to the acceleration levels of the selected aircraft stations. As these plots show, the rigid body and the first five or six modes were the primary contributors.

A study of the plots in Figure 5 shows that total suppression of the structural mode contributions would reduce the rms acceleration by 40 percent at the pilot's station. On the other hand, Figure 5 shows only a small contribution to the rms acceleration by the structural modes at FS 738.

At F/C 2, the responses in Figure 5 show the structural modes are the dominant contributors to the acceleration response. Total suppression of the structural modes would effect nearly a complete reduction in gust-induced accelerations.

TABLE I.- COMPUTED EIGENVALUES FOR F/C 1

Root	Basic 18th-order model without baseline SAS			Transformed 18th-order model without SAS			Simplified model without SAS		
	Quantity	Damping ratio	Frequency, rad/sec	Quantity	Damping ratio	Frequency, rad/sec	Quantity	Damping ratio	Frequency, rad/sec
Z, θ	2	0	0	0	Omitted	----	0	Omitted	----
Rigid body	2	0.37698	1.9927	2	0.2878	2.2876	2	0.3433	1.9929
1st mode	2	0.05232	12.4960	2	0.05250	12.5070	2	0.05570	12.4076
2nd mode	2	0.05096	16.6216	2	0.05087	16.6515	2	0.04705	16.6126
3rd mode	2	0.04310	29.8090	2	0.04306	29.8525	2	0.04286	29.7795
4th mode	2	0.03946	44.6555	2	0.03943	44.7127	2	0.03941	44.5538
5th mode	2	0.04715	49.6822	2	0.04709	49.7628	2	0.04415	49.3676
6th mode	2	0.02823	60.7835	2	0.02822	60.8390	2	0.02808	60.8285
7th mode	2	0.02897	73.7769	2	0.02896	73.8450	2	0.02831	73.8785
8th mode	2	0.03101	86.9578	2	0.03100	87.0434	2	0.03064	87.0373
9th mode	2	0.03077	96.8212	2	0.03075	96.9162	0	Omitted	----
10th mode	2	0.03830	105.7804	2	0.03827	105.9097	0	Omitted	----
11th mode	2	0.02991	124.7189	2	0.02989	124.8380	0	Omitted	----
12th mode	2	0.03647	131.9372	2	0.03644	132.0932	0	Omitted	----
13th mode	2	0.03056	146.7541	2	0.03055	146.8977	0	Omitted	----
14th mode	2	0.03282	150.8634	2	0.03280	151.0222	0	Omitted	----
15th mode	2	0.02822	161.0100	2	0.02821	161.1566	0	Omitted	----
16th mode	2	0.03736	156.5301	2	0.03734	156.7187	0	Omitted	----
Indicial functions	-	Not listed	----	18	----	9.77	10	----	9.77
Series servo	-	Not listed	----	2	0.473	133.0	2	0.473	133.0
Rate gyro	-	Not listed	----	2	0.602	144.0	2	0.602	144.0
Inboard actuator	-	Not listed	----	2	0.637	39.6	2	0.637	39.6
Outboard actuator	-	Not listed	----	2	----	33.9	2	----	33.9
Wind filter	-	Not listed	----	2	----	0.978	2	----	0.978
Gust lag	-	Not listed	----	1	----	4.88	1	----	4.88

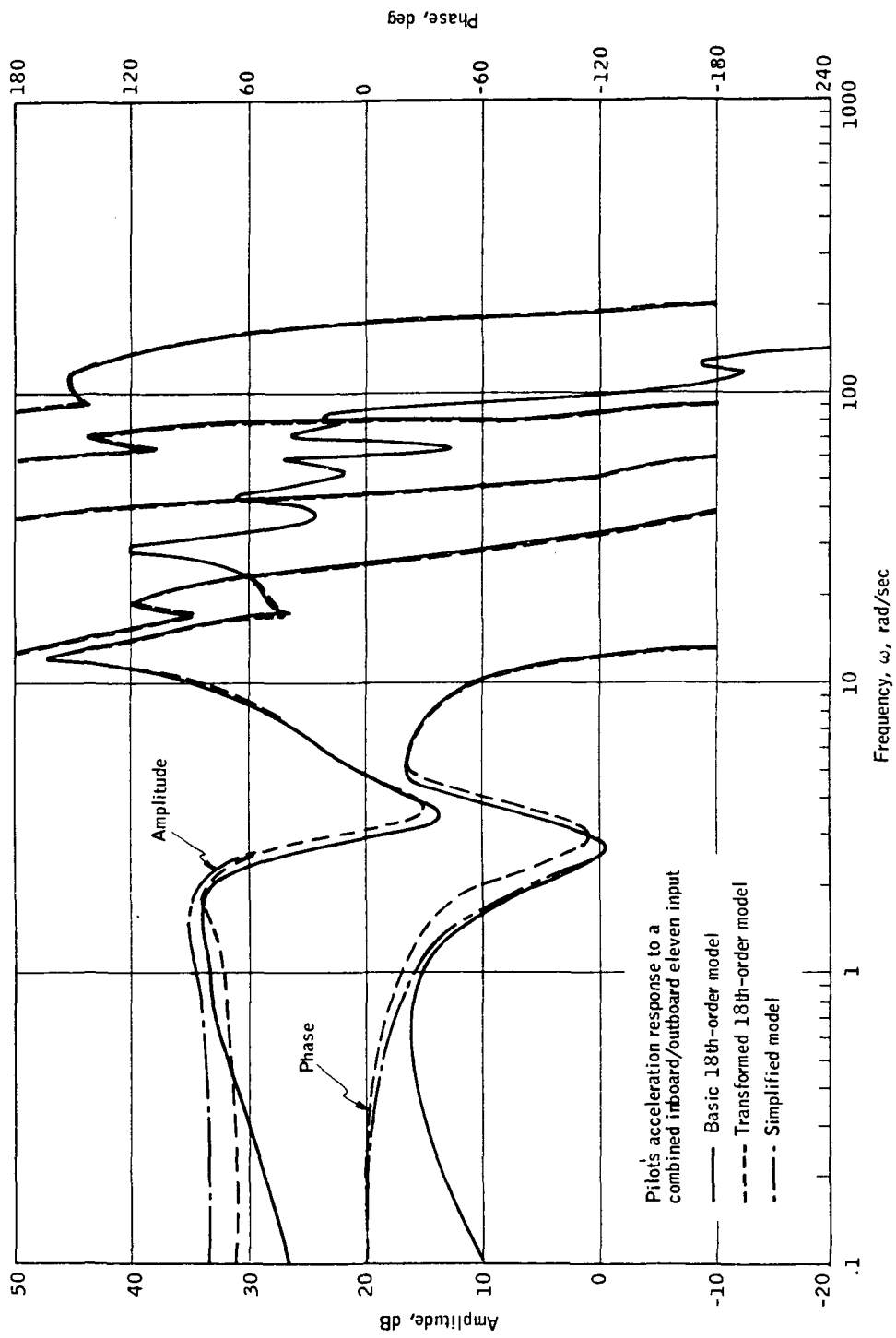

Figure 4. Comparison of Frequency Responses Obtained With Basic 18th-Order Model, Transformed 18th-Order Model, and Simplified Model, Without SAS

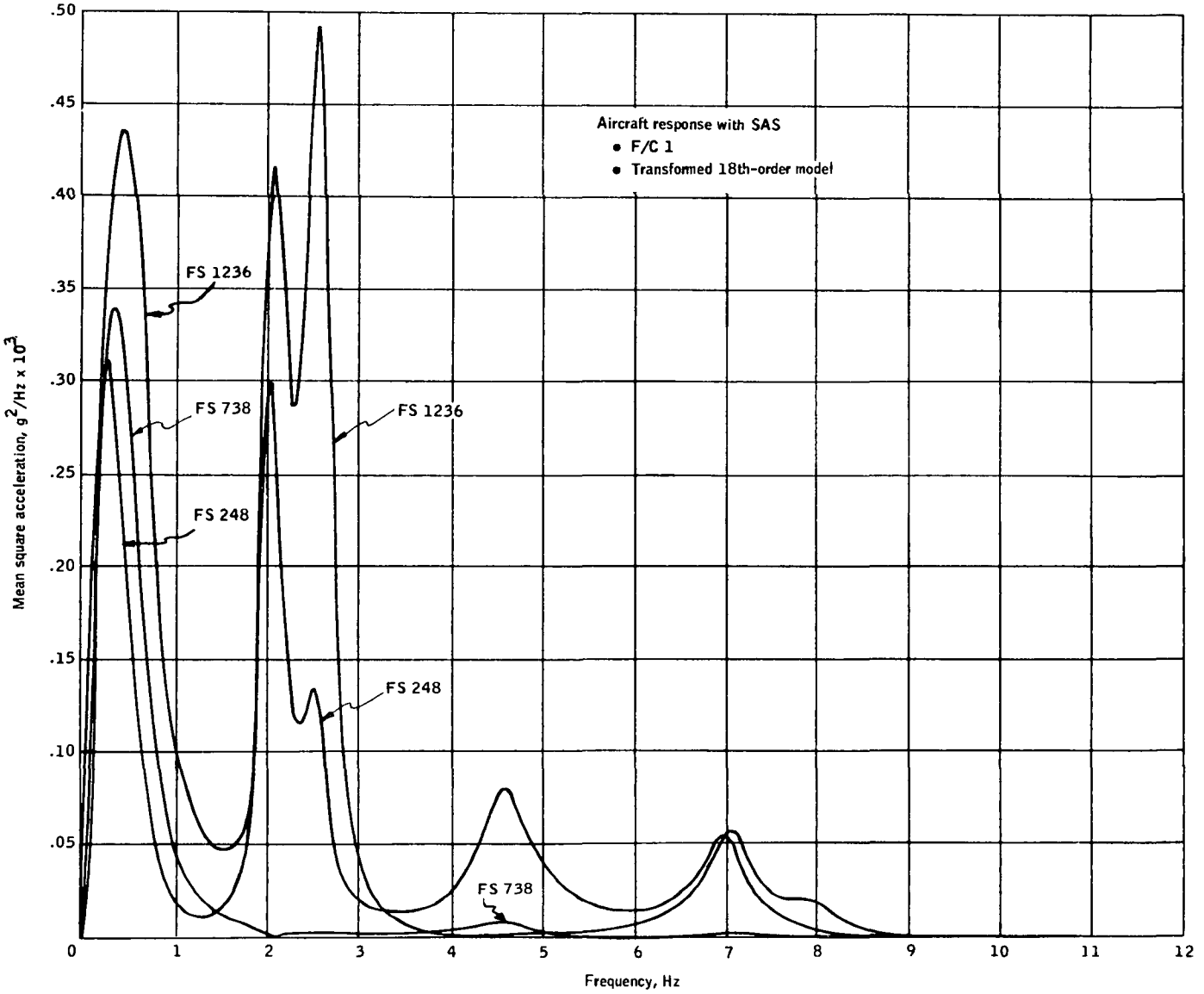

Figure 5A. Mean Square Acceleration at FSs 248, 738, and 1236 for a 1-ft/sec Turbulence Input -- Aircraft With SAS -- F/C 1

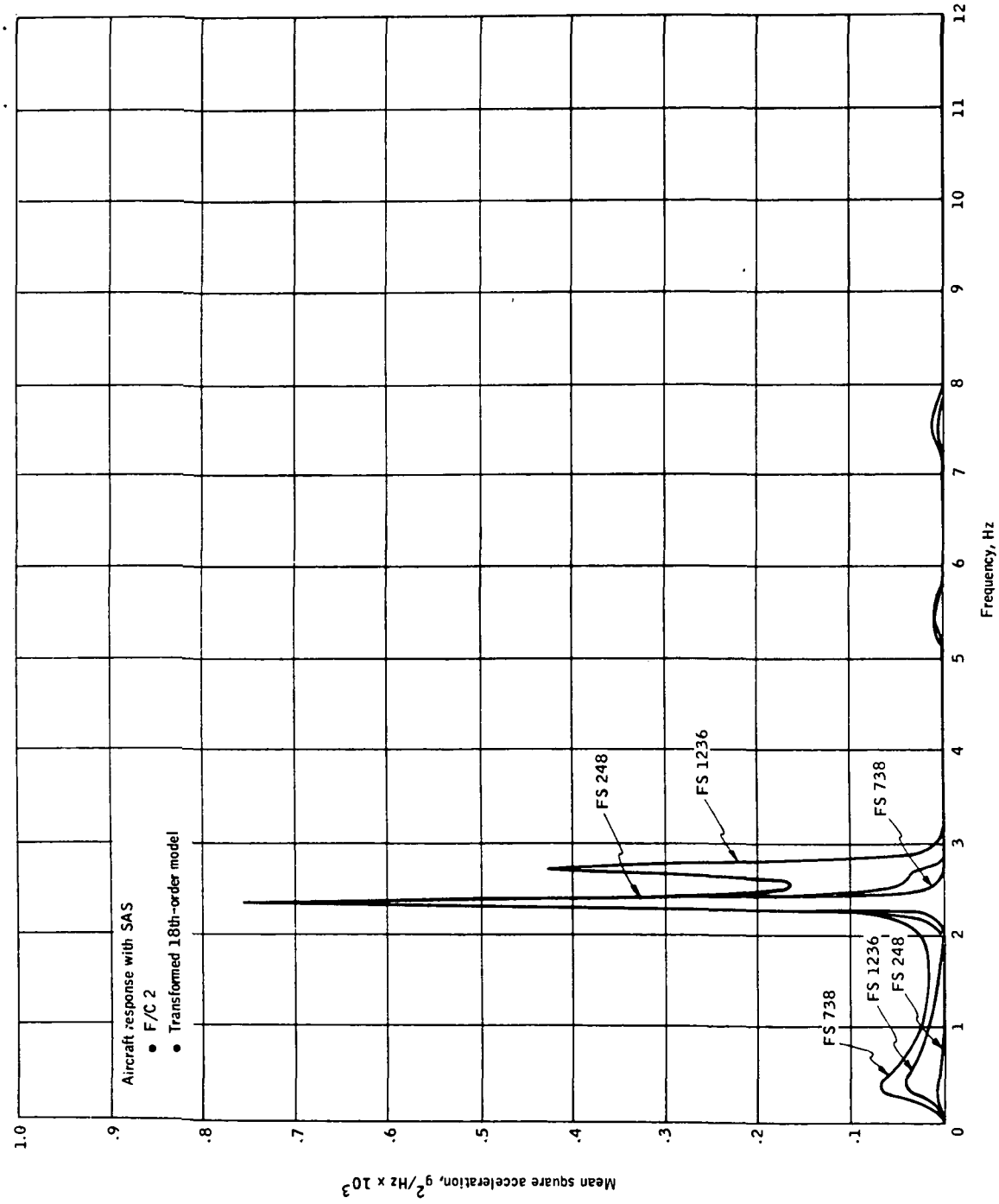

Figure 5B. Mean Square Acceleration at FSs 248, 738, and 1236 for a 1-ft/sec Turbulence Input -- Aircraft With SAS -- F/C 2

Table II compares rms acceleration levels for a unit gust input at all four flight conditions. This table shows that F/Cs 1 and 1A have the largest rms acceleration levels. It is also of interest to note that for the three stations shown, the largest rms acceleration occurs at the aft end of the fuselage.

TABLE II.- RMS ACCELERATION PER 1-FT/SEC GUST INPUT (WITH BASELINE SAS)

Fuselage station	F/C 1, high subsonic, heavyweight condition	F/C 1A, high subsonic, lightweight condition	F/C 2, supersonic cruise condition	F/C 3, low subsonic, lightweight condition
248 (pilot)	0.02118 g	0.02751 g	0.01100 g	0.01478 g
738	0.01473	0.02173	0.00551	0.01492
1236 (aft fuselage)	0.02683	0.04034	0.00996	0.01757

LAMS System Synthesis

Before discussing the detailed system design, it is worthwhile to consider some general aspects of the problem. These aspects include the design criteria and design constraints, the use of force producers to achieve effective mode suppression, and the methods used to synthesize the systems.

Design Criteria and Constraints

A design goal in terms of structural mode suppression was established for the purposes of the study. This goal was to reduce the structural mode contribution to the pilot's rms acceleration by 50 percent for either a gust or control input disturbance. It was assumed that a 50-percent reduction would be sufficient for demonstration purposes.

The systems were to be designed to meet this performance goal, but they also had to satisfy the following design constraints:

- The LAMS system shall not degrade existing handling qualities provided by the baseline SAS.

- The canards or mass-reaction device shall be restricted in size and force output so as not to cause a significant change in the YF-12 aerodynamics and to maintain internal loads within allowable limits. For the study, the design objective was to restrict the force output on the fuselage nose to less than 600 lb.

- The baseline SAS system operation shall not be altered and must remain engaged at all times.
- The mechanical linkage connecting inboard and outboard actuators must be retained.
- LAMS sensor locations must be physically practical.
- The LAMS system shall meet stability margin requirements of a 6-dB gain margin and a 60-deg phase margin.

LAMS Force Producers

As stated above, the ground rules stipulated that the LAMS system could not alter the operation of the baseline SAS nor degrade the rigid-body handling qualities. This requires that any coupling be minimized between the control of the aircraft's structural modes and the control of the rigid-body motion. The coupling between these two control functions may be minimized by either one or a combination of the following methods (assuming a predefined rigid-body SAS):

- Suitably locating and sizing the LAMS force producers
- Properly selecting the LAMS sensor locations
- Properly designing the filtering in the LAMS system.

The LAMS force producers must be selected before the sensor configuration and filtering can be established. To minimize coupling with rigid-body control, it is desirable to locate a LAMS force producer on the aircraft where structural mode deflections are large. This suggests that the force producers for LAMS should be located near the extremities of the aircraft, such as on the wing tips or on the nose. The only existing force producer on the YF-12A which qualifies (in the longitudinal axis) is the outboard elevon. But, on the YF-12A, the outboard elevon is slaved to the inboard elevon through a mechanical linkage. There is also no provision for any other inputs (either mechanical or electrical) to the outboard actuator. Without independent operation of the inboard and outboard elevons, the use of the force producer to separate the rigid-body control from the structural mode control would be ineffective. Hence, in this case, separation of rigid-body and structural mode control functions may be achieved only by a judicious location and blending of sensors and/or by filtering. Locating and blending of sensors is fairly effective, but this method is also limited by space available and environmental factors such as temperature variations. Minimizing coupling between rigid body and structural mode control by filtering is much less effective than either of the other two methods. Reliance on filtering to minimize the coupling generally results in a significant performance compromise between the two functions. This is true especially when the rigid-body short-period frequency is close (less than a factor of 3) to the lowest structural mode frequency. It was concluded that if effective structural mode control was to be achieved on the YF-12A with the existing force producers,

the aircraft would have to be modified. This modification would be necessary to permit independent operation of the inboard and outboard elevons to enhance the effectiveness of the outboard elevons for structural mode control.

Because the outboard elevons are located near the wing tips, they should qualify as an effective LAMS force producer for controlling wing flexure. Control of the aircraft's fuselage modes, however, may be better achieved through the use of a force producer located on the nose of the aircraft. Examination of the structural mode shapes (see Figure 3) shows the mode deflections along the fuselage are largest at the nose and are relatively small at the tail (near the inboard elevons). It was concluded the inboard elevons would be relatively ineffective as a LAMS force producer because of potential coupling problems with the rigid-body control function. Because of these considerations, use of an auxiliary force producer located near the nose of the aircraft was considered in the study. Use of such a force producer would, of course, also require modification of the aircraft.

Three primary factors must be considered before a force producer can be added. First, there must be space available within the aircraft for the force producer actuation. Second, the local structure must be capable of supporting the force producer. Third, the force producer cannot significantly alter the aerodynamics, especially with respect to the engine inlet dynamics. Small canard control surfaces or possibly a mass-reaction device were considered as candidates for the auxiliary force producers. Their location on the aircraft would be as shown in Figure 6.

Canard vanes were selected as one of the candidates because of promising results obtained with them in the XB-70 program. Small canard vanes were installed on the XB-70 primarily for use as a means for exciting the structural modes. The flight testing performed on the XB-70 demonstrated their effectiveness for exciting the modes. If they were effective for exciting the modes, they should be effective for controlling the modes. Furthermore, because of their small size (4 sq ft) the XB-70 canard vanes had only a limited effect on the rigid-body motion. One objective of the YF-12A study was to determine the size of canard vanes required for the YF-12A, keeping in mind the design constraints. The canard size required for mode control had to be evaluated against design constraints on allowable internal loads and on the aerodynamic effects on the engine inlets.

The mass-reaction device was considered because of its potential advantages over an aerodynamic control surface. One advantage is that it is not subject to the gross changes in aerodynamics encountered on vehicles like the YF-12A. This implies that gain scheduling of a system using mass reaction would be relatively simple. Because the mass is mounted internal to the aircraft, its addition would not alter the aerodynamic efficiency or cause potential engine inlet problems.

Use of a mass-reaction device also has disadvantages. First, it appears to be somewhat self-defeating in that it adds weight to the aircraft. Second, it represents a greater design risk than does an aerodynamic surface. This risk stems from the fact that it has not been used in an airplane as a force

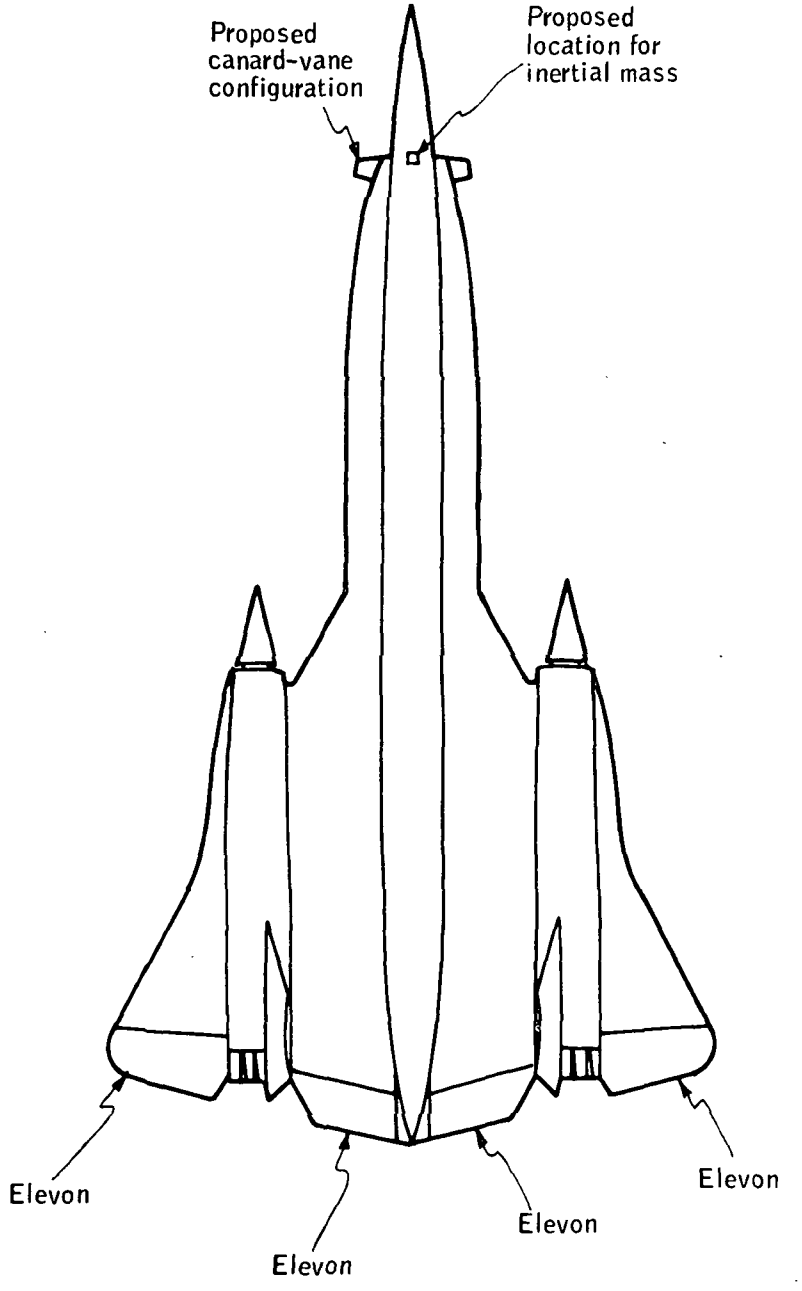

Figure 6. YF-12A Aircraft Showing Possible Locations of Auxiliary Force Producers

producer with feedback control. However, it was decided that the mass-reaction device should be evaluated to determine if the advantages outweigh the disadvantages. As with the canard, it was necessary to determine the size, displacement, and means for actuation of the mass. Finally, it was necessary to analyze these parameters for the YF-12A to determine if such a system would be reasonable for the space available and if the loads produced would be within the allowed limits. Two principal assumptions were made concerning the mass-reaction force producer:

1) It was assumed to be mounted at FS 248. A mass displacement of up to plus or minus 1 ft would be considered acceptable. Significantly larger displacements would have to be considered in more detail than intended for this study to determine the feasibility. At the bulkhead near FS 248, a space approximately 4 ft high is available. Consequently, allowing for packaging of hardware, a plus or minus 1-ft displacement allowance appeared reasonable.

2) The mass was assumed to be free to move in only a vertical plane and was to be positioned by an actuator (most likely hydraulic). In the absence of a command input to the actuator, the mass can be considered as rigidly attached to the airframe through the hydraulic actuator ram.

To summarize, it was evident at the beginning of the study that some modifications of the aircraft would be required in order to demonstrate significant LAMS performance. The purpose of the modifications would be to provide some means of achieving structural mode control without degrading rigid-body control. The modifications would consist of altering the outboard elevon servo to accept inputs from a LAMS system and/or adding an auxiliary force producer near the nose of the aircraft. The auxiliary force producer would be in the form of a small canard vane or a mass-reaction device. Combinations of all force producers were to be evaluated in the study to determine which combination would offer the greatest benefits.

Synthesis Techniques

A special frequency response technique was used as the basic design tool to configure LAMS controllers in the study. The technique was generated during development work on the Lockheed SST ride quality problem (ref. 6). The primary motivation for its development at that time was to provide a means for synthesizing LAMS systems when vehicle data were provided only in a frequency response format. The general principles of the technique are described in Appendix B. The technique basically consists of a set of useful formulas and guidelines for specifying the LAMS sensor configuration and corresponding gains and filtering. The formulas specify requirements for control system gains and filtering in terms of a performance parameter and the imposed stability constraints. This technique has proven to be a useful design tool. However, it also has some limitations. First, it becomes cumbersome to use in multiple-input (i.e., multiple-force-producer) applications. Multiple-input systems designed

with this technique must be done through the usual procedure of designing one control loop at a time. Determining the allocation of control among the available force producers is an iterative trial and error procedure. The second limitation is that one must initially assume an allocation of mode suppression performance for each of the significant structural modes. Whether or not this performance allocation is optimum with regard to all factors, such as system complexity and handling quality constraints, cannot be determined except by trial and error. These are not serious problems for the experienced designer, but it would be desirable to establish a more systematic procedure.

Quadratic optimization from modern control theory (ref. 10) has been used in previous LAMS programs (ref. 4) as an alternate synthesis technique. The primary motivation for its use is the ease with which it can handle the multiple-input/multiple-output problem of which LAMS is typical. By proper selection of weighting factors in a performance cost function, the allocation of control among the force producers is automatically optimized. Furthermore, quadratic optimization provides an effective means for determining the allocation of mode suppression performance among the structural modes.

A limitation in applying quadratic optimization, however, is the fact that the feedbacks determined by the process are not specified in terms of practical sensor outputs (e.g., an accelerometer at a specified location). Rather, the feedbacks are specified directly in terms of the state variables. The transformation from these optimal feedbacks to practical sensor outputs remains a formidable task.

One approach to "practicalizing" the optimal feedbacks is to use the frequency response technique. This is suggested by the fact that the two techniques appear to complement one another. Quadratic optimation provides an allocation of the control function among the given force producers but fails to define feedbacks in terms of practical sensor outputs. The frequency response technique, which lacks the capability for systematic allocation of the control function, offers the capability to define feedbacks in terms of practical sensors. A successful integration of these two techniques could yield a more effective synthesis procedure. An attempt was made in the YF-12A study to integrate these two synthesis techniques. The details of this effort, together with a description of the quadratic optimization technique, are presented in Appendix B.

Quadratic optimization was successfully used in a previous program (ref. 4) to define a LAMS controller for the B-52. In that application, the optimal controller was transformed to a "practical" configuration by trial-and-error analysis on the analog computer.

Design Procedure

The steps of the design procedure used to define the mode suppression systems are described in the following paragraphs.

Three major steps were used. The first step was to assign a control function to each of the available force producers. The second step was to define the control system sensor/filter configuration. The third step was to evaluate system performance. This, of course, was an iterative process, which began with a set of aircraft data already in a suitable form for analysis and the available force producers specified. The three steps are discussed in more detail below.

Step 1. Assign control function to each of the available force producers. - In this step, a control function was assigned to each force producer. This assignment was based on the design objective, and the force producer's location and relative force output capability. The design objective was to minimize the contribution of structural modes to the acceleration response at selected fuselage stations. This was to be accomplished without degrading the rigid-body handling qualities. A force producer was considered ideal for mode suppression if it exhibited the following properties:

- If it was located at or near a station where the acceleration response was to be reduced
- If it possessed relatively large force coefficients for the significant structural modes
- If it possessed relatively small rigid-body force coefficients.

For example, a small canard vane located at the pilot's station would be a logical choice for mode suppression at the pilot's station. However, it would be relatively ineffective for suppressing the acceleration response on the wing tip unless the wing and fuselage flexure modes were strongly coupled. A wing tip-mounted force producer would be a better candidate for suppressing the structural mode acceleration response on the wing tip.

Step 2. Define control system sensor/filter configuration. - Definition of the sensor/filter configuration was started by assuming an acceleration feedback from an accelerometer located near the force producer. This configuration generally guarantees that the sensed structural mode signals will be of the correct phase relative to one another to provide control of the modes through the given force producer (see ref. 3). After picking this initial sensor, the next task was to establish the extent to which the modes could be controlled, i. e. suppressed, taking into account other design objectives such as handling qualities. The rigid-body content of the accelerometer feedback signal generally degrades the handling qualities and, in particular, the short-period damping. As a consequence, the relationship between degraded handling qualities and mode suppression performance was evaluated. This was done by first defining a filter for the accelerometer feedback, using the frequency response technique (see Appendix B), and then by evaluating the closed-loop eigenvalues and PSD plots of acceleration for a gust input.

The next task was to reduce the effect of acceleration feedback on rigid-body response by changing the sensor configuration. There were two basic alternatives to this step. One was to blend two or more accelerometers to

minimize the sensed rigid-body signal. The other alternative was to add a rate gyro feedback to restore the short-period damping. If the force producer is located aft of the center of gravity, blending of accelerometers is preferred. Mounting a single accelerometer aft of the center of gravity (necessary for bending-mode stability) degrades system performance because of the attendant nonminimum phase property. This degradation cannot be eliminated by adding a rate gyro feedback but can be minimized by blending accelerometers. Satisfactory blending of accelerometers can be achieved by placing an accelerometer on each wing, averaging their signals, and subtracting a signal from a fuselage-mounted accelerometer. Ideally, for this purpose, the fuselage-mounted accelerometer should be located the same distance aft of the center of gravity as the wing-mounted accelerometer.

If the force producer is located ahead of the center of gravity, then the second alternative is preferred, that is, to add a rate gyro feedback. Effective cancellation of the rigid-body signal from a blend of accelerometers for a forward fuselage-located force producer generally requires at least three accelerometers. Blending of three accelerometers for this purpose is difficult to achieve while at the same time maintaining favorable structural mode feedback signals. However, with a forward fuselage-located force producer the addition of a rate gyro feedback would restore the short-period characteristics. The problem with the rate gyro is to locate it so as to minimize unfavorable structural mode pickup by the gyro. Since the main function of the gyro is to augment the short period damping, its output could be filtered to further minimize its influence on the structural modes. The filtering required can be computed using the frequency response technique.

The discussion so far has considered the use of only one force producer. If another force producer is available which is effective for controlling the rigid body, then this would offer yet another alternative for restoring the handling qualities without sacrificing the mode suppression performance.

The next task in defining the sensor configuration was to analyze the effects of intermodal coupling and the attendant stability constraints. Intermodal coupling is especially significant when one is attempting to suppress structural mode contributions to acceleration at one station by using a force producer located at some other station. For example, intermodal coupling would be a problem if one were attempting to suppress structural mode contributions to pilot's acceleration by using a wing tip-mounted force producer. Most of the structural mode contribution to pilot's acceleration arises from fuselage flexure. But a wing-mounted force producer has greater effectiveness for suppressing wing modes then for suppressing fuselage modes. The intermodal coupling can dilute the effectiveness of the wing-mounted force producer. The problem was analyzed in the study by using the frequency response technique of Appendix B. The technique was applied to specify allowable ratios of structural mode shape displacements for achieving mode suppression without sacrificing system stability due to intermodal coupling. These ratios served to characterize the required sensor configuration. Knowing the allowed ratios, combinations of sensors were sought which

satisfied this mode shape constraint on the sensor signal content. Having obtained a best "fit" sensor combination, a corresponding filter was defined.

Step 3. Evaluate system performance. - In this step, the performance of the potential system configuration defined in Step 2 was evaluated in terms of the short-period frequency and damping, aircraft-system stability, and mode suppression performance. If the performance objectives were not met, the design procedure was repeated until the deficiencies were eliminated.

Once an acceptable system was defined, additional performance parameters were evaluated. This analysis included an evaluation of structural loads, steady-state stick gradients, and actuator characteristics. The effectiveness of each force producer as a means for introducing a calibrated test input for flight test evaluation was also evaluated.

System Configurations

The LAMS system design was started by examining the possible combinations of force producers. The 11 possible combinations are shown in Table III. Five of the more promising combinations were selected for detailed study. They are:

- System A - Inboard and outboard elevons (operating independently)
- System B - Mass reaction only
- System C - Mass reaction plus outboard elevons
- System D - Canard only
- System E - Canard plus outboard elevons.

Of these five combinations, only one, System A, used the inboard elevons. This system was studied to establish the potential benefits of using only the force producers which presently exist on the aircraft.

TABLE III. - POSSIBLE FORCE PRODUCER COMBINATIONS

Additional force producer(s)	Force Producer			
	Canard	Mass reaction	Inboard elevon	Outboard elevon
None	X	X	X	X
Outboard elevon	X	X	X	----
Inboard elevon	X	X	----	----
Inboard and outboard elevons	X	X	----	----

The design of each of the five systems is described in the following paragraphs. For each system, a block diagram and a description of the function of each element in the system is presented.

System A - Inboard elevon plus outboard elevon. - Figure 7 is an analytical block diagram of System A. This system was defined primarily to demonstrate the performance potential and problem areas associated with using only the existing force producers. One of the design constraints imposed was that the mechanical linkage between the inboard elevon actuator and the outboard elevon series servo could not be altered. This mechanical linkage is the only means available for commanding outboard elevon deflections. Hence, the outboard elevons are slaved to the inboard elevons. For LAMS control, however, it is desirable to have independent control of the outboard and inboard elevons to enhance control of the wing modes. Independent control of the two control surfaces would require modification of the outboard elevon series servo. The series servo would have to be changed to accept both the mechanical linkage input and an electrical input from the LAMS system. In addition, any LAMS input to the inboard elevon must be electrically subtracted from the outboard elevon. Figure 7 shows this cancellation path. The dynamics shown on this path simulate the inboard actuator dynamics. A potential problem would exist with this cancelling of a mechanical signal path with an electrical equivalent. Any variations in the mechanical system (i.e., the power actuator and mechanical linkage) due to nonlinearities (such as hysteresis) and temperature effects would reduce the effectiveness of the cancellation path.

As Figure 7 indicates, the pitch SAS provides an input to only the inboard elevon actuator, while the LAMS system provides inputs to both the inboard and outboard elevon actuators. The primary function of the LAMS outboard elevon controller is to suppress the aircraft's wing bending modes. The LAMS inboard elevon controller functions to control the fuselage bending modes.

The LAMS outboard elevon controller uses three accelerometers. Of these three, one is placed on each wing close to the outboard elevons (i.e., WS 294). These two wing-mounted sensors are averaged together to provide a measurement of wing bending. A third accelerometer is located on the fuselage at station 954 (aft wheel well). The signal from this accelerometer is subtracted from the averaged signal of the wing-mounted sensors. The third accelerometer is required to minimize the net pickup of rigid-body motion and to assure proper phasing on the aeroelastic mode signals. It was desirable to minimize the rigid-body pickup to maintain acceptable handling qualities. Ideally, the rigid-body content of the wing-mounted sensor signals can be cancelled by locating the fuselage-mounted accelerometer at the same distance back from the center of gravity as are the wing-mounted accelerometers. Unfortunately, locating the fuselage-mounted accelerometer in this manner will produce unfavorable phasing on the pickup of higher-frequency aeroelastic modes. But by moving the accelerometer forward on the fuselage, an acceptable compromise can be achieved between rigid-body pickup and phasing of the aeroelastic mode signals. The phasing on the aeroelastic mode signals was most critical for the first two aeroelastic modes. A strong intermodal coupling exists between these two modes because of their close proximity

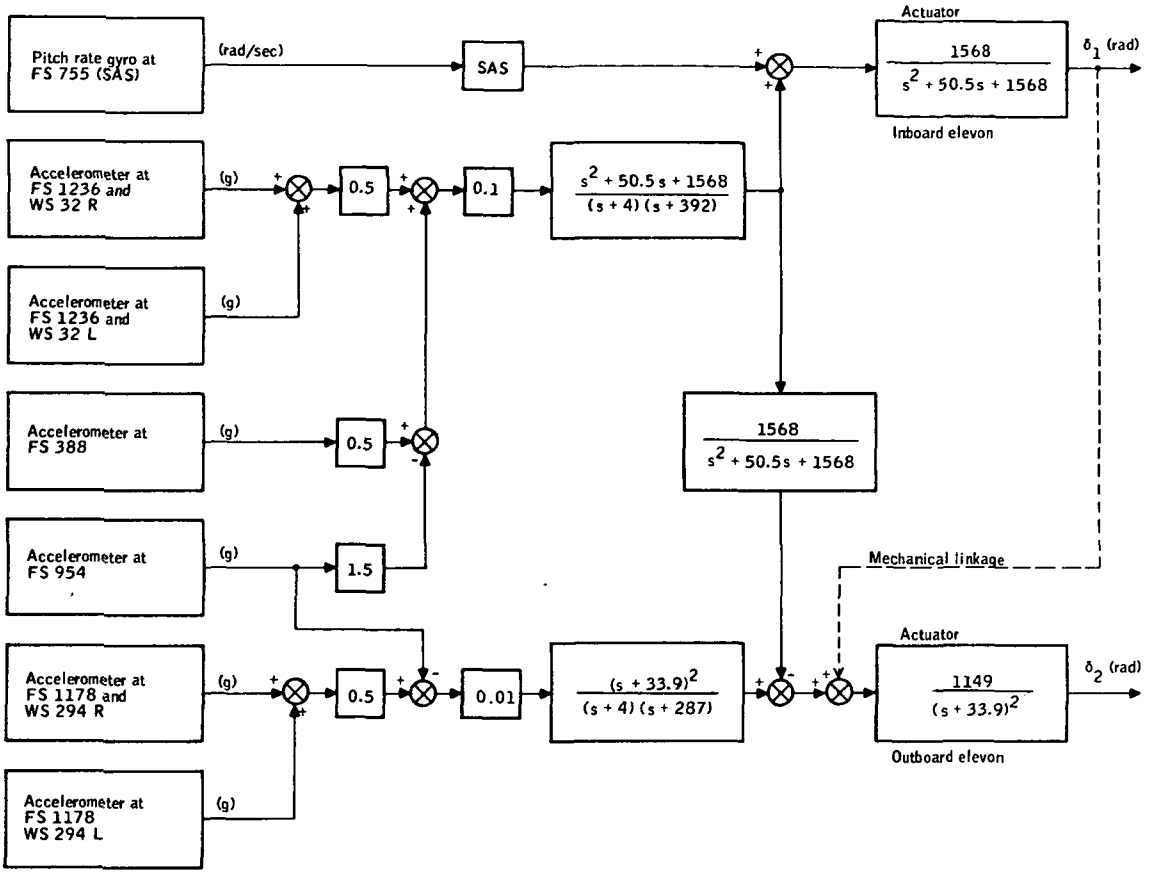

Figure 7. LAMS Inboard/Outboard Elevon Controller

in frequency. The first mode is primarily a fuselage-bending mode while the second mode is primarily a wing-bending mode. The intermodal coupling aggravated the design of a LAMS system because, as control was applied to suppress the wing mode via the outboard elevons, the response of the fuselage mode was made worse. The problem was solved using the frequency response technique (Appendix B) to formulate a design constraint on the required modal pickup and the corresponding filter. The result was the outboard elevon system shown in Figure 7. The filter which was computed provides approximately a 90-deg phase lag over the frequency range of the significant aeroelastic modes. The gain value of 0.01 rad/g was computed to maximize modal suppression performance compatible with stability constraints.

The inboard elevon system uses a blend of four accelerometers mounted along the fuselage. This sensor combination is used to eliminate rigid-body pickup and to provide the required phasing on the structural modes. Two accelerometers are required at FS 1236, since it was assumed a single

accelerometer could not be physically mounted on the centerline. The averaged output of these two aft-mounted accelerometers is blended with an accelerometer mounted just aft of the cockpit at station 388 and an accelerometer mounted in the wheel well at station 954. The gains and shaping shown in Figure 7 for the inboard elevon system provide the required compensation for augmentation of the fuselage bending modes, especially modes 1 and 3.

The synthesis of the inboard elevon system presented the most difficult task of all the control loops considered. The basic difficulty with using this force producer for mode suppression is that the mode deflections are relatively small in the vicinity of the inboard elevons. Hence, the coupling problem with the rigid body was more serious than with the other force producers. Use of an accelerometer near the inboard elevons was ruled out because of the potential degradation in rigid-body dynamics. Various combinations of rate gyros and accelerometers were considered, with the objective of providing favorable pickup on all structural modes while minimizing rigid-body pickup. The end result was the sensor configuration shown in Figure 7. This resulted in favorable pickup of the structural modes while eliminating the rigid-body content.

Although this sensor configuration was considered acceptable for the purposes of the study, it possesses a potentially undesirable feature. This feature has to do with the blending of three (in effect) sensors distributed along the fuselage. Such a configuration is generally sensitive to changes in mode shapes, since proper blending for some of the modes will depend on taking the difference between two large numbers.

System B - Mass reaction only. - Figure 8 is a block diagram of the mass-reaction control system. Since this force producer, like the canard, does not presently exist on the aircraft, the actuator dynamics were not specified. A brief analysis of the mass-reaction dynamics was made prior to synthesizing the mass-reaction system. The objective of this analysis was to establish the desired actuator frequency response characteristic for the mass-reaction system. The actuator response characteristic was determined by examining the aircraft's acceleration response at the mass location for a mass-displacement input. This plot, shown in Figure 9, indicated that a low-frequency, second-order actuator characteristic would be desirable. Such an actuator would provide the following benefits:

- A mass-position feedback
- A 180-deg phase lag over the frequency range of the structural modes
- A high-frequency gain attenuation.

The mass-position feedback is required to keep the mass centered at least on a low-frequency basis. Without this feedback, the mass would be free to drift and eventually hit its displacement limits. A second-order actuator with a natural frequency of 2 rad/sec and a damping ratio of 0.5 was initially selected. An alternative to using this actuator would be to use a low-frequency, first-order actuator. The 180-deg phase lag required

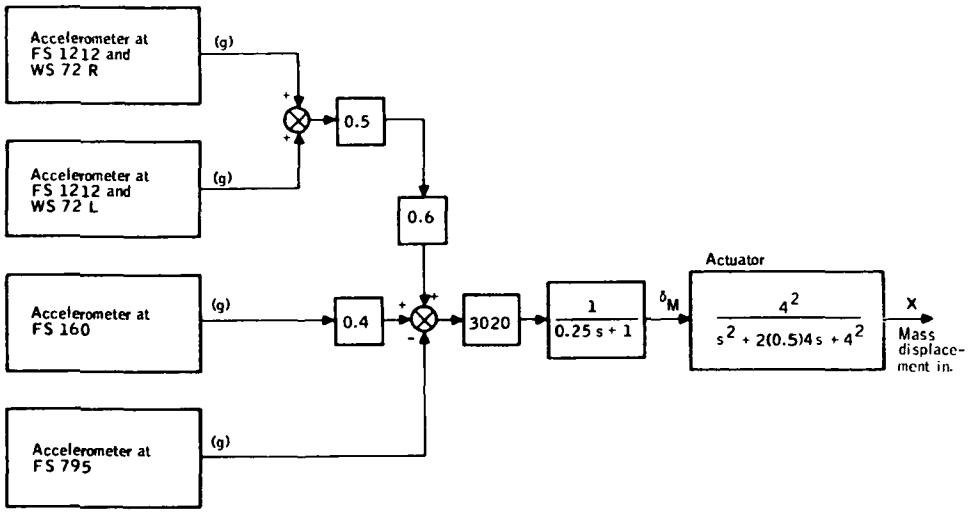

Figure 8. LAMS Mass-Reaction-Only Controller

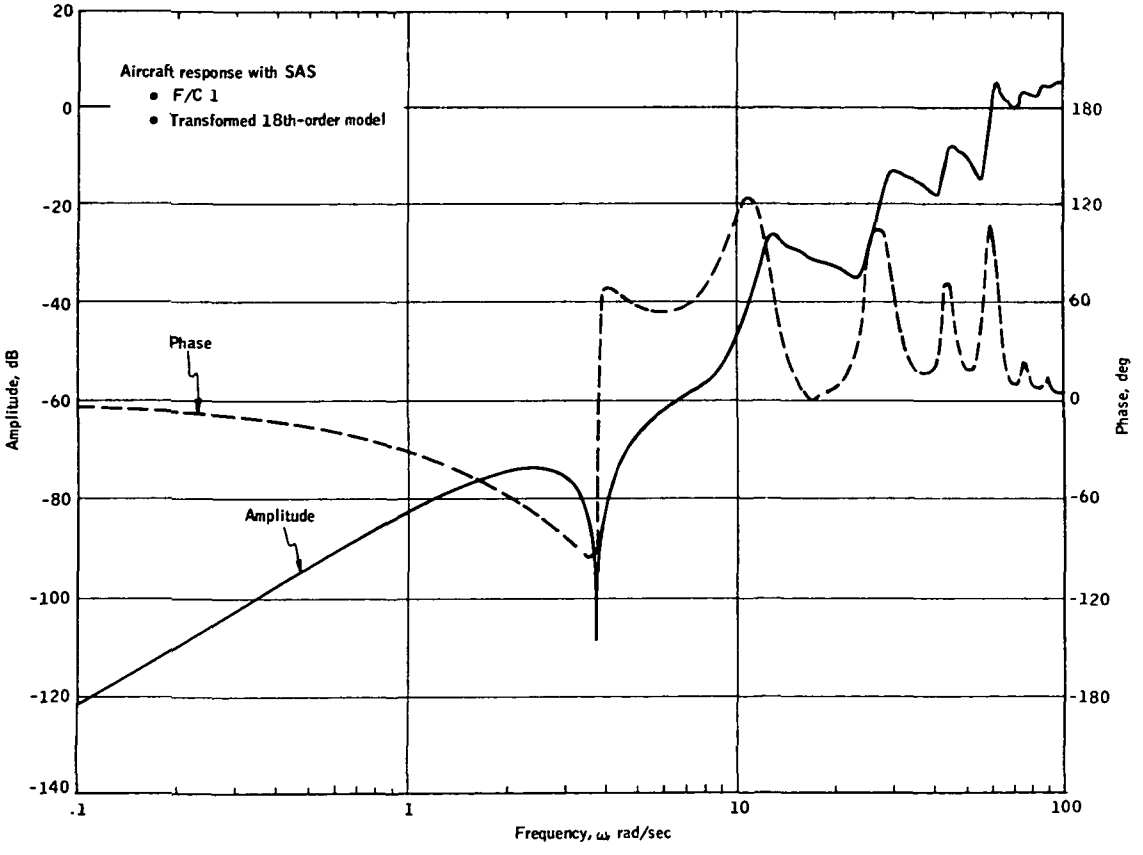

Figure 9. Frequency Response Plot of Acceleration at FS 248 for a White Noise Input Through the Mass Actuator

would have to be obtained through a phase reversal in the control system. However, this approach was discarded in the study because the high-frequency attenuation characteristic was considered to be inadequate.

The sensor configuration shown in Figure 8 consists of four accelerometers located along the fuselage. One accelerometer is located in the nose at FS 160. Another is located at FS 975, which is just aft of the baseline SAS rate gyro. The remaining two accelerometers are placed at FS 1212 on either side of the centerline. As was the case with the outboard elevon controller, it was assumed there would be no space available on the centerline for a sensor at this location. Consequently, the two accelerometers, placed on either side of the centerline, are averaged together. The four sensors were blended together to eliminate all rigid-body pickup while maintaining favorable structural mode pickup. As with the inboard elevon sensor configuration, blending of these accelerometers tends to result in a system which is not tolerant to variations in aircraft dynamics. This intolerance is demonstrated in the performance results. The gain and shaping shown in Figure 8 was defined using the frequency response technique.

System C - Mass reaction plus outboard elevon. - A block diagram of System C is shown in Figure 10. The mass-reaction controller shown in this figure is identical to the one described for System B. The outboard elevon controller shown is identical to the one used in System A except for the following:

- Gain on the net sensor signal is doubled from 0.01 rad/g to 0.02 rad/g.
- The blend of sensors shown calls for using an accelerometer mounted at FS 795. In System A, this sensor was mounted at station 955. This change was made to obtain commonality with the sensors used for the mass-reaction system.

System C contains a rather complex combination of sensors. Refinement of this system would be directed toward simplifying this sensor complement. It is anticipated the two sensors at station 1212 could be eliminated.

System D - Canard only. - An analytical block diagram of System D is shown in Figure 11. It is the simplest of all five candidate systems. The system requires use of a conventional (i.e., no temperature compensation) accelerometer located near the canard at FS 248, and a signal from the baseline SAS rate gyro. The baseline SAS rate gyro is located on the fuselage (FS 765) approximately where the leading edge of the wing joins the fuselage. The only filtering required by the system is provided by the 0.25-sec first-order lag specified for the actuator dynamics.

With the canard located at the pilot's station, synthesis of a mode suppression system is relatively straightforward. The two primary design constraints in the synthesis are retention of handling qualities and system stability. The effects of these constraints are minimized by using an

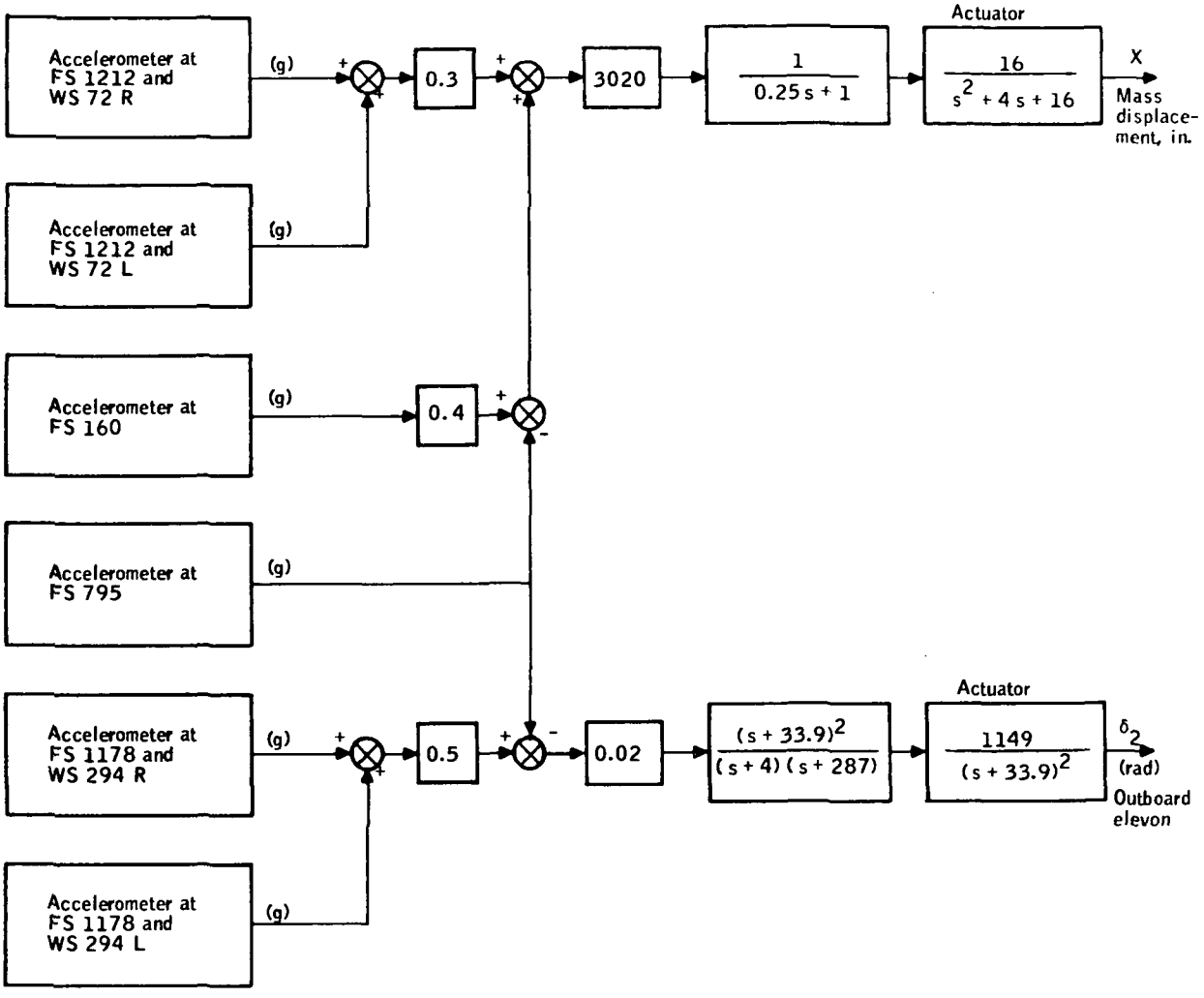

Figure 10. LAMS Outboard Elevon-Plus-Mass Reaction Controller

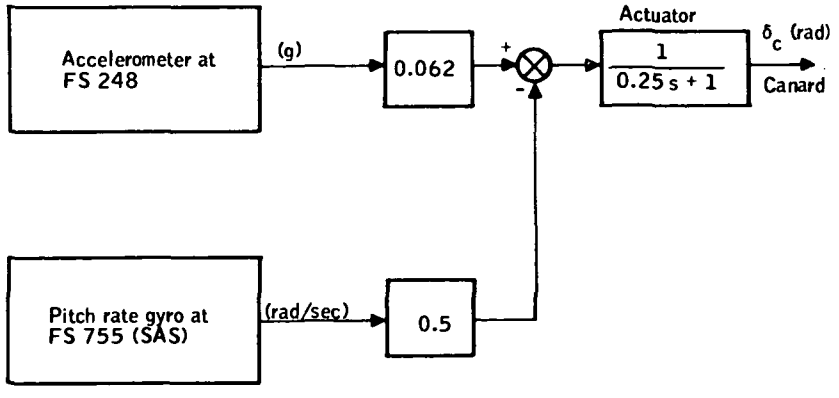

Figure 11. LAMS Canard-Only Controller

accelerometer placed at the same location as the canard. Use of an accelerometer placed in this location offers the following advantages:

- The structural mode pickup is large relative to other vehicle stations. This property minimizes any potential coupling problem with the rigid-body mode.
- Placement of an accelerometer at the same location as the force producer tends to assure proper phasing for stability on all the structural modes. (This concept of locating the sensor at the same location as the force producers is described in ref. 3)
- Phasing on the rigid-body acceleration pickup is such to provide some rigid-body load alleviation.

The acceleration feedback to the canard results in commanding a positive canard deflection (i.e., trailing-edge down) for a positive normal acceleration (i.e., downward). A positive canard deflection results in a nose-up motion to reduce the angle of attack, thereby providing load alleviation. The price paid, however, is reduced short-period damping. The reduction in short-period damping is compensated by adding a pitch rate feedback to the canard.

System E - Canard plus outboard elevons. - Figure 12 shows a block diagram of System E. In this system the outboard elevon loop configured

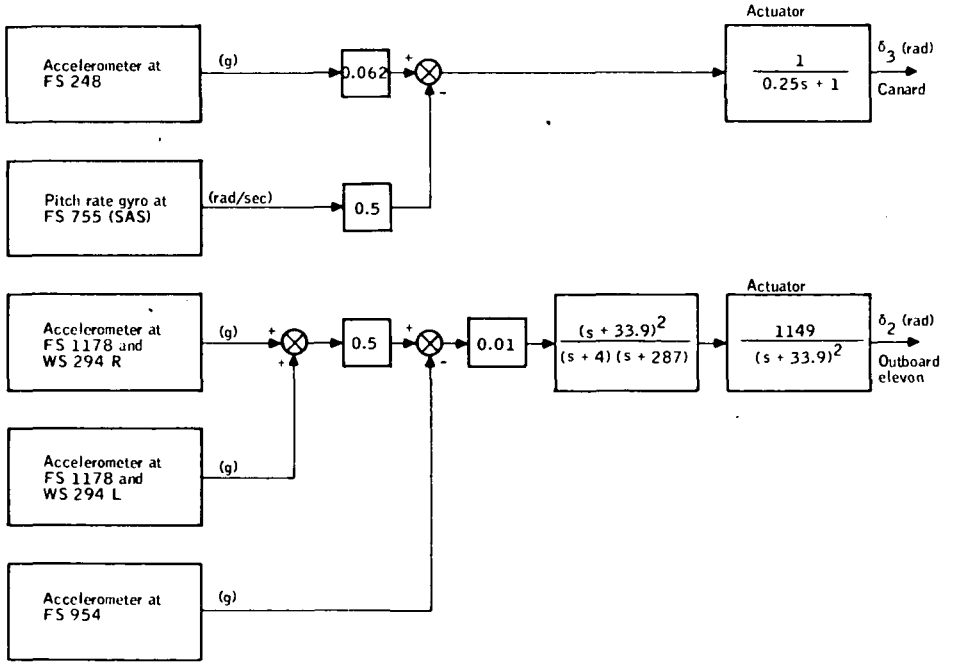

Figure 12. LAMS Outboard Elevon-Plus-Canard Controller

for System A was added to the canard controller of System D. This was done to provide additional mode suppression of the wing aeroelastic modes.

System Mechanization Considerations

Mechanizations for the five candidate systems were examined in the study to the extent necessary to uncover problem areas affecting feasibility and to determine required aircraft modifications. The study indicated no insurmountable problems with respect to mechanization for any of the five candidate systems. All aircraft modifications required to incorporate the auxiliary force producers or to modify the existing force producers were reasonable. Installation of accelerometers in the wings or in the aft body would be constrained by the severe temperature environment, however. Either special high-temperature sensors would have to be designed, or cooling would have to be provided for conventional sensors or else the flight envelope would have to be restricted.

SYSTEM PERFORMANCE

Performance results are presented for each of the five candidate LAMS control systems. These results consist of the following vehicle/system properties:

- Eigenvalues
- Stability margins
- Mode suppression performance at FS 248 (pilot's station), FS 738, and FS 1236 (aft fuselage) for a turbulence input disturbance
- Mode suppression performance at the above three fuselage stations for input disturbances applied via a force producer. The force producer input disturbance was generated by assuming a white noise input into the gust model which was modified by setting L/V_o equal to 20. [See eq. (A34) of Appendix A, Basic Vehicle Data]. The gust model was selected as a convenient means for attenuating the high-frequency content of the white noise input. The output of the modified gust model was summed into the control surface actuator being used to excite the aircraft. For the cases where the canard was used to excite the aircraft, actuator dynamics were ignored.

Handling quality performance and the effects of nonlinearities are described collectively for the five systems at the end of the section.

System A - Inboard/Outboard Elevon System

Table IV shows a comparison of the open- and closed-loop roots obtained with the inboard/outboard elevon system. Examination of these roots shows that the rigid-body damping was reduced and the frequency increased. The resultant frequency and damping were considered acceptable, however. The excessively high damping obtained on the first structural mode indicates the mode is being overcontrolled. These results indicate the gain on the inboard elevon controller should have been lower. If the gain were halved there would be less of a change in the short-period dynamics and probably no significant change in the mode suppression performance for the first mode. The mode suppression performance of the higher-frequency modes would have been reduced, but this could probably be restored via a change in the outboard elevon system.

TABLE IV. - COMPARISON OF OPEN- AND CLOSED-LOOP POLES WITH SYSTEM A - F/C 1 - SIMPLIFIED MODEL

Mode	Baseline SAS only		With LAMS	
	Damping ratio	Frequency, rad/sec	Damping ratio	Frequency, rad/sec
Short-period	0.610	3.70	0.443	5.76
1st mode	0.068	12.7	0.969	11.64
2nd mode	0.056	16.2	0.109	16.2
3rd mode	0.076	29.1	0.111	28.0
4th mode	0.042	44.1	0.097	44.1
5th mode	0.043	49.4	0.058	49.1
6th mode	0.029	60.8	0.038	60.8
7th mode	0.032	74.1	0.044	74.3
8th mode	0.029	86.8	0.074	86.1

The stability results for the inboard/outboard elevon system are shown in Table V. Stability margins shown for F/C 1 tend to support the above observation concerning the inboard elevon control gain. Table V indicates only a 4-dB margin exists at F/C 1. Reducing the inboard elevon control gain level would, of course, enhance this margin. The control gains were not changed for the computation of stability at F/C 1A. As the table indicates, the inboard elevon system causes a stability problem with the second mode at

TABLE V. - STABILITY MARGINS - SYSTEM A - TRANSFORMED 18TH-ORDER MODEL

Flight condition	Inboard elevon loop closed		Outboard elevon loop closed	
	Gain margin, dB	Phase margin, deg	Gain margin, dB	Phase margin, deg
1	----	180	4	63
1A	Unstable 2nd mode		10	63
2	Unstable higher-frequency mode		14	67

this flight condition. However, closure of both the inboard and outboard control loops restored the stability of this mode. The stability problem with the second mode is most likely due to intermodal coupling between the first and second modes. It is expected that a reduced gain for the inboard elevon loop would solve the problem. Stability at F/C 2 was computed with the inboard elevon gain increased by a factor of 10 and the outboard elevon gain increased by a factor of 6. These gain adjustments were made to compensate for the decrease in surface effectiveness in going from F/C 1 to F/C 2. As is evident from the table, the inboard elevon controller causes an instability in a higher-frequency structural mode. This could be easily corrected by a gain reduction or by the addition of some high-frequency filtering.

Table VI shows mode suppression performance obtained with the inboard plus outboard elevon system at two flight conditions. These results show a reduction in rms acceleration of approximately 30 percent at the subsonic

TABLE VI. - MODE SUPPRESSION PERFORMANCE FOR A 1-FT/SEC TURBULENCE INPUT DISTURBANCE WITH SYSTEM A - TRANSFORMED 18TH-ORDER MODEL

Fuselage station	F/C 1, high subsonic, heavyweight condition[a]		F/C 2, supersonic cruise condition[b]	
	SAS only	LAMS	SAS only	LAMS
248 (pilot)	0.0212 g	0.0159 g	0.0110 g	0.0051 g
738	0.0147	0.0142	0.0055	0.0040
1236 (aft fuselage)	0.0268	0.0189	0.010	0.0050

[a]Simplified model

[b]Transformed 18th-order model

condition and 50 percent at the supersonic condition. It should be noted that these rms values are misleading. The contribution of the rigid-body mode, which was intentionally not reduced, masks the true mode suppression performance. The corresponding PSD plots of mean square acceleration at the subsonic condition are shown in Figures 13, 14, and 15. The mode suppression performance obtained is more evident from these plots.

Tables VII and VIII show rms accelerations obtained for force producer input disturbances at the subsonic and supersonic conditions, respectively. Performance at the subsonic condition shows rms acceleration reductions up to 70 percent for an inboard/outboard elevon input. Performance obtained at the supersonic condition (see Table VIII) shows reductions in rms accelerations on the order of 50 percent for a canard input and 75 percent for an inboard/outboard elevon input.

TABLE VII. - RMS ACCELERATION RESPONSE FOR A 1-RAD FORCE PRODUCER INPUT DISTURBANCE - SYSTEM A - F/C 1 - SIMPLIFIED MODEL

Fuselage station	Input to canards		Input to inboard/ outboard elevons	
	SAS only	LAMS	SAS only	LAMS
248	6.52 g	6.16 g	2.16 g	0.825g
738	1.79	1.75	0.576	0.337
1236	2.91	2.23	1.96	0.586

TABLE VIII. - RMS ACCELERATION RESPONSE FOR A 1-RAD FORCE PRODUCER INPUT DISTURBANCE - SYSTEM A - F/C 2 - TRANSFORMED 18TH-ORDER MODEL

Fuselage station	Input to canards		Input to inboard/ outboard elevons	
	SAS only	LAMS	SAS only	LAMS
248	0.621g	0.493g	0.526g	0.134g
738	0.220	0.167	0.222	0.076
1236	0.300	0.149	0.376	0.106

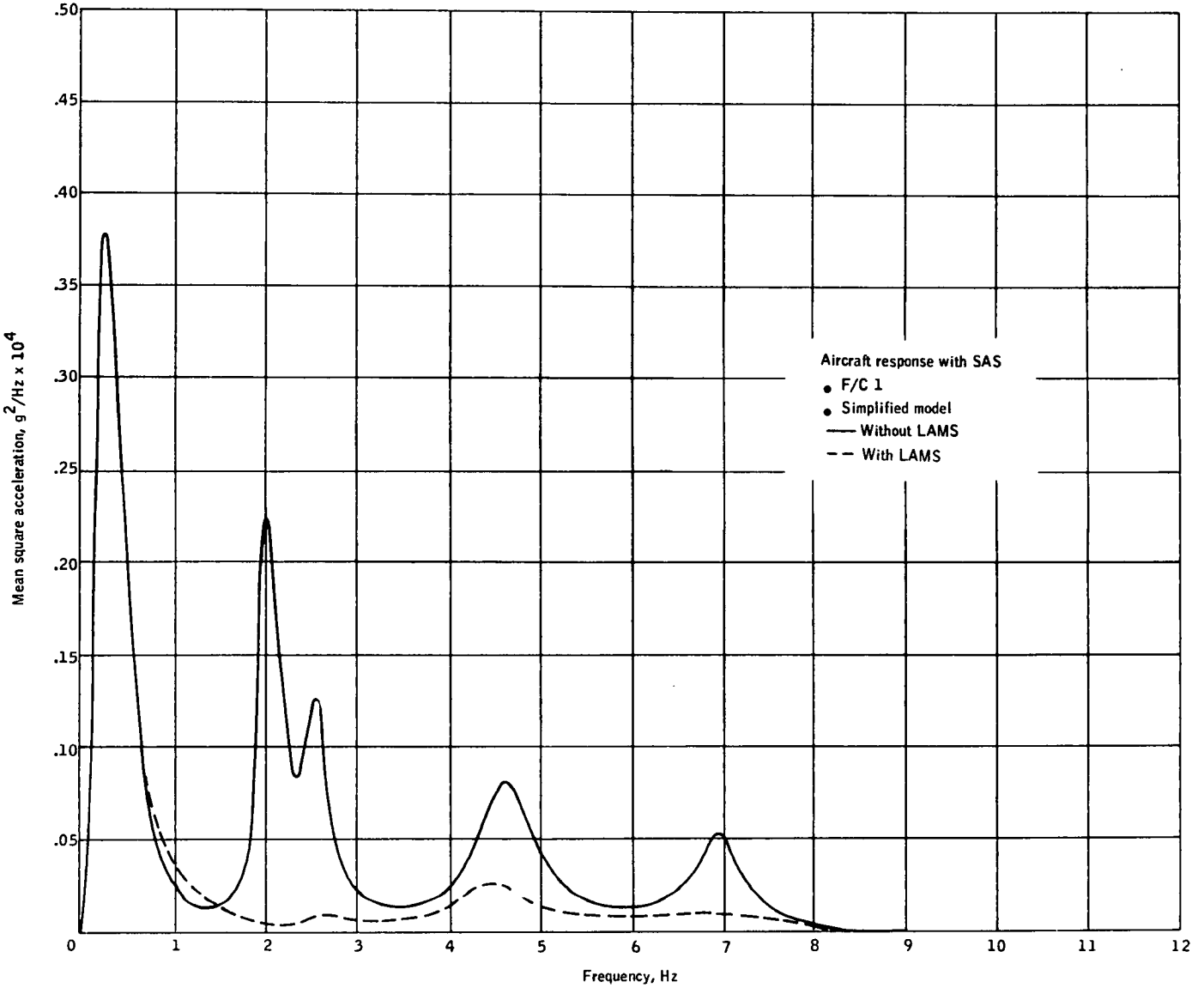

Figure 13. Mean Square Acceleration at FS 248 for a 1-ft/sec Turbulence Input With and Without LAMS System A -- F/C 1

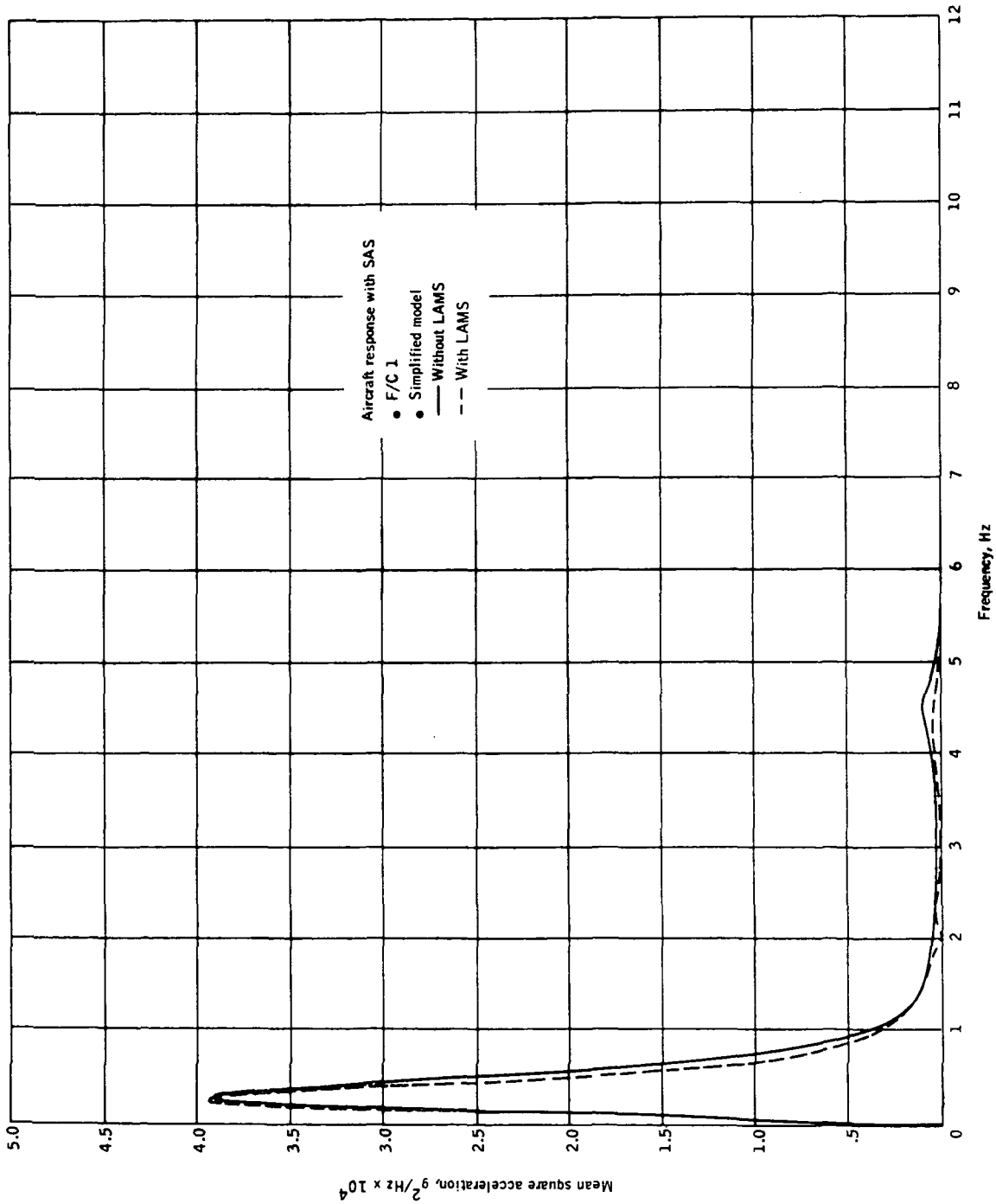

Figure 14. Mean Square Acceleration at FS 738 for a 1-ft/sec Turbulence Input With and Without LAMS System A -- F/C 1

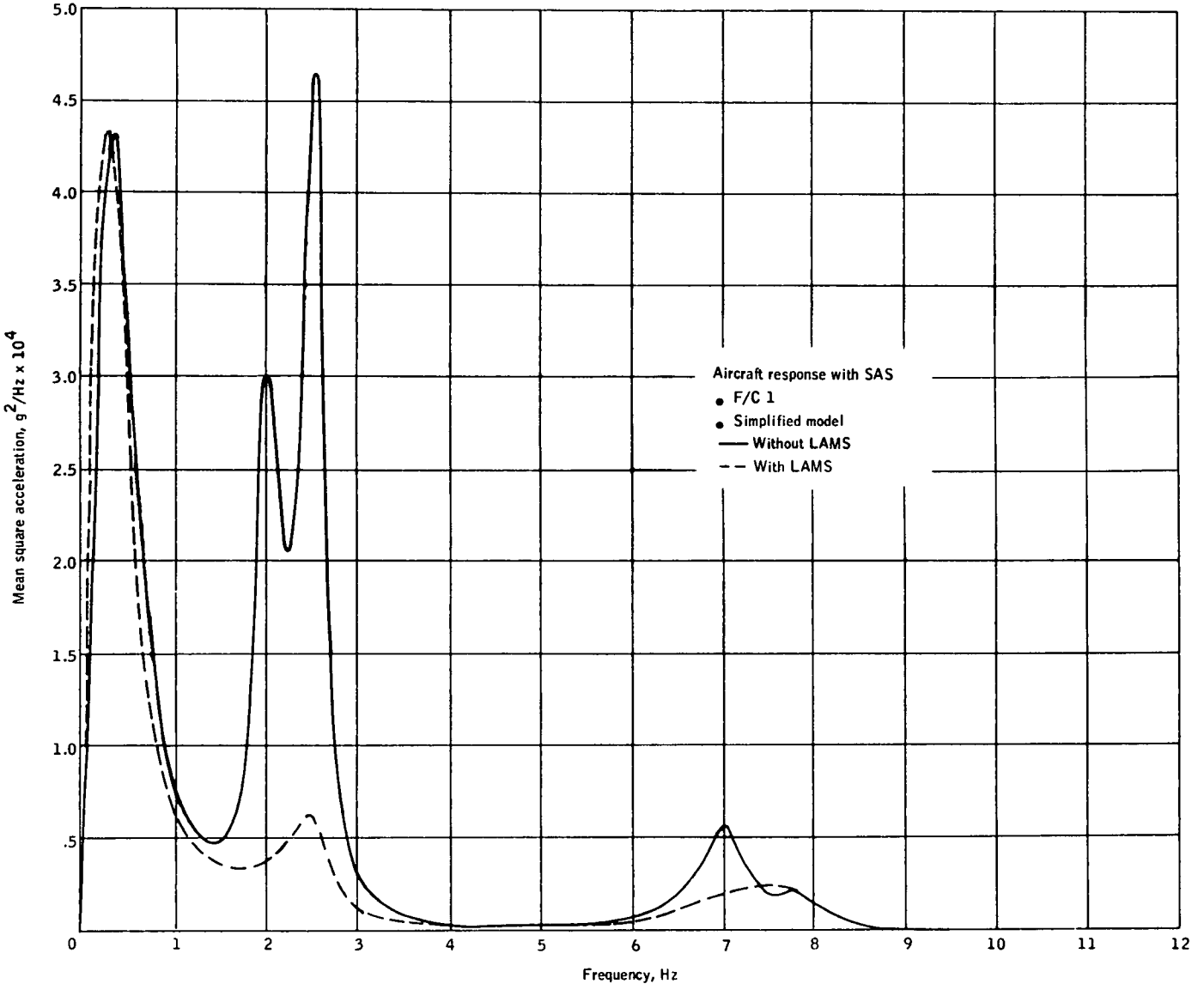

Figure 15. Mean Square Acceleration at FS 1236 for a 1-ft/sec Turbulence Input With and Without LAMS System A -- F/C 1

Table IX shows rms elevon displacements and rates obtained for each of the disturbances inputs. Surface displacements obtained for a turbulence input indicate that only 0.3 deg of inboard elevon and 0.11 deg of outboard elevon rms displacement would be required for a 3σ (12-ft/sec) gust. These values represent only the LAMS system surface displacements. Actual surface displacements would also include the contribution due to the baseline SAS command. Hence, it cannot be readily assessed from these results whether or not hysteresis in the actuator dynamics will seriously degrade the LAMS performance with this system. But since these rms values are indeed small, it is expected that hysteresis may pose a significant problem for turbulence inputs.

TABLE IX. - RMS SURFACE MOTION FOR EACH DISTURBANCE INPUT - SYSTEM A - F/C 1 - SIMPLIFIED MODEL

Disturbance input	RMS inboard elevon		RMS outboard elevon	
	Displacement, rad	Rate, rad/sec	Displacement, rad	Rate rad/sec
1-ft/sec turbulence input	0.473×10^{-3}	Not available	0.973×10^{-4}	0.00243
1 rad input to canards	0.085	Not available	0.00912	0.349
1 rad input to inboard/outboard elevons	0.0275	1.0	0.0078	0.218

The rms surface displacements and rates obtained for the input disturbances applied to the force producers serve only to size the allowable level of input disturbance. The results obtained indicate no problems exist for reasonable rms acceleration levels.

System B - Mass Reaction Only

Table X shows the eigenvalues obtained with the mass-reaction system. These roots indicate the system augmented the lower-frequency fuselage modes (modes 1 and 3) without affecting the primary wing mode (mode 2). This illustrates the ineffectiveness of a nose-mounted force producer for suppressing wing modes.

Table XI shows the stability margins computed at each flight condition with the transformed 18th-order model. The gain of the mass-reaction system was held constant for all three conditions. At F/C 1A the third mode was unstable. This situation was caused by a sign reveral on the force coefficient for this mode. This suggests the mass should be moved forward to improve its tolerance to variations. A second alternative would be to change the sensor configuration.

TABLE X. - COMPARISON OF OPEN- AND CLOSED-LOOP POLES WITH SYSTEM B - F/C 1 - SIMPLIFIED MODEL

Mode	Baseline SAS only		With LAMS	
	Damping ratio	Frequency, rad/sec	Damping ratio	Frequency, rad/sec
Short-period	0.61	3.70	0.74	2.94
1st mode	0.068	12.7	0.46	10.2
2nd mode	0.056	16.2	0.056	16.3
3rd mode	0.076	29.1	0.157	28.0
4th mode	0.042	44.1	0.045	44.0
5th mode	0.043	49.4	0.043	49.4
6th mode	0.029	60.8	0.058	60.2
7th mode	0.032	74.1	0.042	73.7
8th mode	0.029	86.8	0.034	86.7
Actuator	0.5	4.0	0.277	4.47

TABLE XI. - STABILITY MARGINS - SYSTEM B - TRANSFORMED 18TH-ORDER MODEL

Flight Condition	Gain margin, dB	Phase margin, deg
1	9	65
1A	Unstable 3rd mode	Unstable 3rd mode
2	21	55

Table XII shows mode suppression performance for both turbulence and force producer inputs. This performance was computed at the high subsonic, heavyweight condition. Performance was not computed at the supersonic condition. It was felt that the canard performance obtained at the supersonic condition would suffice to show the feasibility of an auxiliary force producer. Figures 16, 17, and 18 show the PSD plots for a turbulence input. These plots show that the mass-reaction system is fairly effective for suppressing the lower-frequency modes. However, the system provides little benefit at frequencies above 6 Hz for a gust input. The mass-reaction system provides little improvement for the wing modes, especially at station 1236.

TABLE XII. - RMS ACCELERATION RESPONSE TO TURBULENCE AND FORCE PRODUCER INPUTS - SYSTEM B - F/C 1 - SIMPLIFIED MODEL

Fuselage station	1-ft/sec turbulence input		1-in. input to mass reaction		1-rad input to inboard/outboard elevons	
	SAS only	LAMS	SAS only	LAMS	SAS only	LAMS
248 (pilot)	0.0211 g	0.0164 g	1.22×10^{-4} g	0.911×10^{-4} g	2.16 g	0.897 g
738	0.0148	0.0146	0.334×10^{-4}	0.220×10^{-4}	0.576	0.397
1236 (aft fuselage)	0.0253	0.0232	0.550×10^{-4}	0.364×10^{-4}	1.96	1.20

Table XIII shows the rms values of mass displacement, rate, acceleration, and force output computed for a turbulence input. These results indicate that a 100-lb weight will require approximately a 1-ft displacement to produce the performance described in the previous paragraphs. If necessary, this displacement can be reduced by a proportionate increase in the weight of the mass.

TABLE XIII. - MASS VARIABLES FOR A TURBULENCE INPUT DISTURBANCE - SYSTEM B - F/C 1 - SIMPLIFIED MODEL

RMS mass variables[a]	Unit turbulence input, 1 ft/sec	3σ turbulence input, 12 ft/sec
Displacement	1.1 in.	13.2 in.
Rate	7.44 in./sec	89.3 in./sec
Acceleration	89.0 in./sec^2	1070 in./sec^2
Force output[a]	23.0 lb	277 lb

[a]Assumes 100-lb weight for the mass.

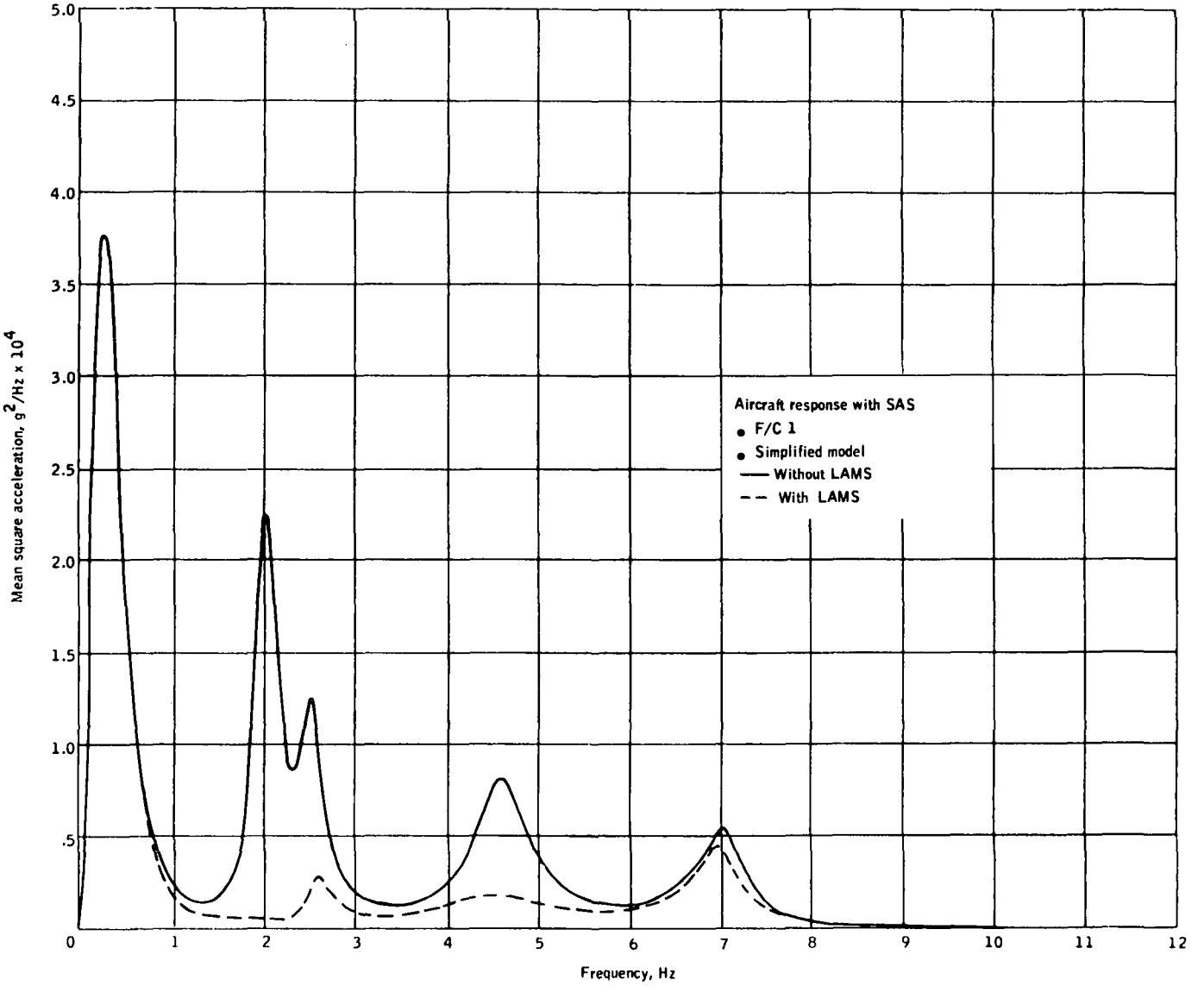

Figure 16. Mean Square Acceleration at FS 248 for a 1-ft/sec Turbulence Input With and Without LAMS System B -- F/C 1

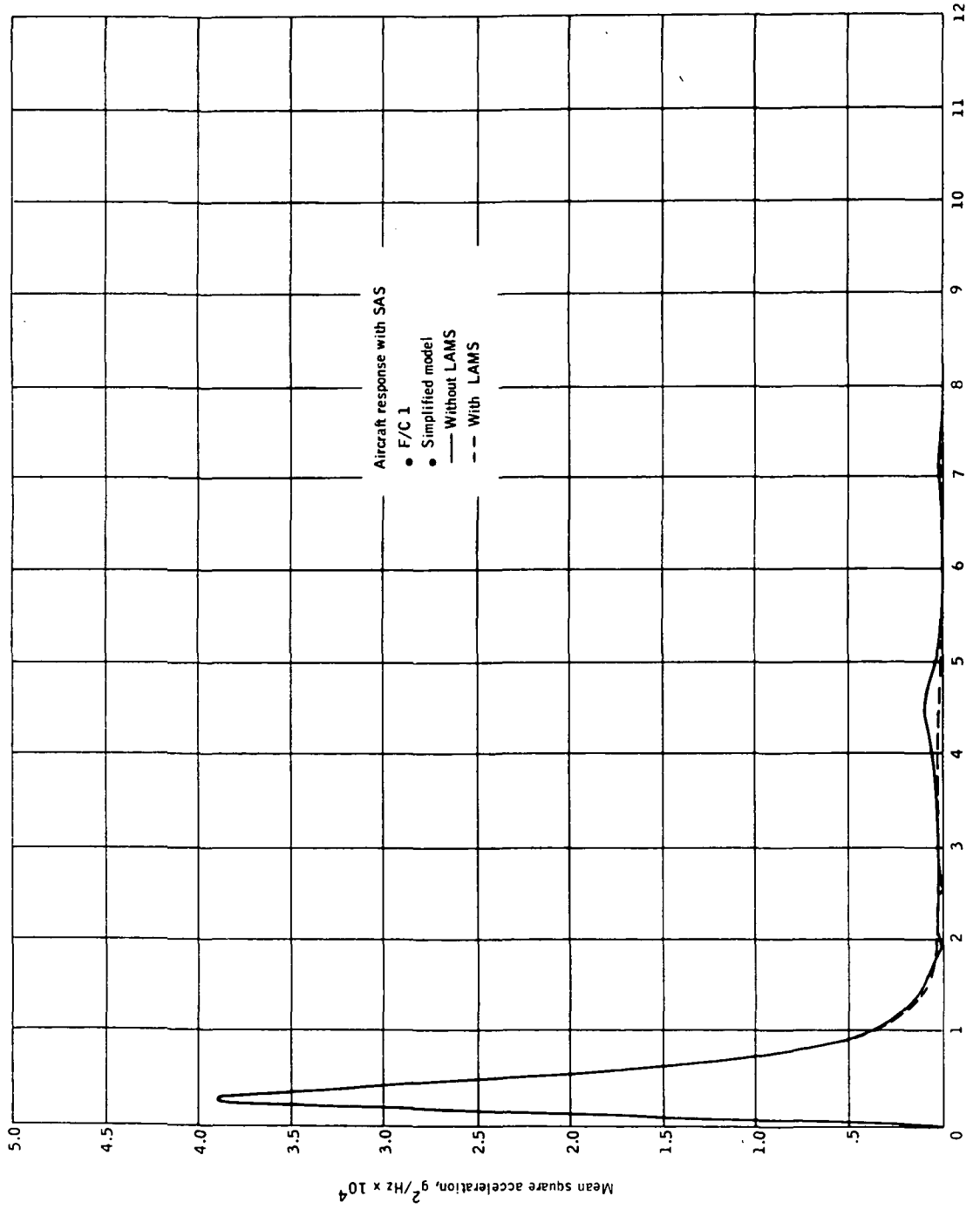

Figure 17. Mean Square Acceleration at FS 738 for a 1-ft/sec Turbulence Input With and Without LAMS System B -- F/C 1

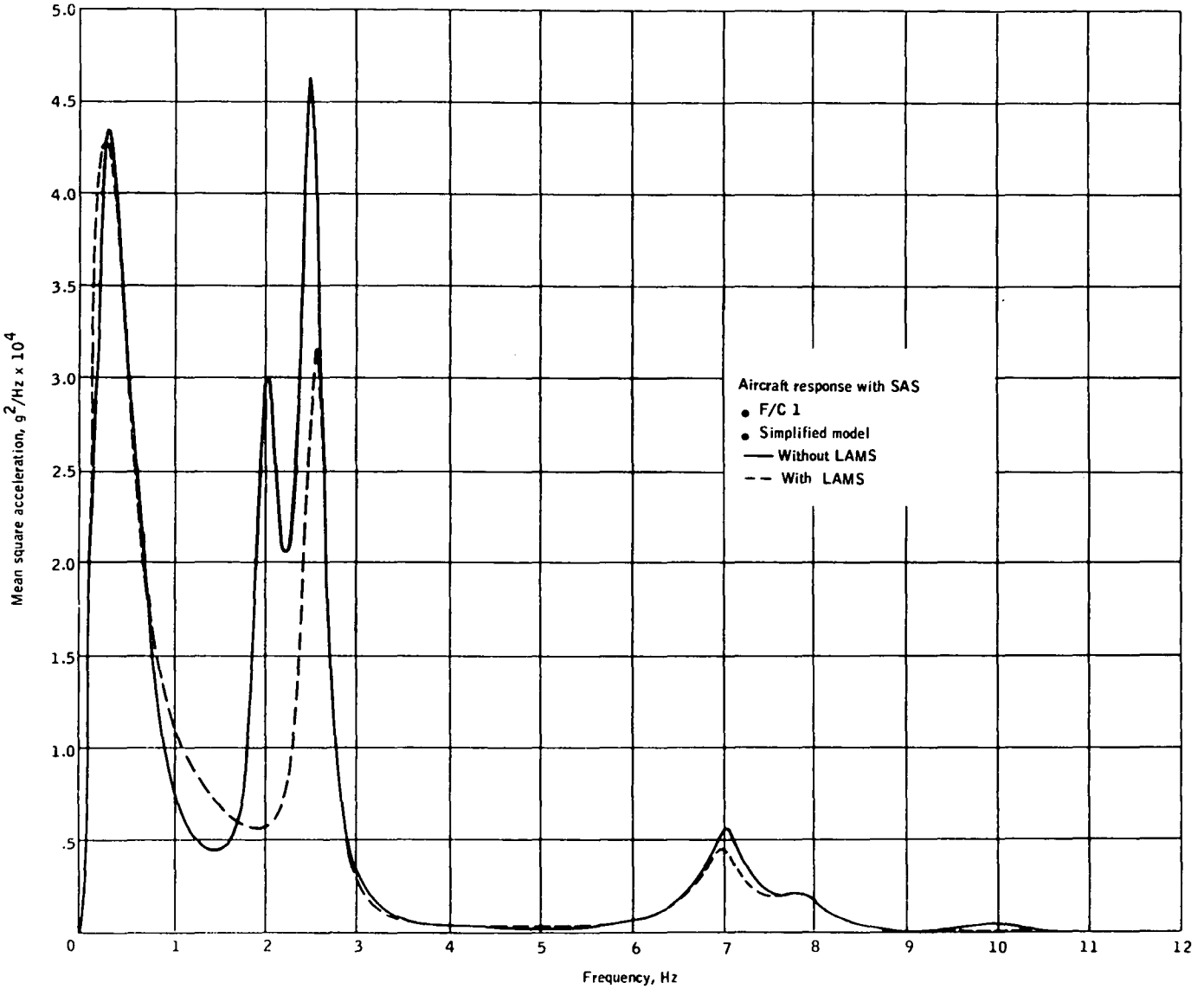

Figure 18. Mean Square Acceleration at FS 1236 for a 1-ft/sec Turbulence Input With and Without LAMS System B -- F/C 1

Table XIII shows that the force output on the nose was 277 lb for a 3σ gust input. This is well within the assumed force constraint of 600 lb.

System C - Mass Reaction Plus Outboard Elevon

The open- and closed-loop roots are compared in Table XIV for the mass-reaction-plus-outboard elevon system. These roots show significant augmentation of the first three structural modes. These results, when compared with the results obtained with the mass-reaction system only, indicate the effectiveness of the outboard elevon system to control the wing modes.

TABLE XIV. - COMPARISON OF OPEN- AND CLOSED-LOOP POLES WITH SYSTEM C - SUBSONIC, HEAVYWEIGHT CONDITION - SIMPLIFIED MODEL

Mode	Baseline SAS only		With LAMS	
	Damping ratio	Frequency, rad/sec	Damping ratio	Frequency, rad/sec
Short-period	0.610	3.70	0.743	2.94
1st mode	0.068	12.7	0.418	10.6
2nd mode	0.056	16.2	0.217	16.4
3rd mode	0.076	29.1	0.203	27.8
4th mode	0.042	44.1	0.083	45.0
5th mode	0.043	49.4	0.096	47.7
6th mode	0.029	60.8	0.059	60.2
7th mode	0.032	74.1	0.042	73.7
8th mode	0.029	86.8	0.034	86.7
Actuator	0.5	4.0	0.267	4.46

Table XV shows the stability margins obtained with this control system for three flight conditions. The results show a stability problem exists with the third mode at F/C 1A. This instability results from closure of the mass-reaction control loop. This same problem was evident with the mass-reaction system only. It should be noted, however, that with both loops closed the system was stable. The outboard elevon loop compensated for the destabilizing effect of the mass-reaction system. The control gains were held constant between conditions 1 and 2, but the outboard elevon gain was increased by a factor of 6 at F/C 2.

TABLE XV. - STABILITY MARGINS - SYSTEM C - TRANSFORMED 18TH-ORDER MODEL

Flight condition	Mass reaction loop closed		Outboard elevon loop closed	
	Gain margin, dB	Phase margin, deg	Gain margin, dB	Phase margin, deg
1	----	88	9	64
1A	Unstable 3rd mode		3	87
2	----	102	10	57

Table XVI shows the rms acceleration performance obtained for both gust and force producer inputs. PSD plots for a turbulence input disturbance are shown in Figures 19. 20, and 21. As expected, this rms acceleration performance is similar to the mass-reaction-only performance. The major differences to be noted are for the improved rms acceleration performance obtained at station 1236. This additional performance is attributed to suppression of the wing modes by the outboard elevon system. Performance of this system was computed for only the high subsonic, heavyweight condition.

TABLE XVI. - RMS ACCELERATION RESPONSE TO TURBULENCE AND FORCE PRODUCER INPUTS - SYSTEM C - F/C 1 - SIMPLIFIED MODEL

Fuselage station	1 ft/sec turbulence input		1-in. input to mass reaction		1-rad input to inboard/ outboard elevons	
	SAS only	LAMS	SAS only	LAMS	SAS only	LAMS
248	0.0211 g	0.0162 g	1.22×10^{-4} g	0.902×10^{-4} g	2.16 g	0.729 g
738	0.0148	0.0147	0.334×10^{-4}	0.217×10^{-4}	0.576	0.338
1236	0.0253	0.0222	0.550×10^{-4}	0.361×10^{-4}	1.96	0.833

Table XVII shows rms values for the mass system variables obtained for a turbulence input. These results show the mass variables were increased by approximately 10 percent with the addition of the outboard elevon. The rms mass displacement of 14.6 in. obtained with a 3σ gust is larger than desired, although the force level remains well below the allowable force of 600 lb. As noted previously, the displacement of the mass can be reduced by increasing the weight of the mass.

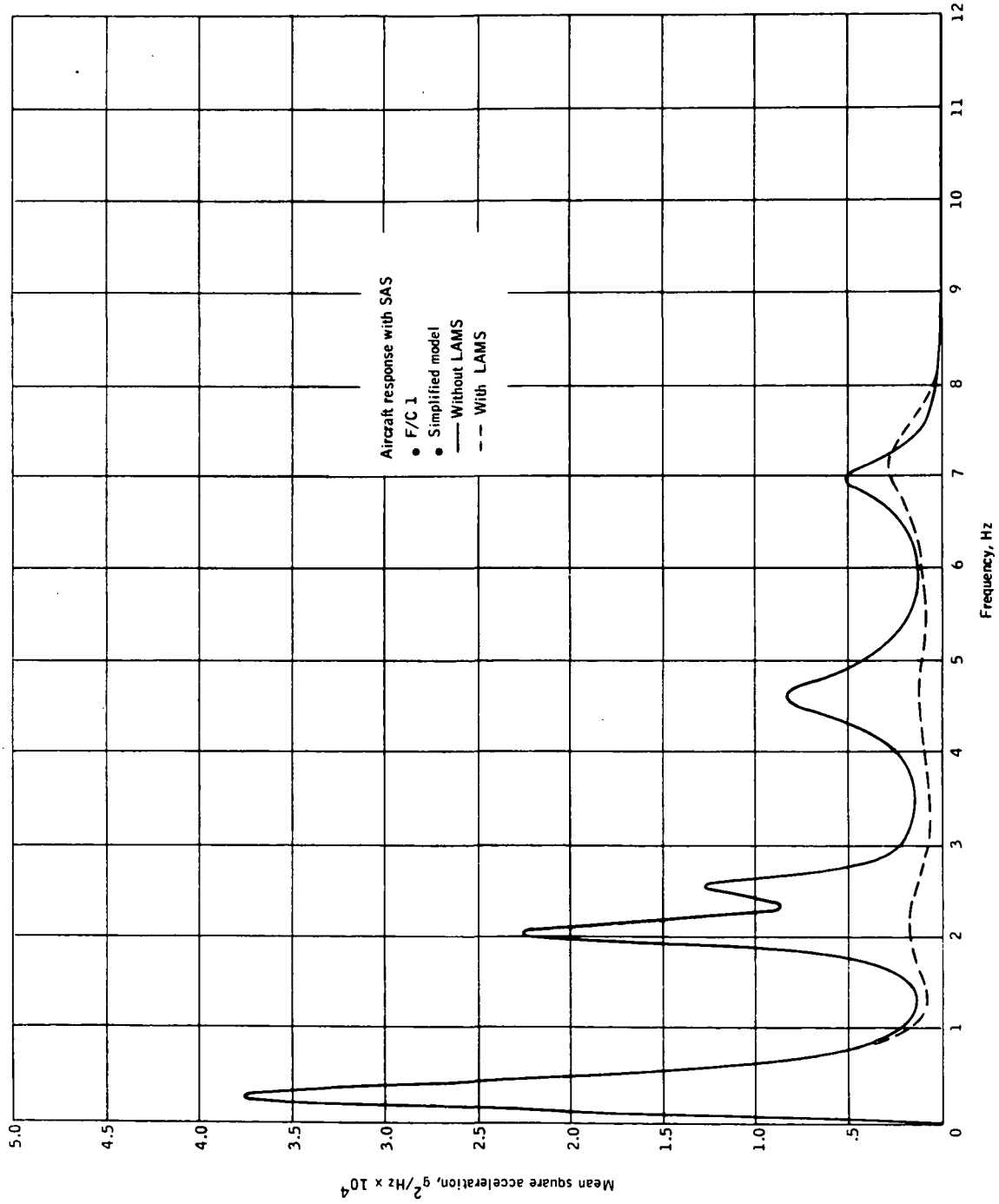

Figure 19. Mean Square Acceleration at FS 248 for a 1-ft/sec Turbulence Input With and Without LAMS System C -- F/C 1

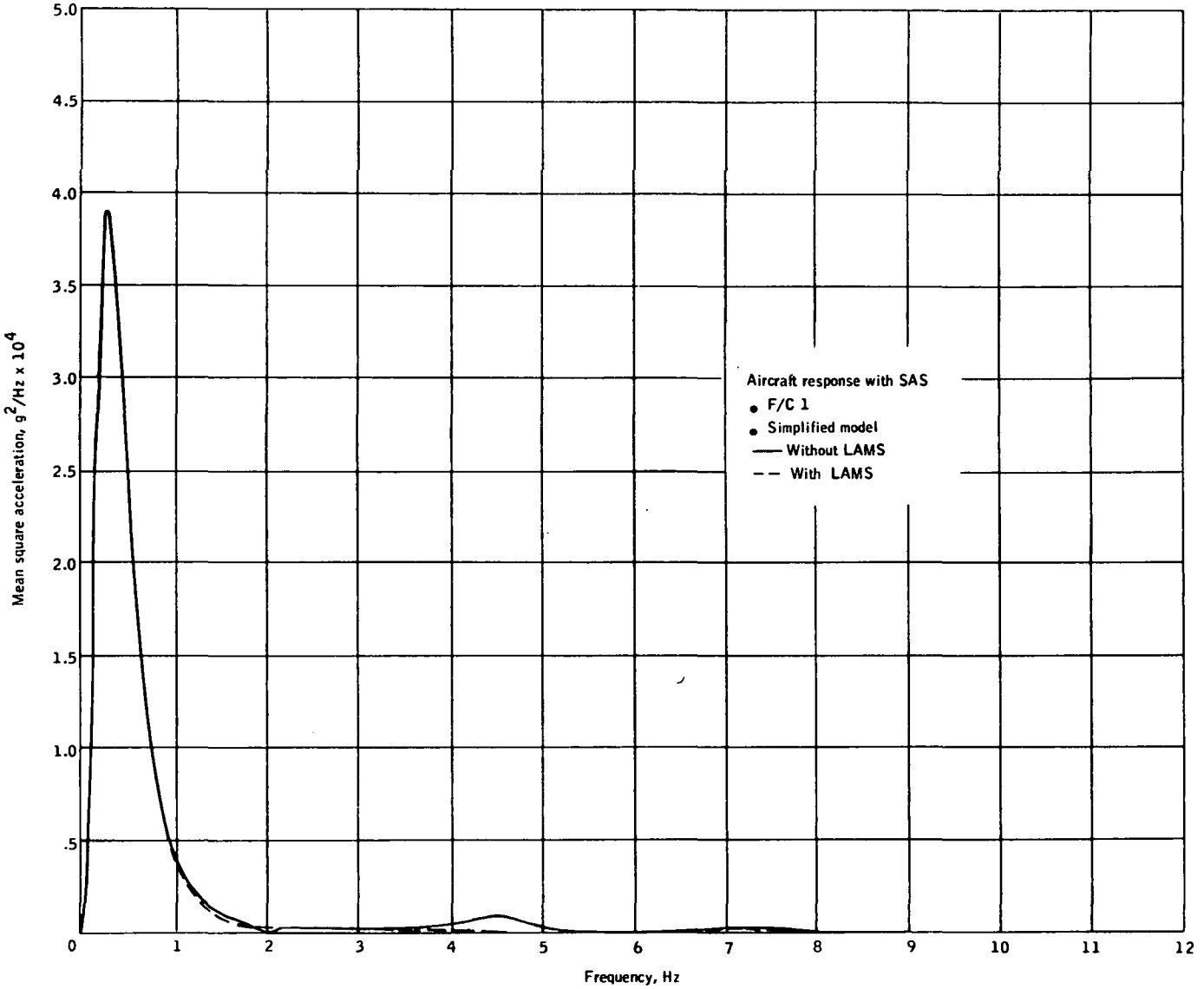

Figure 20. Mean Square Acceleration at FS 738 for a 1-ft/sec Turbulence Input With and Without LAMS System C -- F/C 1

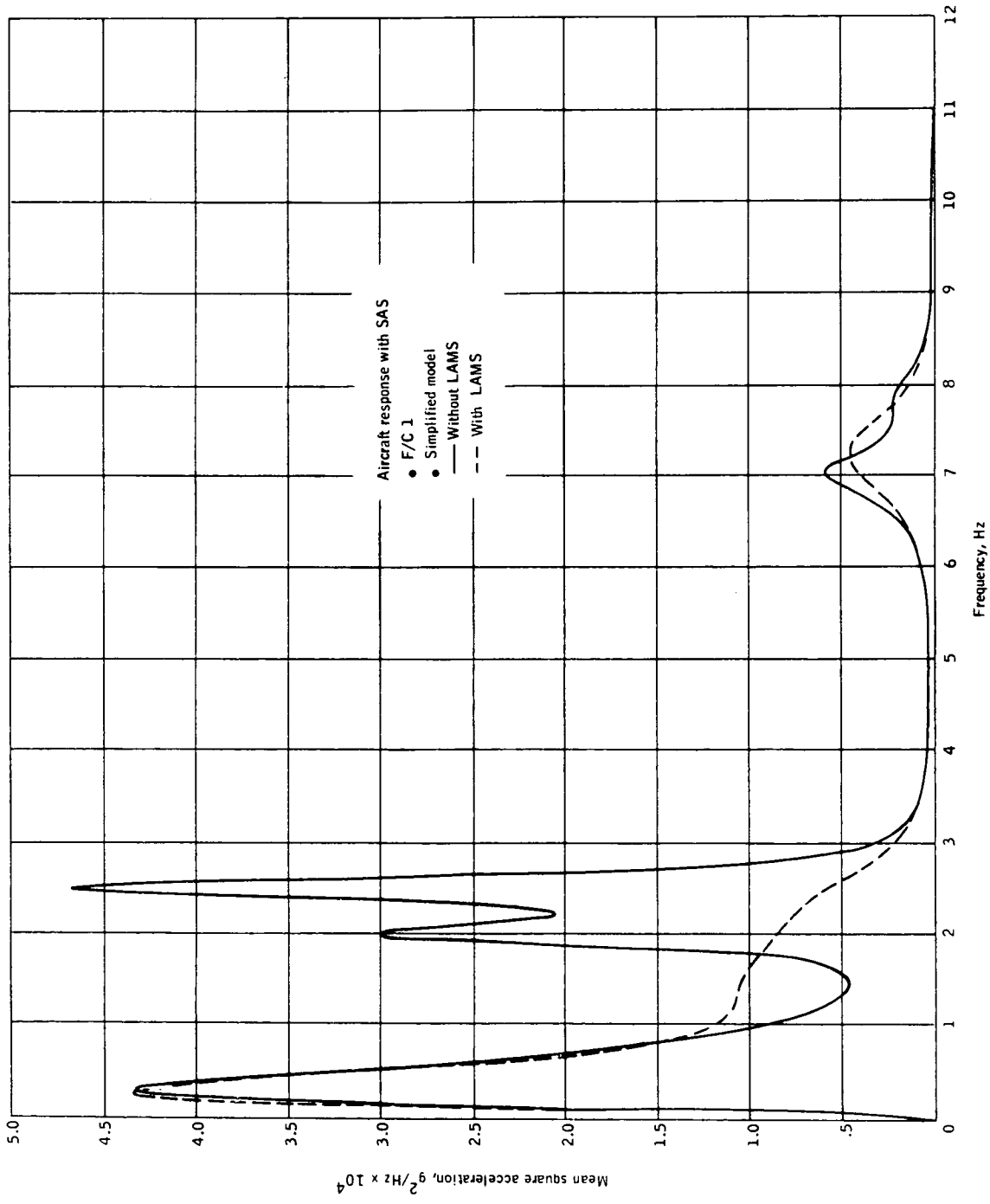

Figure 21. Mean Square Acceleration at FS 1236 for a 1-ft/sec Turbulence Input With and Without LAMS System C -- F/C 1

TABLE XVII. - MASS VARIABLES FOR A TURBULENCE INPUT DISTURBANCE - SYSTEM C - F/C 1 - SIMPLIFIED MODEL

RMS Mass variables[a]	Unit turbulence input, 1 ft/sec	3σ turbulence input, 12 ft/sec
Displacement, in.	1.22	14.6
Rate, in./sec	9.13	110
Acceleration, in./sec^2	102	1220
Force output, lb	26.5	318

[a]Assumes 100-lb weight for the mass.

System D - Canard-Only Controller

Table XVIII shows the eigenvalues obtained with the canard-only controller at F/C 1. Not too surprising is the fact that the damping of the second mode, a wing mode, is not significantly affected. As will be shown, however, its contribution to pilot's acceleration is significantly reduced.

Table XIX shows the stability margins of this system at the two high subsonic, heavyweight flight conditions (1 and 1A) and at the supersonic cruise flight condition (F/C 2). These stability margins were extracted from open-loop frequency responses computed using the transformed 18th-order model. At F/C 2, the control gain in the canard system was increased by a factor of 10 over the one used at F/C 1 (or F/C 1A).

Table XX shows rms acceleration performance obtained at the three fuselage stations for 1-ft/sec turbulence input. These results were computed using the transformed 18th-order vehicle model. The canard-only system is the only one for which performance was computed at the high subsonic, lightweight condition. It is also the only configuration for which performance was computed at all conditions with the transformed 18th-order model. The performance shown in Table XX shows significant reductions in rms acceleration at the pilot's station for all three conditions. A 40-percent reduction was obtained at the subsonic conditions and a 62-percent reduction was obtained at the supersonic condition. This performance is especially significant when the relatively large contribution of the rigid-body mode to rms acceleration is considered. As the subsonic, heavyweight condition the rigid-body mode contributes approximately 60 percent to rms

TABLE XVIII. - COMPARISON OF OPEN- AND CLOSED-LOOP POLES WITH SYSTEM D - F/C 1 - SIMPLIFIED MODEL

Mode	Baseline SAS only		With LAMS	
	Damping ratio	Frequency, rad/sec	Damping ratio	Frequency, rad/sec
Short-period	0.610	3.70	0.59	4.24
1st mode	0.068	12.7	0.202	9.89
2nd mode	0.056	16.2	0.059	16.3
3rd mode	0.076	29.1	0.141	25.9
4th mode	0.042	44.1	0.059	43.2
5th mode	0.043	49.4	0.044	49.4
6th mode	0.029	60.8	0.067	59.8
7th mode	0.032	74.1	0.038	73.9
8th mode	0.029	86.8	0.032	86.7

TABLE XIX. - STABILITY MARGINS - SYSTEM D - TRANSFORMED 18TH-ORDER MODEL

Flight condition	Gain margin, db	Phase margin, deg
1	10	90
1A	----	88
2	10	78

acceleration at the pilot's station. Figures 22 and 23 show the PSD plots of pilot's acceleration at the high subsonic, heavyweight and supersonic cruise conditions.

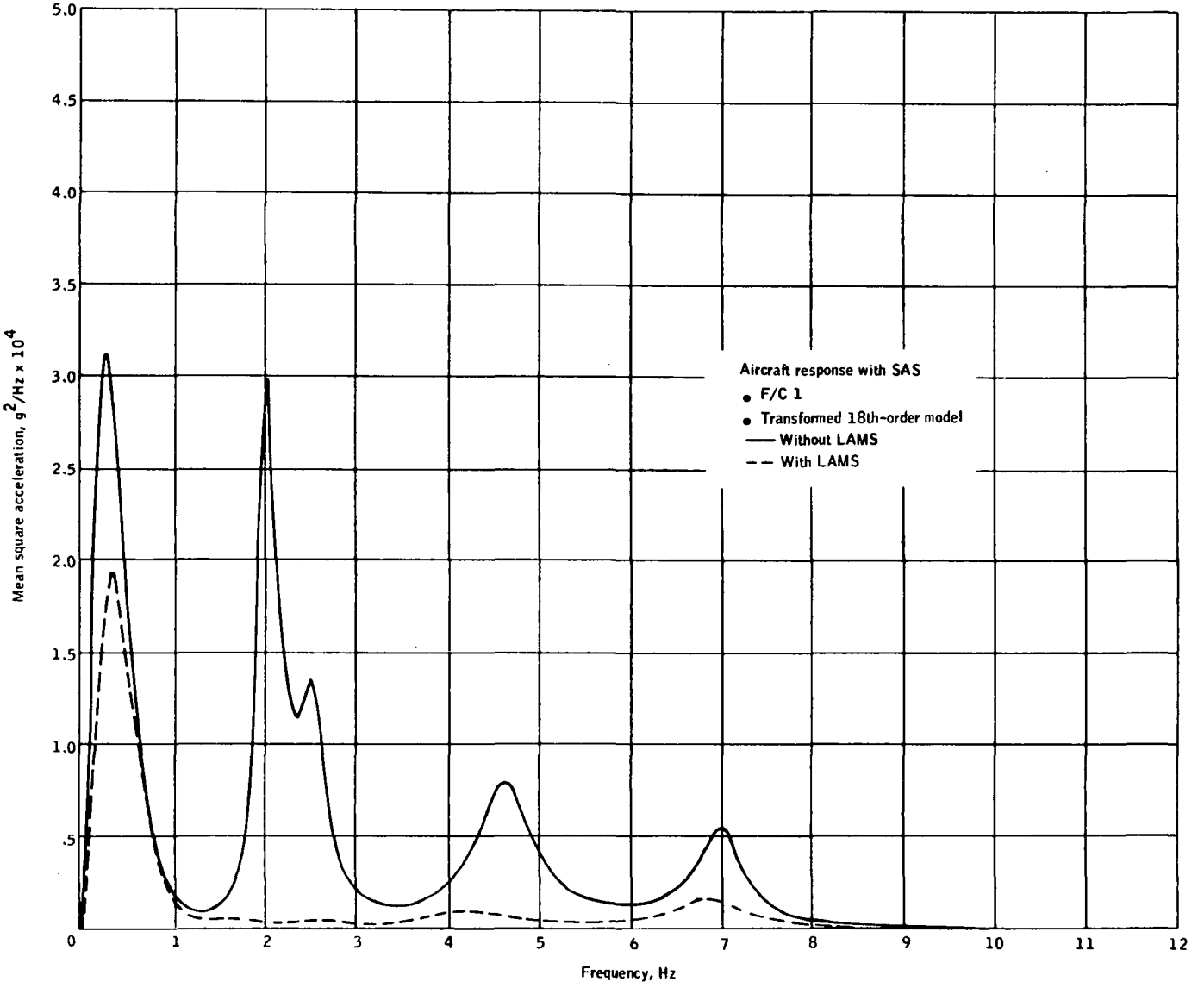

Figure 22. Mean Square Acceleration at FS 248 for a 1-ft/sec Turbulence Input With and Without LAMS System D -- F/C 1

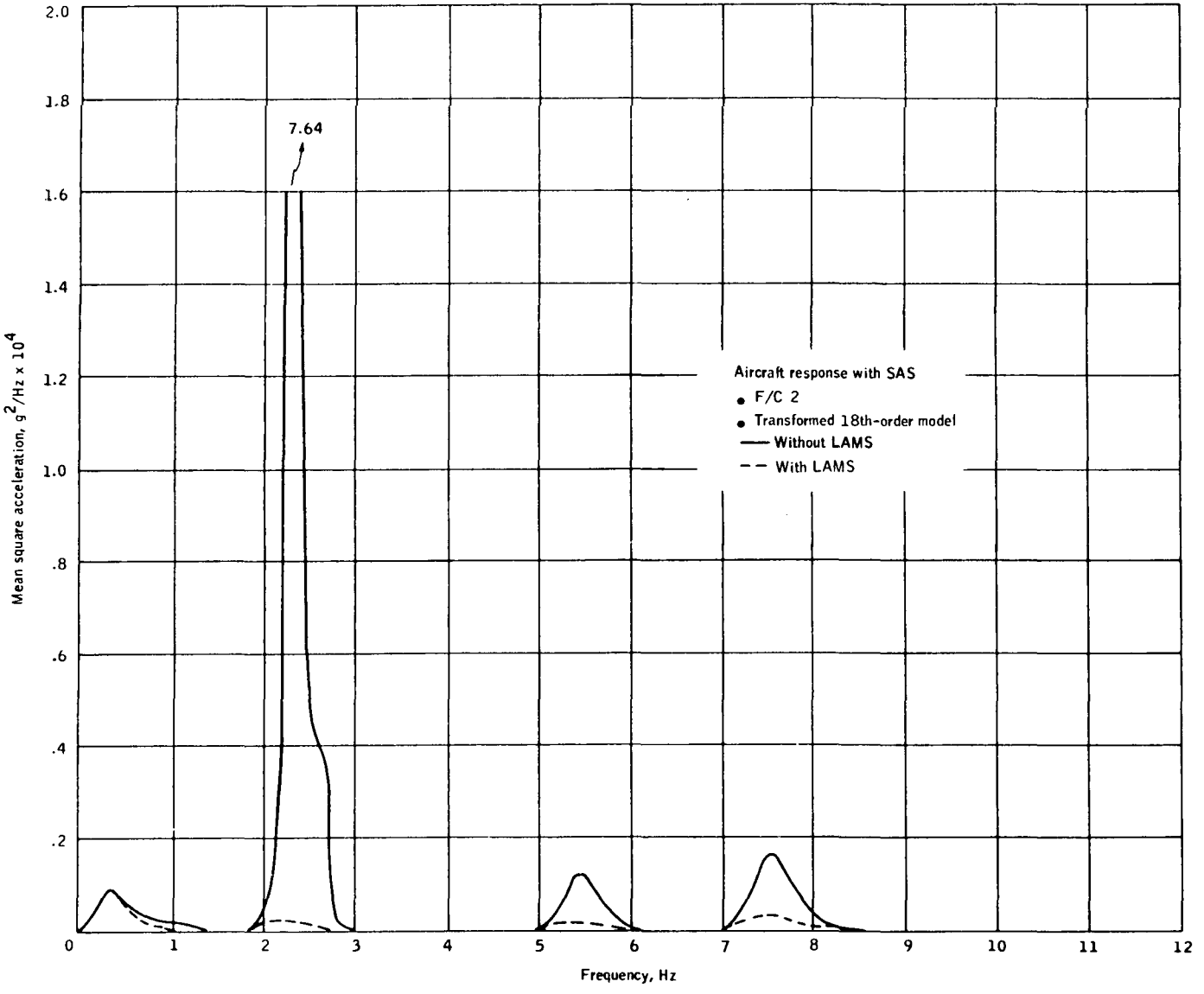

Figure 23. Mean Square Acceleration at FS 248 for a 1-ft/sec Turbulence Input With and Without LAMS System D -- F/C 2

The data in Table XX also show the relative ineffectiveness of the canard in providing mode suppression at the aft end of the fuselage. The inability to provide mode suppression at station 1236 is attributed to two factors. First, it was a design constraint not to provide rigid-body load alleviation with the canard. This constraint was imposed to minimize canard size requirement. Second, because the canard is located on the nose, it is ineffective for controlling wing modes, such as the second structural mode. Figures 24 through 27 show the performance at both stations 738 and 1236 for the high subsonic, heavyweight and the supersonic conditions.

TABLE XX. - MODE SUPPRESSION PERFORMANCE FOR A 1-FT/SEC TURBULENCE INPUT DISTURBANCE - SYSTEM D - TRANSFORMED 18TH-ORDER MODEL

Fuselage station	F/C 1, high subsonic, heavyweight condition		F/C 1A, high subsonic, lightweight condition		F/C 2, supersonic cruise condition	
	SAS only	LAMS	SAS only	LAMS	SAS only	LAMS
248 (pilot)	0.0212 g	0.0124 g	0.0275 g	0.0166 g	0.0111 g	0.0042 g
738	0.0147	0.0127	0.0217	0.0104	0.0055	0.0035
1236 (aft fuselage)	0.0268	0.0247	0.0403	0.0394	0.0100	0.0074

The mode suppression performance described in the preceding paragraphs definitely shows the feasibility of demonstrating mode suppression techniques on the YF-12A aircraft. The canard is shown to be effective for mode suppression at the pilot's station, although it is relatively ineffective at the aft end of the fuselage. However, mode suppression at the aft fuselage station can be obtained through the use of inboard and outboard elevons.

Tables XXI and XXII show the rms accelerations obtained with the canard-only system for various force producer input disturbances. At the supersonic condition the input disturbance was introduced into the inboard elevon series servo to effect displacement of both the inboard and outboard elevons. Performance is comparable at the two flight conditions. Reduction in rms acceleration ranges from 73 percent at the pilot's station for supersonic cruise to 25 percent reduction at station 1236 for the subsonic condition.

RMS canard surface displacements and rates were computed at the subsonic, heavyweight condition for both gust and force producer disturbance inputs. Table XXIII shows the computed rms canard displacements and rates for a canard having a total area of 3.6 sq. ft. The canard was sized using aerodynamic data derived from the USAF DATCOM Handbook and is similar in size to the XB-70 vanes (ref. 3).

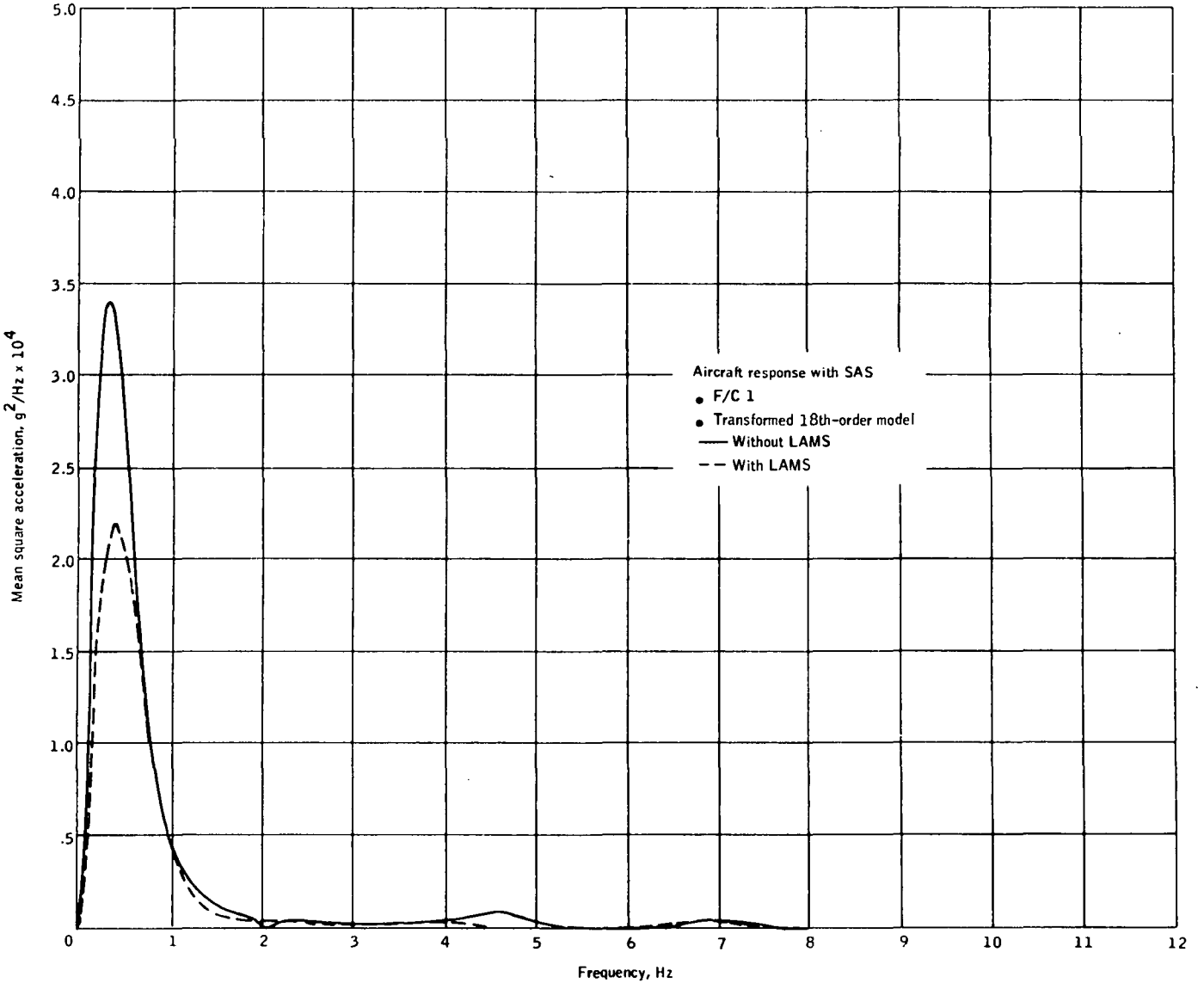

Figure 24. Mean Square Acceleration at FS 738 for a 1-ft/sec Turbulence Input With and Without LAMS System D -- F/C 1

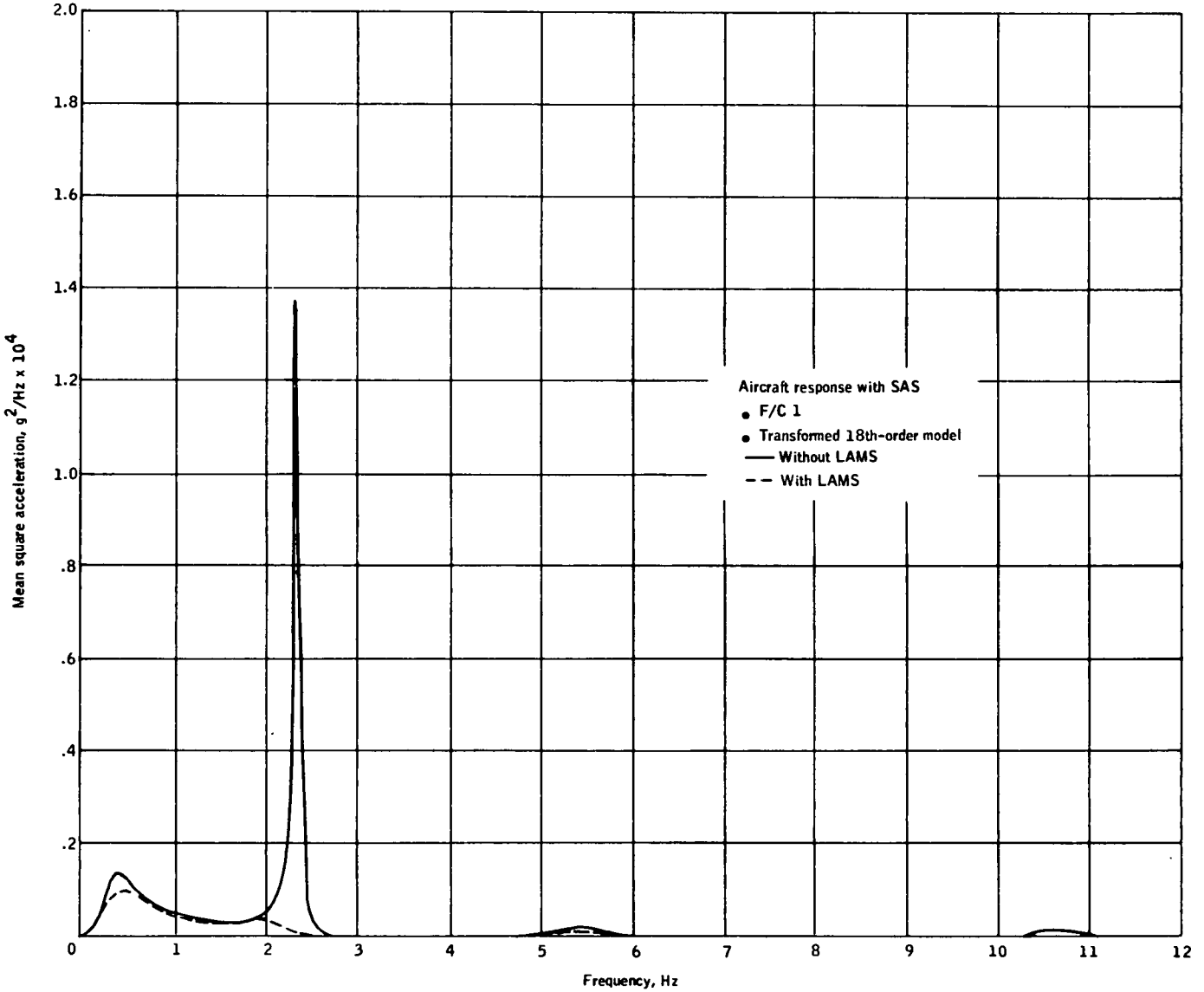

Figure 25. Mean Square Acceleration at FS 738 for a 1-ft/sec Turbulence Input With and Without LAMS System D -- F/C 2

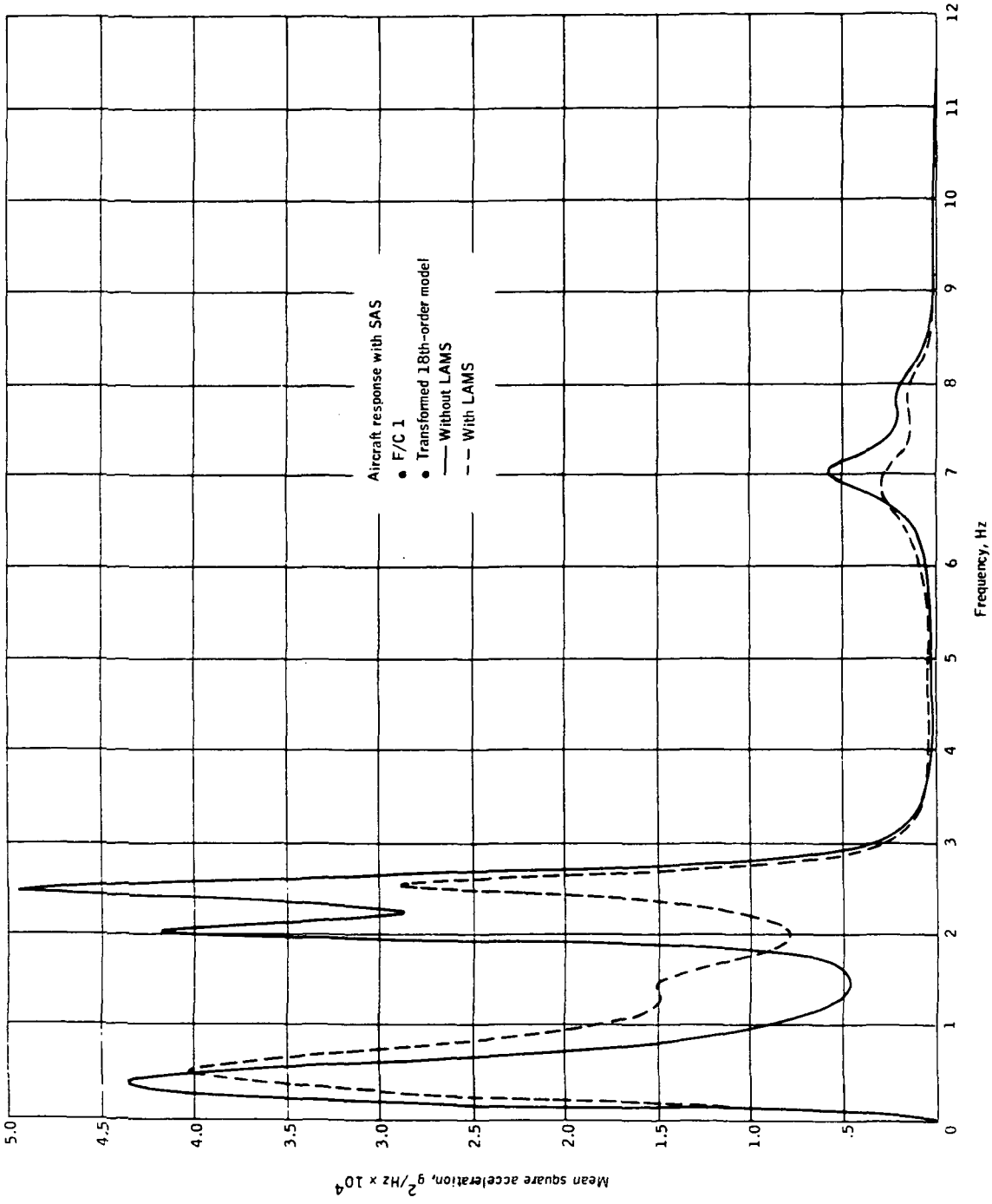

Figure 26. Mean Square Acceleration at FS 1236 for a 1-ft/sec Turbulence Input With and Without LAMS System D -- F/C 1

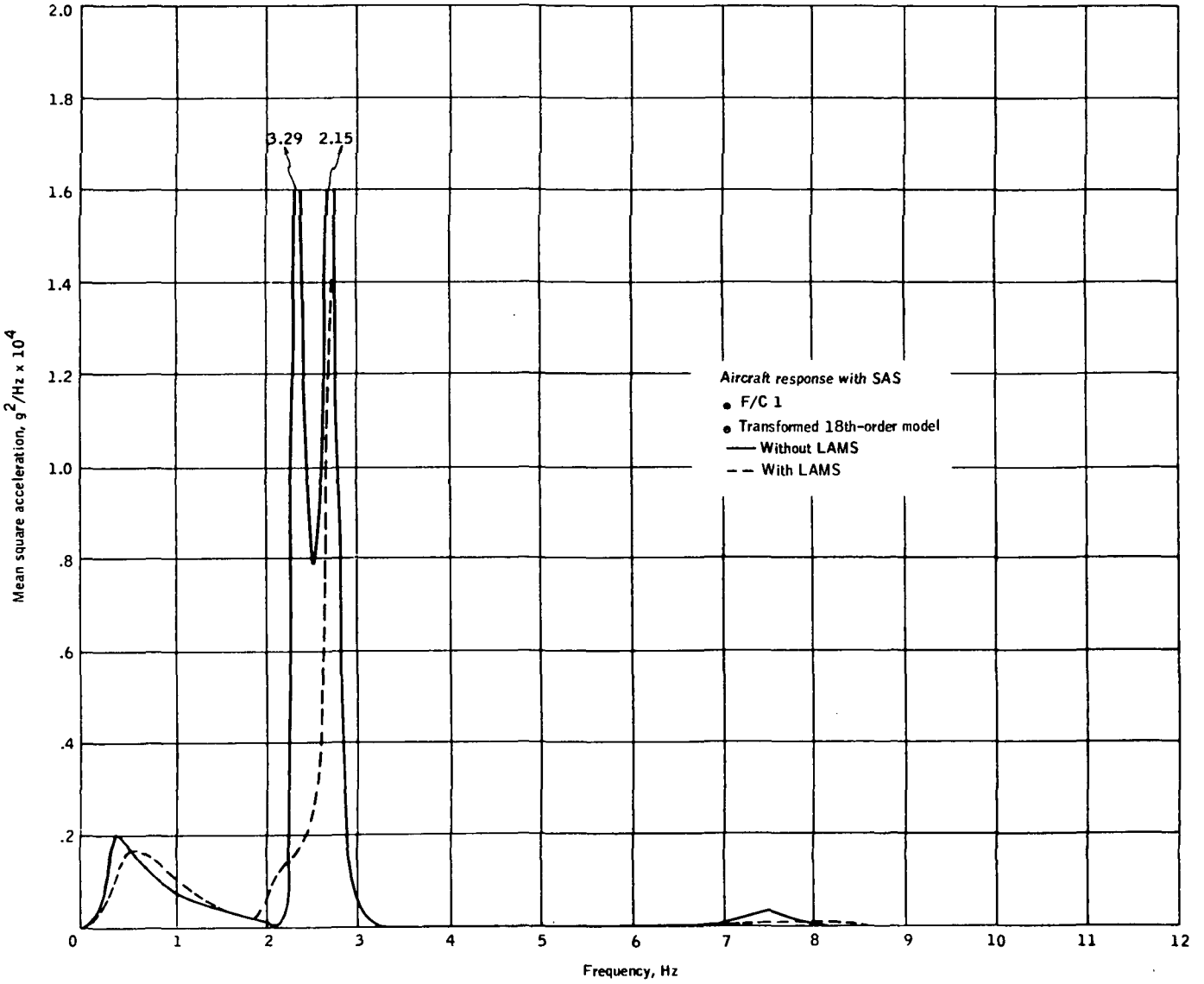

Figure 27. Mean Square Acceleration at FS 1236 for a 1-ft/sec Turbulence Input With and Without LAMS System D -- F/C 2

TABLE XXI. - RMS ACCELERATION RESPONSE TO A 1-RAD FORCE PRODUCER INPUT DISTURBANCE - SYSTEM D - F/C 1 - TRANSFORMED 18TH-ORDER MODEL

Fuselage station	Input to canards		Input to inboard elevons		Input to outboard elevons	
	SAS only	LAMS	SAS only	LAMS	SAS only	LAMS
248 (pilot)	6.52g	4.45g	1.27g	0.430g	1.39g	0.427g
738	1.79	0.967	0.338	0.227	0.355	0.258
1236 (aft fuselage)	2.91	1.53	1.06	0.791	1.47	1.07

TABLE XXII. - RMS ACCELERATION RESPONSE TO A 1-RAD FORCE PRODUCER INPUT DISTURBANCE - SYSTEM D - F/C 2 - TRANSFORMED 18TH-ORDER MODEL

Fuselage station	Input to canards		Input to inboard/ outboard elevons	
	SAS only	LAMS	SAS only	LAMS
248	0.621g	0.391g	0.526g	0.143g
738	0.220	0.111	0.222	0.108
1236	0.300	0.148	0.376	0.237

Based on the data in Table XXIII a 3σ gust (12-ft/sec) will result in a 3σ rms canard deflection of 6.5 deg and a surface rate of 199 deg/sec. The total force produced by the canard in this gust environment is 985 lb. This force level exceeds the design goal of 600 lb. Whether or not this force level is acceptable can only be determined by an internal loads analysis.

The maximum allowable forces determine the maximum magnitude of the test input allowed through a force producer. Inboard and outboard elevon test inputs were sized to produce the same rms acceleration at station 248 as a 3σ gust input. The equivalent test input for the inboard elevon was computed to be 11.5 deg and for the outboard elevon, 10.5 deg.

TABLE XXIII. - RMS CANARD SURFACE DISPLACEMENT AND RATES FOR GIVEN DISTURBANCE INPUTS - SYSTEM D - F/C 1 - TRANSFORMED 18TH-ORDER MODEL

Disturbance input	Canard surface displacement, deg	Canard surface rate, deg/sec
1-ft/sec turbulence input	0.63	8.33
1-rad input to inboard elevons	32.0	540.0
1-rad input to outboard elevons	27.4	535.0
1-rad input to canards	1.93	Not available

System E - Canard Plus Outboard Elevons

Table XXIV compares roots of the canard-only system and the canard-plus-outboard elevon system. This comparison shows an improvement primarily in the damping of the second and fifth modes.

Table XXV shows the stability margins obtained with the transformed 18th-order model at the three flight conditions. At F/C 2 the stability was computed with the canard loop gain increased by a factor of 10 and the outboard elevon loop gain increased by a factor of 6.

Table XXVI shows mode suppression performance obtained with this system for a turbulence input. The corresponding PSD plots are shown in Figures 28 through 33. These rms acceleration levels indicate mode suppression performance essentially identical with that obtained using the canard alone. The difference between the two systems shows up at station 1236, especially at the supersonic condition. The improved mode suppression can be seen better by comparing PSD plots (see Figures 27 and 33). The reduction in rms acceleration at station 1236 is 43 percent versus 26 percent obtained with canard alone. It is expected that an outboard elevon system designed especially for use with a canard controller would yield further improvements.

The reduction in rms acceleration for a 1-rad white noise input applied to a force producer actuator is shown in Tables XXVII and XXVIII. These data show similar trends in performance as did the turbulence input responses. The only indicated improvements in rms accelerations over the canard-only system are at the aft fuselage station (i.e., 1236). This is especially evident at the supersonic condition, where an additional 35-percent reduction in rms acceleration was obtained.

TABLE XXIV. - COMPARISON OF ROOTS OBTAINED WITH SYSTEM E - F/C 1 - SIMPLIFIED MODEL

Mode	Canard only		Canard plus outboard elevon	
	Damping ratio	Frequency, rad/sec	Damping ratio	Frequency, rad/sec
Short-period	0.59	4.24	0.59	4.24
1st mode	0.202	9.89	0.196	9.96
2nd mode	0.059	16.3	0.132	16.1
3rd mode	0.141	25.9	0.157	25.7
4th mode	0.059	43.2	0.077	43.3
5th mode	0.044	49.4	0.070	49.1
6th mode	0.067	59.8	0.068	59.8
7th mode	0.038	73.9	0.038	73.9
8th mode	0.032	86.7	0.033	86.7

TABLE XXV. - STABILITY MARGINS - SYSTEM E - TRANSFORMED 18TH-ORDER MODEL

Flight condition	Canard loop closed		Outboard elevon loop closed	
	Gain margin	Phase margin, deg	Gain margin, dB	Gain margin, deg
1	----	52	18	90
1A	----	----	----	90
2	----	120	11	72

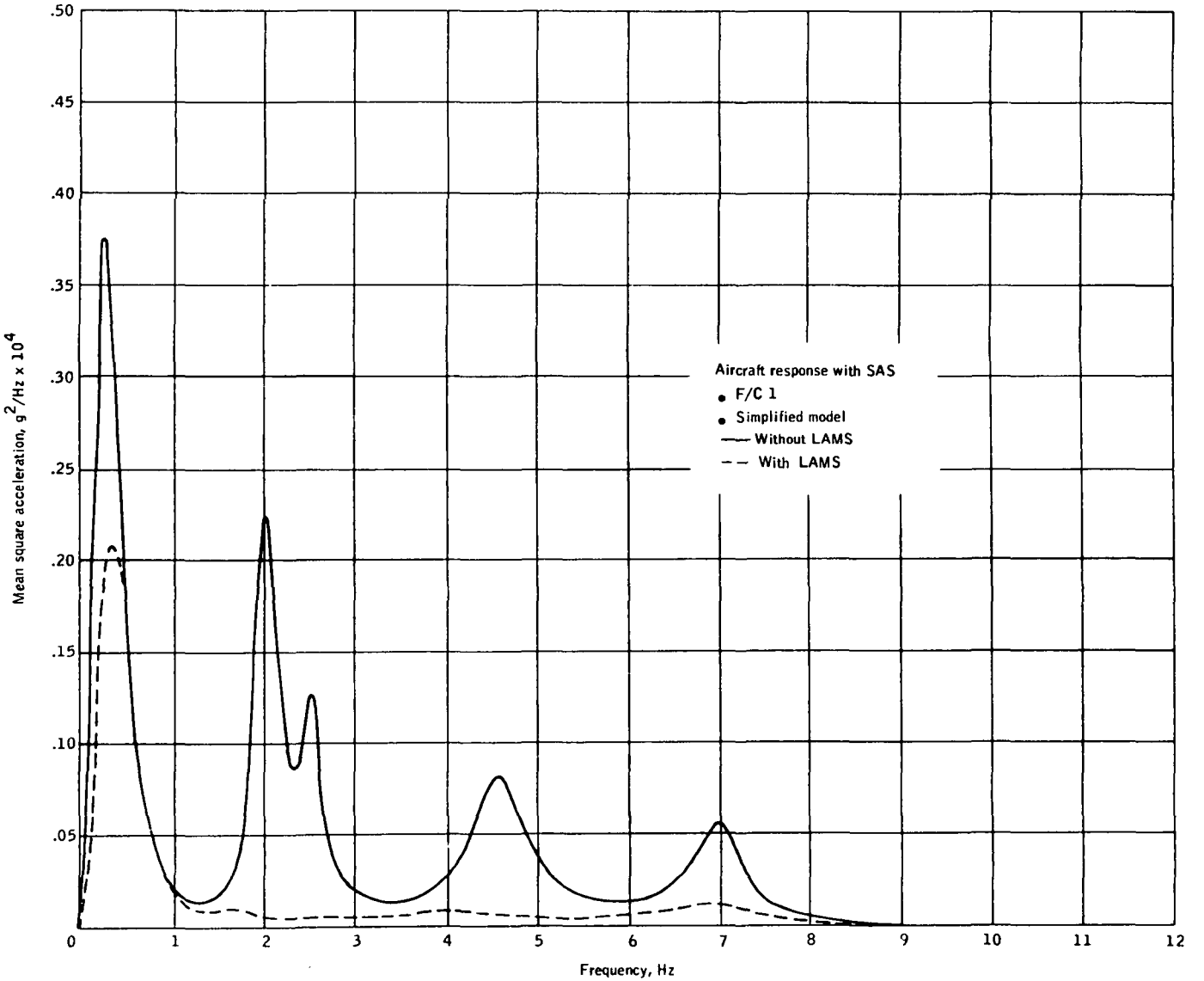

Figure 28. Mean Square Acceleration at FS 248 for a 1-ft/sec Turbulence Input With and Without LAMS System E -- F/C 1

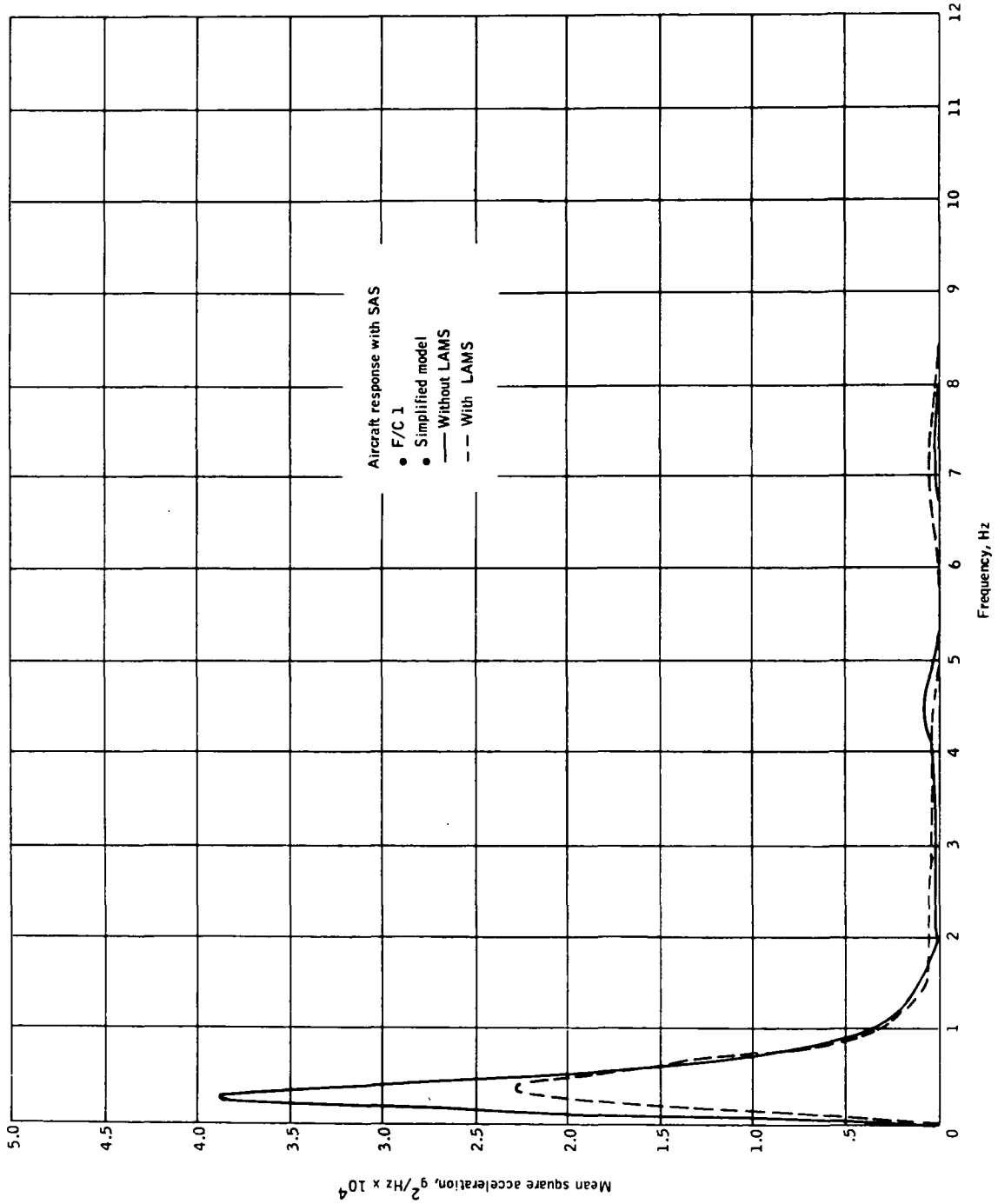

Figure 29. Mean Square Acceleration at FS 738 for a 1-ft/sec Turbulence Input With and Without LAMS System E -- F/C 1

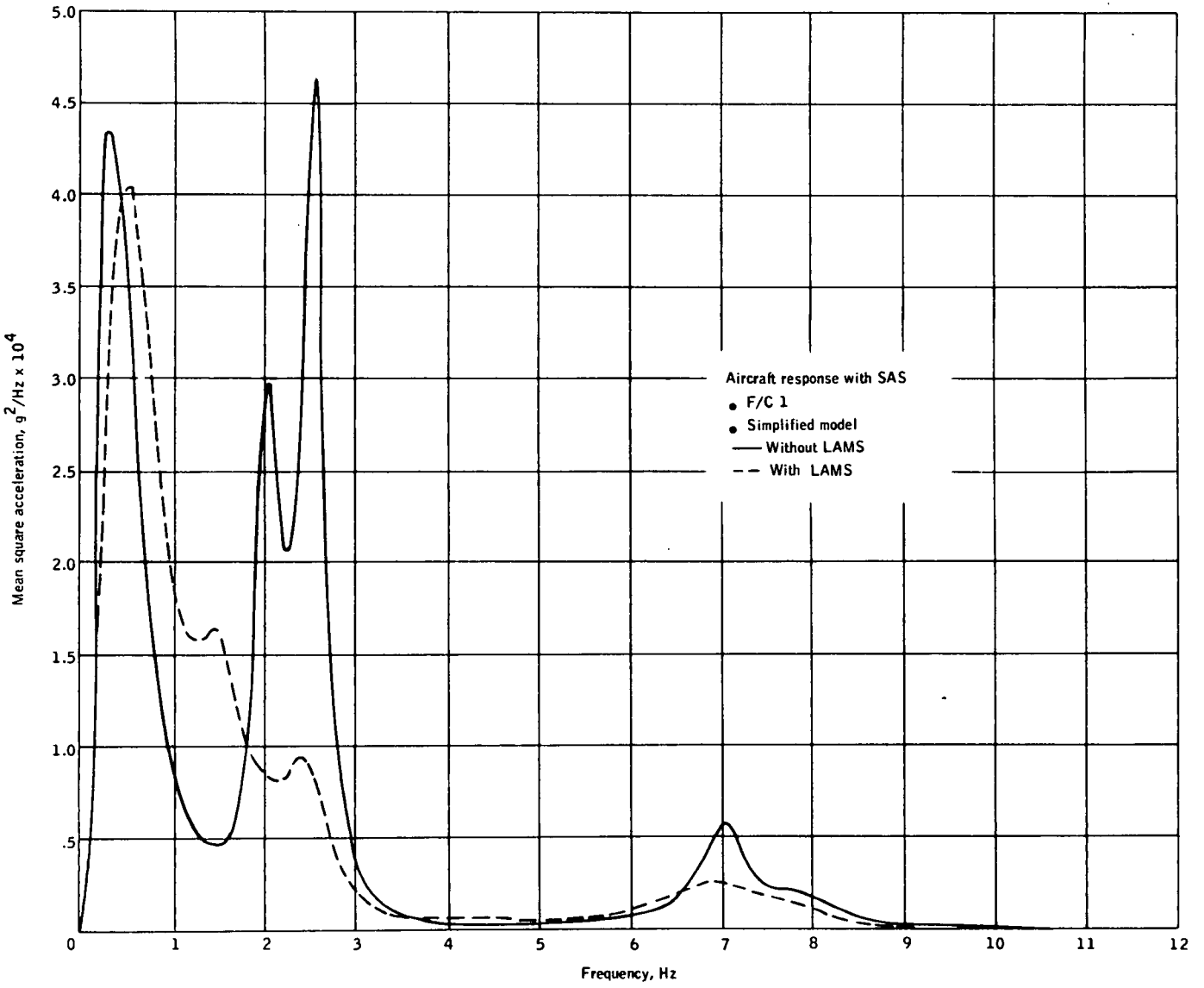

Figure 30. Mean Square Acceleration at FS 1236 for a 1-ft/sec Turbulence Input With and Without LAMS System E -- F/C 1

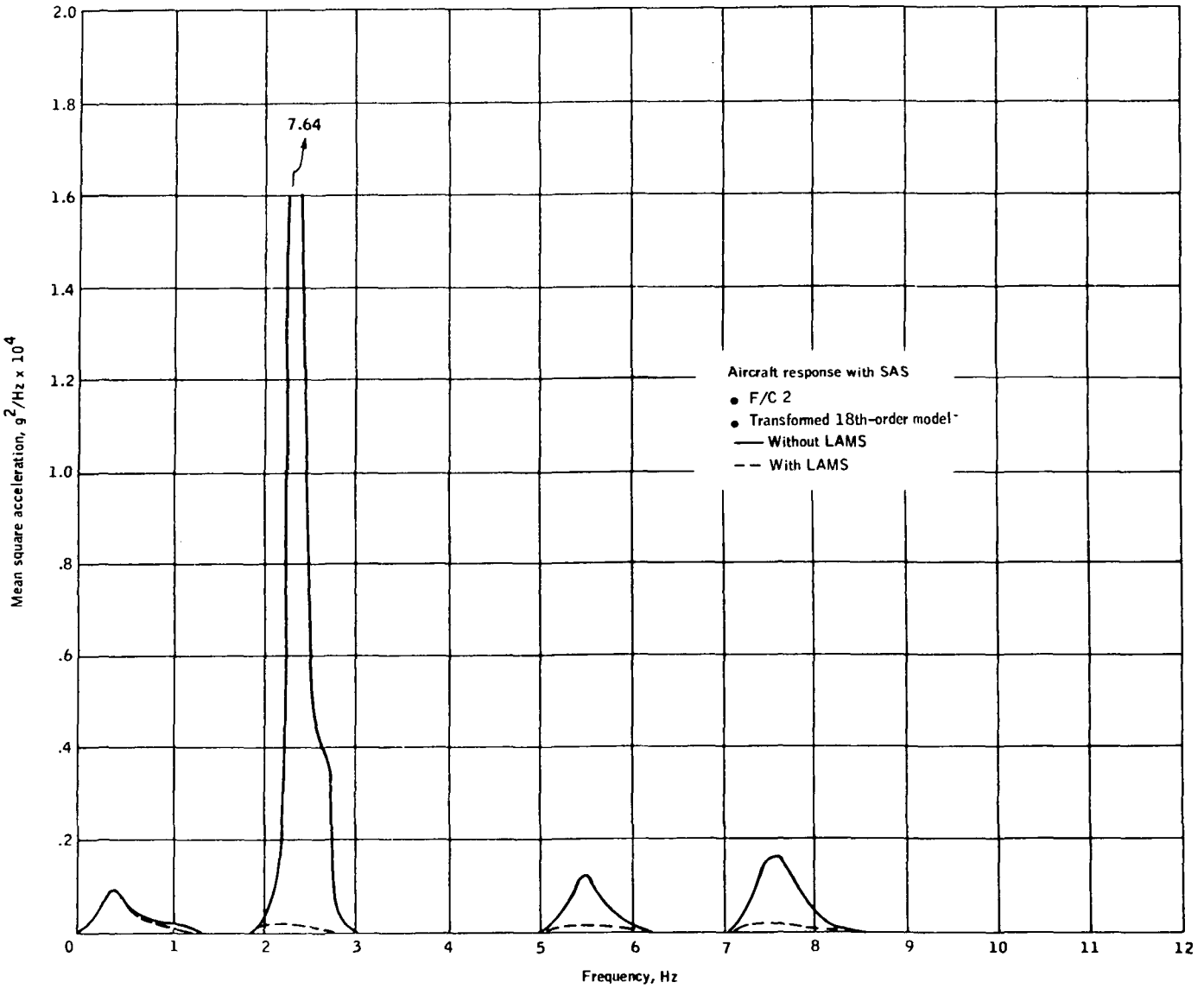

Figure 31. Mean Square Acceleration at FS 248 for a 1-ft/sec Turbulence Input With and Without LAMS System E -- F/C 2

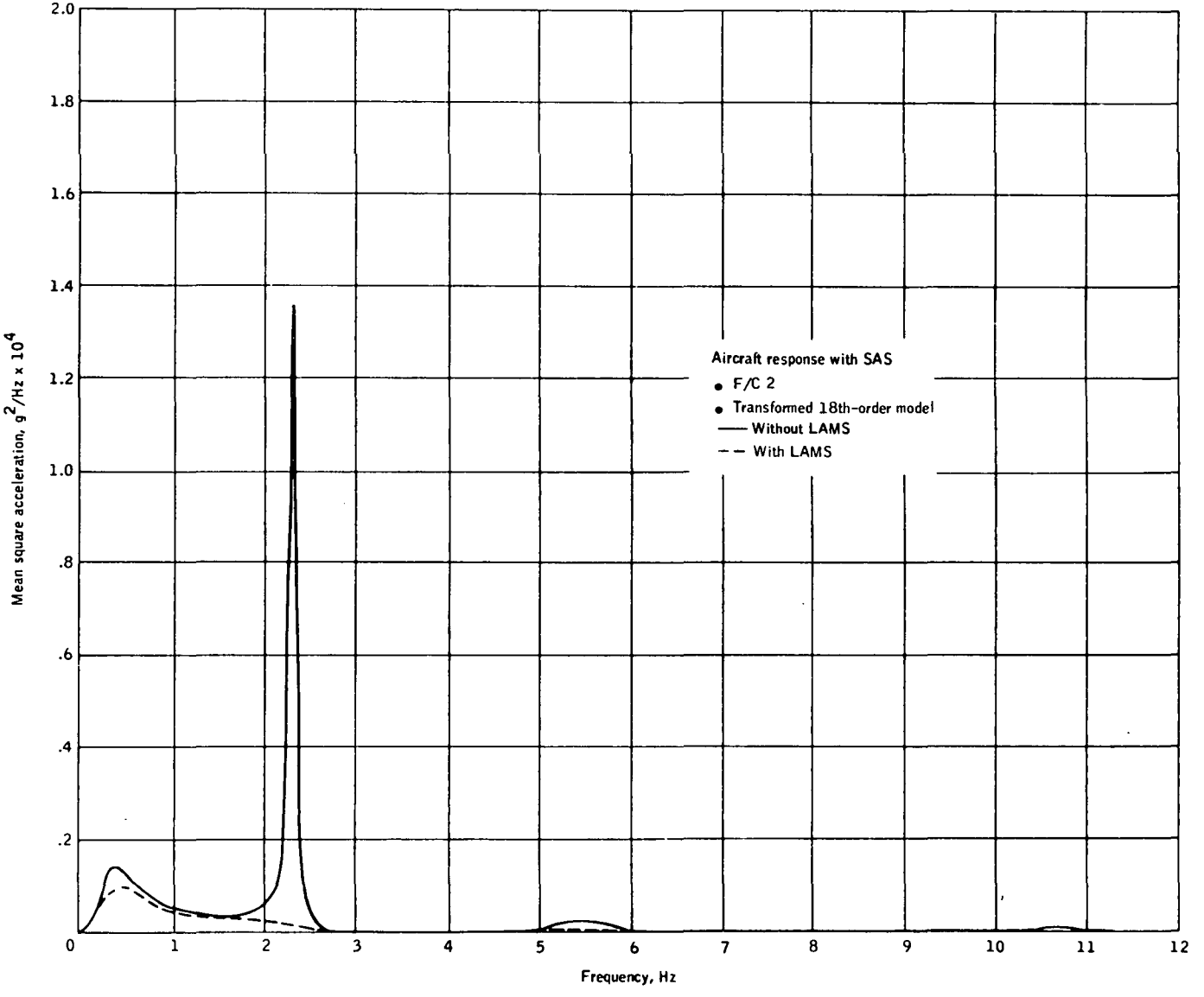

Figure 32. Mean Square Acceleration at FS 738 for a 1-ft/sec Turbulence Input With and Without LAMS System E -- F/C 2

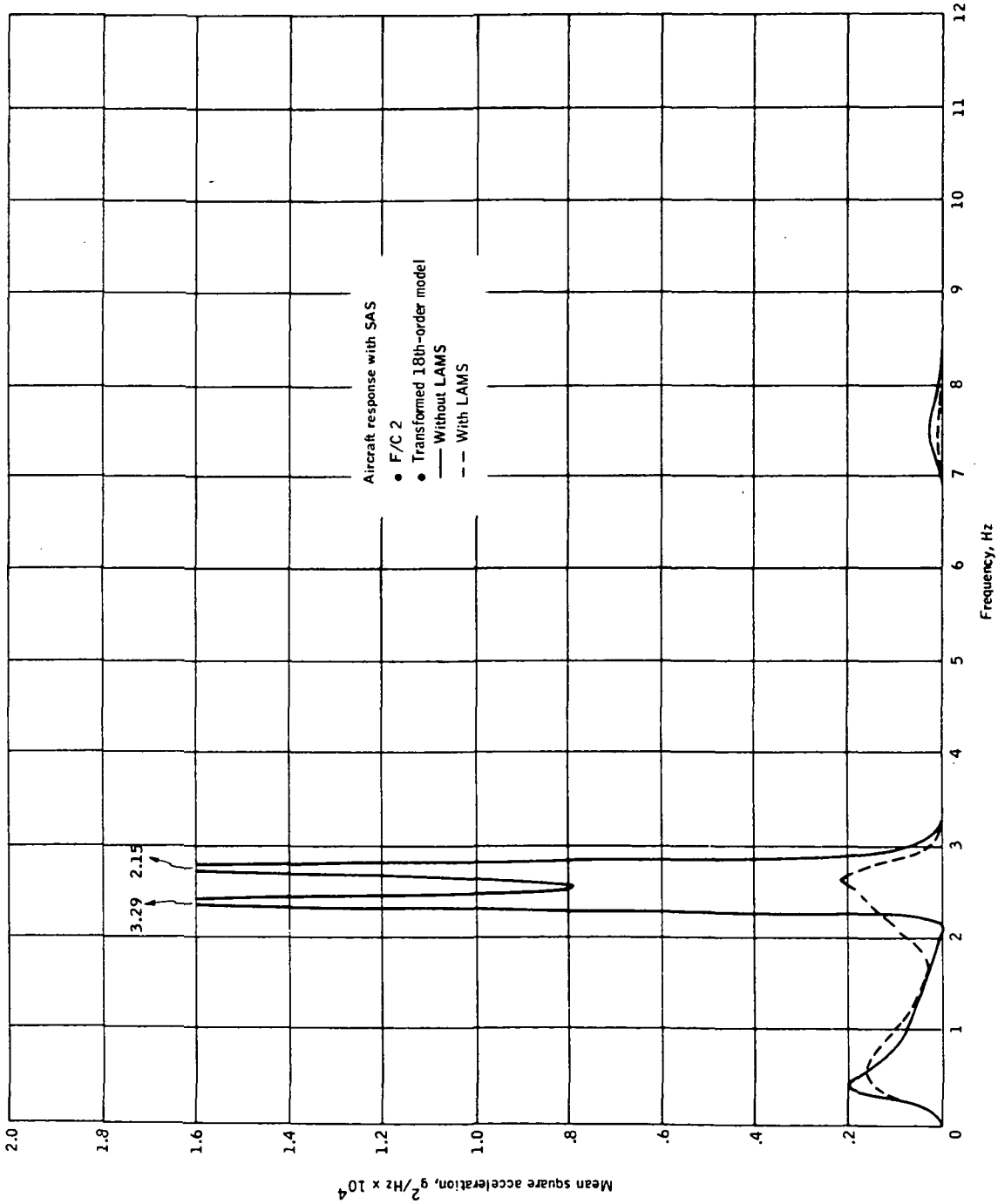

Figure 33. Mean Square Acceleration at FS 1236 for a 1-ft/sec Turbulence Input With and Without LAMS System E -- F/C 2

TABLE XXVI. - MODE SUPPRESSION PERFORMANCE FOR A 1-FT/SEC TURBULENCE INPUT DISTURBANCE - SYSTEM E

Fuselage station	F/C 1, high subsonic heavyweight condition[a]		F/C 2, supersonic cruise condition[b]	
	SAS only	LAMS	SAS only	LAMS
248 (pilot)	0.0211 g	0.0125 g	0.0111 g	0.00402 g
738	0.0148	0.0127	0.0055	0.00345
1236 (aft fuselage)	0.0253	0.0234	0.0100	0.00570

[a]Simplified model

[b]Transformed 18th-order model

TABLE XXVII. - RMS ACCELERATION RESPONSE TO 1-RAD FORCE PRODUCER INPUT DISTURBANCE - SYSTEM E - F/C 1 - SIMPLIFIED MODEL

Fuselage station	Input to canards		Input to inboard/ outboard elevons	
	SAS only	LAMS	SAS only	LAMS
248	6.52 g	4.44 g	2.156 g	0.7003 g
738	1.79	0.958	0.576	0.3036
1236	2.90	1.53	1.958	0.876

TABLE XXVIII. - RMS ACCELERATION RESPONSE TO 1-RAD FORCE PRODUCER INPUT DISTURBANCE - SYSTEM E - F/C 2 - TRANSFORMED 18TH-ORDER MODEL

Fuselage station	Input to canards		Input to inboard/ outboard elevons	
	SAS only	LAMS	SAS only	LAMS
248	0.621 g	0.3876 g	0.526 g	0.1249 g
738	0.220	0.1076	0.222	0.0967
1236	0.300	0.1461	0.376	0.1574

Surface motion was not computed for this system configuration. It was assumed the surface motion computed for the canard-only system would not change appreciably for this system. Surface motion for the outboard elevon system was computed for System A, the inboard/outboard elevon system. These data were also considered to be representative of those for the canard-plus-outboard elevon system.

Handling Qualities

A brief analysis was performed on the analog computer to evaluate the effects of the LAMS control on aircraft handling qualities. The analysis was performed on the analog computer using only the rigid-body pitch-and-plunge degrees of freedom plus the first three aeroelastic modes. The handling qualities were evaluated at F/C 1.

The YF-12A primary control system uses a mechanical linkage between the control stick and the inboard elevon actuator. This configuration provides a surface position command in proportion to stick position, but does not augment the aircraft's handling qualities. The short-period dynamics and static stability are augmented by the pitch SAS, however.

A LAMS system can affect the handling qualities both in the transient response behavior and in the steady-state stick effectiveness. Providing mode suppression actually improved the transient response due to the damping augmentation provided for the lower-frequency structural modes. This was true for all LAMS system configurations. The short-period frequency and damping were not degraded by the LAMS systems because of the design constraints imposed during the LAMS system synthesis. For the canard system, however, it was necessary to add a pilot stick input to the actuator. This input was necessary because the canard controller used an acceleration and rate feedback which acted to oppose pilot commands. This caused large deflections and tended to reduce the steady-state stick effectiveness. The addition of a pilot input to the canard actuator restored the effectiveness and reduced the canard displacement during a pilot command. Reduction of the canard displacement in turn reduced the loads imposed on the aircraft forward fuselage during pilot commands.

Nonlinearities

The analog computer simulation used for evaluating handling qualities included actuator rate and displacement limits. Generally, mode suppression performance is degraded by any limiting action of the actuator. The degradation is caused by an effective reduction in force output relative to the actuator input command. This was not the case for the mass-reaction system. Whenever the mass would strike its displacement limit, its force output would be momentarily increased, thereby enhancing the mode suppression performance.

Nonlinearities, such as actuator hysteresis, were not evaluated, per se, in the study. However, previous studies established (e.g., see ref. 4) that nonlinearities such as hysteresis can result in a significant degradation in LAMS system performance. Hysteresis can have a significant effect because

surface motion required for mode suppression in the presence of a gust is generally small. For example, typical values of hysteresis for the inboard and outboard elevon actuators (and linkage) are 0.15 deg and 0.25 deg, respectively. Table IX shows the rms surface displacement for System A to be only 0.32 deg for the inboard elevon and 0.67 deg for the outboard elevon for a 12-ft/sec gust disturbance. Certainly, hysteresis would have a significant effect on the performance of System A. It is expected that by using a small, lightweight, dedicated surface, such as the canard vanes, the hysteresis effects on mode suppression performance could be minimized.

CONCLUSIONS

The study has shown that the application of the LAMS technology to the YF-12A achieves significant improvement in vehicle rms structural load factor for both gust inputs and for force producer inputs. Therefore, the YF-12A aircraft can be an effective research tool for expanding LAMS technology and for developing improved application techniques.

The canard vanes were found to be the single most effective force producer for reducing structural mode contributions to local accelerations along the fuselage. Use of a dedicated force producer, such as the canard vanes, also offers the advantage of allowing the design to be optimized for the mode suppression function.

Of the five candidate systems evaluated, the one using the canard vanes plus the outboard elevons offers the greatest potential for continued development of mode suppression. There are no major technical obstacles, existing or anticipated, that would preclude implementation of the system on the YF-12A.

APPENDIX A
BASIC VEHICLE DATA

The basic vehicle description used in the LAMS YF-12A study is presented in this appendix. This description includes the symmetric structural, aerodynamic, and gust models for the four flight conditions that were studied. The choice of flight conditions was based partly on what was considered to be critical areas of the flight envelope from a loads and dynamics standpoint and also on the availability of data during the initial part of the study. The flight conditions studied are listed below:

Flight condition	Weight, lb	Altitude, ft	Mach no.
1	124 271	25 000	0.95
1A	68 693	25 000	0.95
2	90 703	--- Cruise condition ---	
3	68 693	22 000	0.68

NOMENCLATURE, SIGN CONVENTIONS AND COORDINATE SYSTEMS

This section contains the nomenclature for the material presented in this appendix, as well as all sign conventions and coordinate systems used to describe the vehicle.

Nomenclature

Matrix notation. -

$[\ ]$	rectangular or square matrix
$\lfloor\ \rceil$	diagonal matrix
$\{\ \}$	column matrix
$\lfloor\ \rfloor$	row matrix
$[\ ]^T$	matrix transpose
$\lfloor I \rceil$	unit diagonal matrix

$*$ convolution operator; e. g.,

$$\left[C_{\ell_\alpha}(t)\right] * \left\{\frac{d\alpha}{dt}\right\} = \left[\int_0^t C_{\ell_\alpha}(t-t') \frac{d\alpha}{dt'} dt'\right]$$

Coordinates and forces. -

z_o	displacement of reference point
θ_o	rotation of reference point
z_i	displacement of i^{th} coordinate
θ_i	rotation of i^{th} coordinate
δ_1, δ_2	rotation of inner and outer elevons with respect to hingeline, rad
δ_3	rotation of canard surface, rad
δ_m	displacement of mass of mass-reaction device
r_i	i^{th} generalized displacement
$[D_Z]$	transformation of deflections at structural nodes to aerodynamic nodes
$[D_\theta]$	transformation of deflections at structural nodes into thetas at aerodynamic nodes
Z_o	force at reference point
M_o	pitching moment at reference point
Z_i	force at i^{th} coordinate
M_i	pitching moment at reference point
Q_i	i^{th} generalized force
A_{LW}, A_{NAC}	aerodynamic influence coefficient matrix

$A_{Z_1}, A_{Z_2}, A_{\theta_1}, A_{\theta_2}, A_{g_1}, A_{g_2}, A_{\delta_1}, A_{\delta_2}, A_{\delta_3}, A_Z, A_\theta$	generalized aerodynamic matrices
A_{δ_m}	generalized mass-reaction force matrix
$[M]$, $[\bar{M}]$	mass and generalized mass matrices
$[K]$, $[\bar{K}]$	stiffness and generalized stiffness matrices
$[D_i]$	transformation of relative degrees of freedom to absolute degrees of freedom
$[V_m]$	matrix of mode shapes used to compute generalized forces
$[T]$	$[T] = [D_i][V_m]$
$\{v_i\}$	eigenvector or mode shape
$\{w\}$	downwash on structure, $w_i = V\theta_i + \dot{z}_i$
$\{w_g\}$	gust downwash

Parameters. -

V	free-stream velocity, in/sec
ρ	density of air, lb-sec^2/in.^{4}
q	dynamic pressure = $1/2\ \rho V^2$
b_o	semiroot chord, in.
ℓ	semispan of wing, in.
g_i	damping coefficient
ω_i	i^{th} elastic mode frequency, rad/sec
λ_i	$\lambda_i = \omega_i^2$

s	$s = i\omega = \sqrt{-1}\ \omega$
$\Phi(\omega)$	power spectral density
σ_u^2	mean square gust velocity, ft^2/sec^2
L	scale of turbulence, ft
V_o	velocity, ft/sec
ω	frequency, rad/sec
a_i, b_i	coefficients for indicial lag, $i = 1, 2$

Subscript. -

abs	denotes quantity in absolute coordinate system
rel	denotes quantity in relative coordinate system
i, j	integers

Sign Conventions and Coordinate Systems

The basic sign conventions for forces, moments, deflections, and rotations for the symmetric analysis are shown in Figure A1.

Two basic coordinate systems are used in presenting the vehicle dynamics. Both systems have the same axis orientation as in Figure A1. The first system is the "absolute" coordinate system and is defined by the motion of the vehicle as seen by an observer stationed on the ground. The other system is the "relative" coordinate system and is defined by the motion of the vehicle as seen by an observer stationed at some reference point on the vehicle, which for this study is FS 900, WL 100, and WS 32.

These coordinate systems can be related to one another, and this relationship will be used in the remaining sections of this appendix in defining the basic data.

Transformations for displacements and rotations. - The equations governing the relationship between the absolute and relative displacements and rotations are:

$$z_{o_{abs}} = z_{o_{rel}} \tag{A1a}$$

$$\theta_{o_{abs}} = \theta_{o_{rel}} \tag{A1b}$$

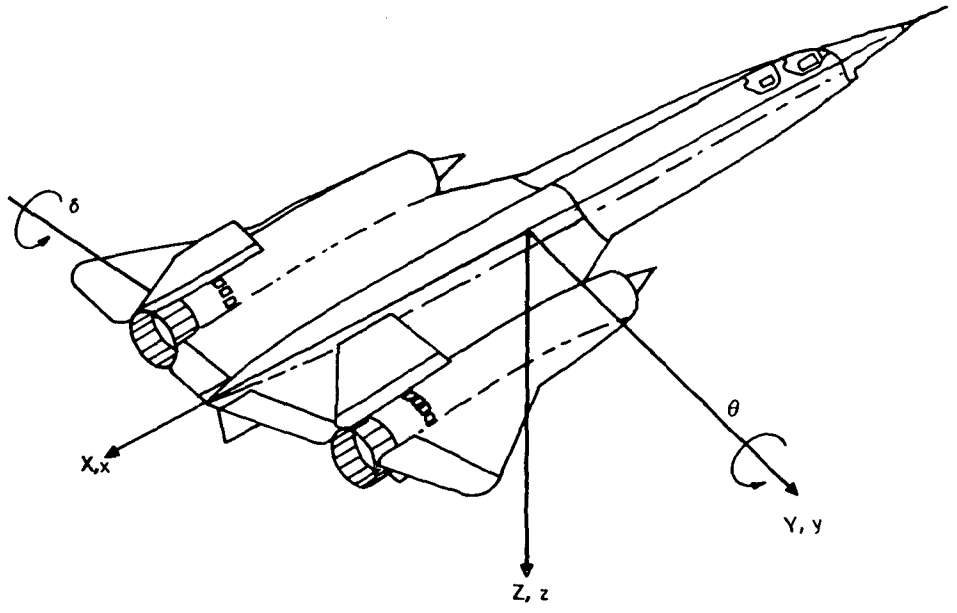

Figure A1. Sign Convention

$$z_{i_{abs}} = z_{i_{rel}} + z_{o_{rel}} + \bar{x}_i \, \theta_{o_{rel}} \tag{A1c}$$

$$\theta_{i_{abs}} = \theta_{i_{rel}} + \theta_{o_{rel}} \tag{A1d}$$

where $\bar{x}_i$ is the streamwise distance from the i^{th} coordinate to FS 900, with $\bar{x}_i$ positive for coordinates aft of FS 900.

Since the vehicle description will be given in matrix form, the above transformation can be written as:

$$\begin{Bmatrix} z_o \\ \theta_o \\ z_1 \\ \vdots \\ z_n \\ \theta_1 \\ \vdots \\ \theta_n \end{Bmatrix}_{abs} = \begin{bmatrix} 1 & 0 & 0 & \cdots & 0 \\ 0 & 1 & 0 & \cdots & 0 \\ 1 & \bar{x}_1 & & & \\ \vdots & \vdots & & & \\ 1 & \bar{x}_n & & I & \\ 0 & 1 & & & \\ \vdots & \vdots & & & \\ 0 & 1 & & & \end{bmatrix} \begin{Bmatrix} z_o \\ \theta_o \\ z_1 \\ \vdots \\ z_n \\ \theta_1 \\ \vdots \\ \theta_n \end{Bmatrix}_{rel} \tag{A1}$$

Transformation for forces and moments. - The equations relating the forces and moments in the relative and absolute coordinate systems are:

$$Z_{o_{rel}} = Z_{o_{abs}} + \sum_{i=1}^{n} Z_{i_{abs}} \tag{A2a}$$

$$M_{o_{rel}} = M_{o_{abs}} + \sum_{i=1}^{n} M_{i_{abs}} + \sum_{i=1}^{n} \bar{x}_i Z_{i_{abs}} \tag{A2b}$$

$$Z_{i_{rel}} = Z_{i_{abs}} \tag{A2c}$$

$$M_{i_{rel}} = M_{i_{abs}} \tag{A2d}$$

The above equations can be written in matrix form as

$$\begin{Bmatrix} Z_o \\ M_o \\ Z_1 \\ \vdots \\ Z_n \\ M_1 \\ \vdots \\ M_n \end{Bmatrix}_{rel} = \begin{bmatrix} 1 & 0 & 1 & \cdots & 1 & 0 & \cdots & 0 \\ 0 & 1 & \bar{x}_1 & \cdots & \bar{x}_n & 1 & \cdots & 1 \\ 0 & & & & & & & \\ \vdots & & & & & & & \\ & & & & & & & \end{bmatrix} \begin{Bmatrix} Z_o \\ M_o \\ Z_1 \\ \vdots \\ Z_n \\ M_1 \\ \vdots \\ M_n \end{Bmatrix}_{abs} \tag{A2}$$

If one examines the matrices in transformations (A1) and (A2), one notes that the matrix in (A2) is just the transpose of the matrix in (A1).

The actual coordinates used in describing the vehicle dynamics are all displacements, except for θ_o ; hence, there are no local moments M_i or rotations θ_i . For this system, transformation (A1) becomes

$$\begin{Bmatrix} z_o \\ \theta_o \\ z_1 \\ \vdots \\ z_n \end{Bmatrix}_{abs} = \begin{bmatrix} 1 & 0 & \cdots & 0 \\ 0 & 1 & 0 \cdots & 0 \\ 1 & \bar{x}_1 & & \\ \vdots & \vdots & & \\ 1 & \bar{x}_n & & \end{bmatrix} \begin{Bmatrix} z_o \\ \theta_o \\ z_1 \\ \vdots \\ z_n \end{Bmatrix}_{rel} = \begin{bmatrix} \\ D_i \\ \\ \end{bmatrix} \begin{Bmatrix} z_o \\ \theta_o \\ z_1 \\ \vdots \\ z_n \end{Bmatrix}_{rel} \quad \text{(A3)}$$

STRUCTURAL MODEL

The structural model was obtained by using a two-dimensional finite element representation, where structural members were lumped together in order to keep the size of the model small but still provide a good description of the dynamic behavior of the vehicle. The resulting model was then transformed as described below to obtain a description of the vehicle in terms of generalized forces and displacements.

Structural Node Locations

The stiffness matrix for the vehicle is defined in the relative coordinate system and contains 66 degrees of freedom, including the reference pitch and displacement degrees of freedom θ_o and z_o. All of these degrees of freedom are displacements, except for θ_o. Their locations are listed in Table A1 and are also shown in Figure A2.

Stiffness and Mass Representation

The stiffness matrix was determined using a two-dimensional finite element representation, and symmetric boundary conditions were imposed. This matrix was transformed into the relative coordinate system by imposing a pitch and plunge constraint at FS 900, WS 32. The form of this matrix is

$$\begin{Bmatrix} Z_o \\ M_o \\ Z_1 \\ \vdots \\ Z_n \end{Bmatrix}_{rel} = \begin{bmatrix} 0 & 0 & \cdots & 0 \\ \cdot & 0 & \cdots & 0 \\ \cdot & 0 & & \\ \vdots & \vdots & \text{Constrained K, lb/in} & \\ 0 & 0 & & \end{bmatrix} \begin{Bmatrix} z_o \\ \theta_o \\ z_1 \\ \vdots \\ z_n \end{Bmatrix}_{rel} = \begin{bmatrix} \\ K \\ \\ \end{bmatrix} \begin{Bmatrix} z_o \\ \theta_o \\ z_1 \\ \vdots \\ z_n \end{Bmatrix}_{rel} \quad \text{(A4)}$$

TABLE A1. - STRUCTURAL NODE LOCATIONS

	Node	FS	WS	Node	FS	WS	Node	FS	WS
(z_o)	1	900	32	23	1034	72	45	1212	133
(θ_o)	2	900	32	24	1130	72	46	795	207
	3	160	32	25	1178	72	47	914	207
	4	248	32	26	1212	72	48	1034	213
	5	388	32	27	1236	72	49	1130	213
	6	555	32	28	1262	72	50	1178	213
	7	640	32	29	795	100	51	1212	207
	8	738	32	30	882	100	52	1212	213
	9	795	32	31	914	100	53	1034	240
	10	954	32	32	954	100	54	1082	240
	11	1034	32	33	1034	100	55	1130	240
	12	1130	32	34	1130	100	56	1178	240
	13	1178	32	35	1178	100	57	1212	240
	14	1212	32	36	1212	100	58	1082	267
	15	1288	0	37	1236	100	59	1130	267
	16	1236	32	38	1262	100	60	1178	267
	17	1262	32	39	795	133	61	1212	267
	18	738	72	40	914	133	62	1130	294
	19	795	72	41	1034	127	63	1178	294
	20	882	72	42	1130	127	64	1212	294
	21	914	72	43	1178	127	65	1178	320
	22	954	72	44	1212	127	66	1212	320

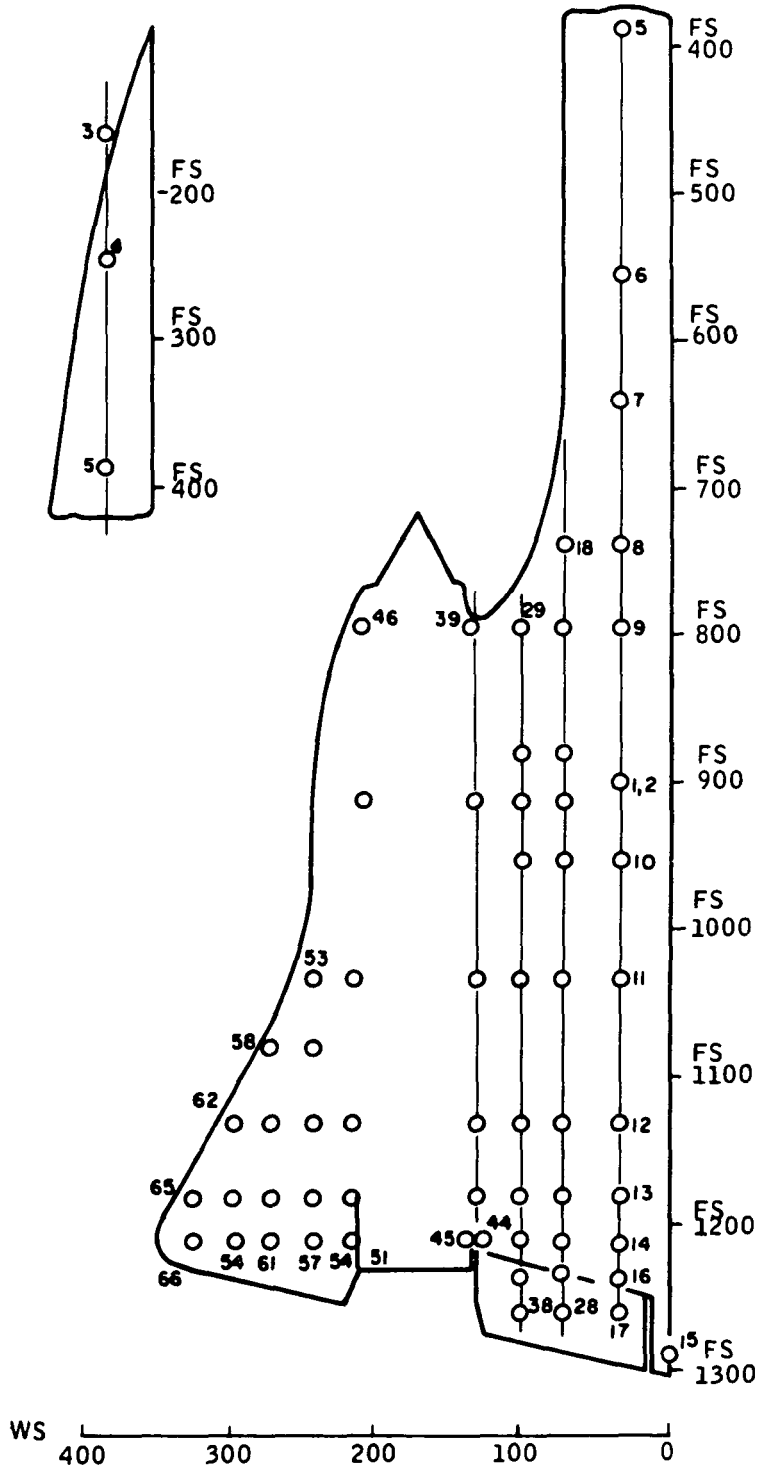

Figure A2. Structural Node Locations

where Z_o and M_o are the elastic force and moment at FS 900, which must be zero for equilibrium.

The inertia description of the vehicle consists of a matrix of lumped weights at the node points. This description is in the absolute coordinate system and hence must be transformed. Thus, the description of the mass in the relative coordinate system becomes:

$$[M]_{rel} = \frac{1}{g} [D_i]^T \lfloor W \rceil [D_i] \tag{A5}$$

where

g = acceleration due to gravity, in./sec^2

$\lfloor W \rceil$ = diagonal matrix of weights in lb for some specified weight condition

Determination of Generalized Forces and Displacements

Due to the lumped parameter representation of the vehicle, the generalized forces can be easily determined. One first finds the nonzero eigenvalues and their corresponding eigenvectors for the following vibration problem:

$$\left(\lambda_i [M] - [K]\right) \left\{ V_i \right\} = \left\{ 0 \right\} \tag{A6}$$

where

$\lambda_i = \omega_i^2 = i^{th}$ natural frequency squared of the elastic vehicle

V_i = associated eigenvector for λ_i

Let $[V_m]$ be the matrix described below:

$$\left[V_m \right] = \left[\begin{matrix} 1.0 & 0 \\ 0 & 1.0 \\ . & 0 \\ . & . \\ . & . \\ . & . \\ 0 & 0 \end{matrix} \quad \left\{ V_1 \right\} \cdots \left\{ V_n \right\} \right] \tag{A7}$$

From the above matrix, the generalized forces and displacements can be defined for the vibration problem as:

$$z_i = \sum_{j=1}^{n+2} V_{m_{ij}} r_j$$

$$Q_i = \sum_{j=1}^{n+2} V_{m_{ji}} F_j$$

where Q_i are the generalized forces and r_j are the generalized displacements.

The above transformation can be carried out by use of $[V_m]$ and its transpose. The form of the generalized mass and stiffness matrices becomes

$$[\bar{K}] = [V_m]^T [K] [V_m] \tag{A8}$$

$$[\bar{M}] = [V_m]^T [M] [V_m] \tag{A9}$$

The same procedure is used for converting the aerodynamic matrices, since the airloads are lumped at many stations and, hence, is a good approximation to the integral form of the generalized forces.

Sixteen modes, corresponding to the 16 lowest-frequency symmetric modes of the free-free vehicle, were used to modalize the data for this study. This representation allows one to work in the 0- to 25-Hz range for dynamic calculations.

Representation of Structural Damping

The structural damping of the vehicle is assumed to be proportional to the displacement and in phase with the velocity. This representation is usually carried out by multiplying $[\bar{K}]$ by a diagonal matrix of the form $[1 + ig_j]$, where g_j is the damping coefficient for the j^{th} mode. In this study, it was advantageous to keep all matrices real; hence, an equivalent viscous damping formulation was used. Since the natural frequencies of the system with and without aerodynamics are more or less constant, the equivalent viscous form of the damping can be approximated as

$$d_{jj} = \frac{g_j \bar{K}_{jj}}{\omega_j}$$

$$d_{ij} = 0 \text{ for } i \neq j$$

where

$\bar{K}_{jj}$ = j^{th} generalized stiffness

ω_j = j^{th} vibration natural frequency, rad/sec

g_j = damping coefficient assumed to be 0.02 for the first two modes and 0.05 for the rest

The damped vibration equation is then written as:

$$[\bar{M}]\{\ddot{r}\} + [D]\{\dot{r}\} + [\bar{K}]\{r\} = \{0\} \tag{A10}$$

where

$$[D] = \begin{bmatrix} 0 & 0 & \cdots & 0 \\ \vdots & \vdots & & \vdots \\ 0 & 0 & \cdots & 0 \end{bmatrix}$$

$\{r\}$ = generalized coordinate or displacement vector.

AERODYNAMIC MODEL

The aerodynamics used in this study were formulated in the time domain instead of the frequency domain. This formulation was needed for the control theory problem discussed in Appendix B.

Subsonic Aerodynamic Model

For the subsonic flight conditions, the aerodynamics for the wing and forebody were based on the subsonic kernel function or lifting surface theory (ref. 3), and used in conjunction with a uniform indicial lag. The airloads on the nacelle and those on the vehicle due to elevon rotation were determined from wind-tunnel measurements and were used without a lag function.

A steady-state aerodynamic influence coefficient matrix for the wing and forebody was computed, and adjustments to the airload distributions, based on pressure measurement tests, were made. This matrix is used to represent the airloads at the structural degrees of freedom due to the displacements and slopes of the structure at the nodes.

To account for the lag in the buildup of lift due to the motion of the structure, a uniform lag of the form $1 - a_1 e^{-b_1 \hat{t}}$ was used. The values of a_1 and b_1 were estimated from ref. 7. The effect of this lag was checked when a

flutter analysis of the vehicle was performed using both the uniform lag aerodynamics and the unsteady kernel function aerodynamics. That analysis showed that the flutter results for the vehicle were basically the same for both representations.

The form of the indicial aerodynamics is outlined below:

$$\left\{Z(\hat{t})_{lift}\right\}_{abs} = 4\pi\ell^2 q\left[A_{LW}(\hat{t})\right] * \left\{\frac{d\frac{w(\hat{t})}{V}}{d\hat{t}}\right\}_{abs} + 4\pi\ell^2 q\left[A_{NAC}\right] * \left\{\frac{d\frac{w(\hat{t})}{V}}{d\hat{t}}\right\}_{abs} \tag{A11}$$

where

$*$ = represents the convolution operator

$\hat{t}$ = semiroot chord lengths traveled

$\frac{w(\hat{t})}{V}$ = nondimensional downwash at the structural degrees of freedom

$A_{LW}(\hat{t}) = \left[1 - a_1 e^{-b_1\hat{t}}\right] [A_{LW}]$

The above equation can be transformed into the frequency domain and has the following form:

$$\left\{Z(s)_{lift}\right\}_{abs} = 4\pi\ell^2 q\left[1 - \frac{a_1 s}{s + b_1\left(\frac{V}{b_o}\right)}\right][A_{LW}]\left(\left[D_{\theta_1}\right] + \frac{s}{V}\left[D_{Z_1}\right]\right)\{z_i\}_{abs} + 4\pi\ell^2 q\,[A_{NAC}]\left(\left[D_{\theta_2}\right] + \frac{s}{V}\left[D_{Z_2}\right]\right)\{z_i\}_{rel} \tag{A12}$$

where

s = $i\omega$

$\left[D_{\theta_i}\right]$ = represents a transformation of the deflections, z_i, at the structural modes into slopes at the collocation points used in the formation of the aerodynamic influence coefficient matrix $[Q(i\omega)]$, i = 1 for wing forebody, i = 2 for nacelle.

$\left[D_{Z_i}\right]$ = similar to $\left[D_{\theta_i}\right]$, except it relates the deflections at the structural modes to the deflections at the collocation points.

Since the above formulation is in the absolute coordinate system, the transformation $\left[D_i\right]$ can be applied to transform into the relative system. This transformation and the reduction to generalized forces and displacements will be performed simultaneously by using the following transformation:

$$\left[T\right] = \left[D_i\right]\left[V_m\right]$$

Under the above transformation, one has

$$\left\{A(s)_{aero}\right\}_{rel} = 4\pi \ell^2 q \left[T\right]^T \left\{\left[1 - \frac{a_1 s}{s+b_1\left(\frac{V}{b_o}\right)}\right]\left[A_{LW}\right]\left\langle\left[D_{\theta_1}\right] + \frac{s}{V}\left[D_{Z_1}\right]\right\rangle + \left[A_{NAC}\right]\left\langle\left[D_{\theta_2}\right] + \frac{s}{V}\left[D_{Z_2}\right]\right\rangle\right\}\left[T\right]\{r\}_{rel} \tag{A13}$$

or for fixed q and V

$$\left\{A(s)_{aero}\right\}_{rel} = -\left\{\left[1 - \frac{a_1 s}{s+b_1\left(\frac{V}{bo}\right)}\right]\left\langle\left[A_{\theta_1}\right] + s\left[A_{Z_1}\right]\right\rangle + \left[A_{\theta_2}\right] + s\left[A_{Z_2}\right]\right\}\{r\}_{rel} \tag{A14}$$

The aerodynamics due to elevon rotation were needed in the study. The forces due to the inboard and outboard elevons were calculated separately and were not lagged. These forces were determined from wind tunnel test data and include the induced effects on the wing itself, as well as surface forces. The form of these forces is given below:

$$\left\{Z_{lift_{\delta_1}}\right\}_{abs} = q\left\{L_{\delta_1}\right\}\delta_1 \tag{A15}$$

$$\left\{Z_{lift_{\delta_2}}\right\}_{abs} = q\left\{L_{\delta_2}\right\}\delta_2 \tag{A16}$$

where

δ_1 = surface angle of inboard elevon relative to wing

δ_2 = surface angle of outboard elevon relative to wing

δ_1, δ_2 = positive for elevon trailing edge down

By use of the transformation, T, one obtains the generalized forces due to elevon rotation, for fixed q, as

$$\left\{Q_{\delta_1}\right\}_{rel} = q[T]^T \left\{L_{\delta_1}\right\} \delta_1 = \left\{A_{\delta_1}\right\}\delta_1 \tag{A17}$$

$$\left\{Q_{\delta_2}\right\}_{rel} = q[T]^T \left\{L_{\delta_2}\right\} \delta_2 = \left\{A_{\delta_2}\right\}\delta_2 \tag{A18}$$

The gust aerodynamics for the study presented a problem since they had to be formulated as indicial-type aerodynamics. An interim uniform lag function of the form

$$1 - e^{-b_2\hat{t}}$$

was used, and the value of b_2 was based on results presented in refs. 5, 7, and 8.

The interim gust aerodynamics was defined to be:

$$\left\{Z_{gust}\right\}_{abs} = 4\pi \ell^2 q \left[\left[1-e^{-b_2\hat{t}}\right] [A_{LW}] * \left\{\frac{\frac{d^{w}g}{V}}{d\hat{t}}\right\} + [A_{NAC}] * \left\{\frac{\frac{d^{w}g}{V}}{d\hat{t}}\right\}\right] \tag{A19}$$

or using the transformation, T, one obtains the forces in relative system for fixed q and v, as

$$\{Q_{gust}(s)\}_{rel} = \left[1 - \frac{s}{s + b_2\left(\frac{V}{b_o}\right)}\right] \left\{A_{g_1}\right\} w_g + \left\{A_{g_2}\right\} w_g \tag{A20}$$

Appendix A

Supersonic Aerodynamic Model

For the supersonic flight condition, i.e., the cruise condition, the aerodynamics were formulated using piston theory due to the high Mach number. Because of the Mach number considered, no aerodynamic lag was used on the aerodynamics due to the motion of the structure. A lag on the gust aerodynamics was used in the gust analysis of this vehicle and was retained for this study.

The form of the aerodynamics is basically the same as that used for the subsonic conditions, except that the lag term is deleted in all but the gust formation. Thus, one has:

$$\left\{Z_{lift}\right\}_{abs} = q\,[A]\left\{[D_\theta] + \frac{s}{V}\,[D_Z]\right\} \tag{A21}$$

$$\left\{Z_{\delta_1}\right\}_{abs} = q\left[L_{\delta_1}\right]\delta_1 \tag{A22}$$

$$\left\{Z_{\delta_2}\right\}_{abs} = q\left[L_{\delta_2}\right]\delta_2 \tag{A23}$$

$$\left\{Z_{gust}\right\}_{abs} = q\left[1-e^{-b_2\hat{t}}\right][A_{wing}]^* \frac{dw_g}{d\hat{t}} + q\,[A_{forebody}]^* \left\{\frac{dw_g}{d\hat{t}}\right\} \tag{A24}$$

By applying the transformation, T, the above forces are transformed to the relative system and become generalized forces and displacement for fixed q, V

$$\left\{Q_{lift}(s)\right\}_{rel} = -\left\{[A_\theta] + \frac{s}{V}\,[A_Z]\right\}\{r\}_{rel} \tag{A25}$$

$$\left\{Q_{\delta_1}\right\}_{rel} = \left\{A_{\delta_1}\right\}\delta_1 \tag{A26}$$

$$\left\{Q_{\delta_2}\right\}_{rel} = \left\{A_{\delta_2}\right\}\delta_2 \tag{A27}$$

$$\left\{Q_{gust}(s)\right\}_{rel} = \left[1 - \frac{s}{s + b_2\left(\frac{V}{b_o}\right)}\right]\left\{A_{g_1}\right\} w_g + \left\{A_{g_2}\right\} w_g \tag{A28}$$

Appendix A

EQUATIONS GOVERNING THE ELASTIC VEHICLE

This section contains the equations governing the elastic model, and describes the internal loads calculation and gust models.

Equations Governing the Vehicle Motion

The equations of motion for the elastic vehicle without the baseline pitch SAS are given as:

$$\left\{ s^2 [\bar{M}] + \left[1 - \frac{a_1 s}{s + b_1 \left(\frac{\bar{V}}{b_o} \right)} \right] \left(s \left[A_{Z_1} \right] + \left[A_{\theta_1} \right] \right) + s \left(\left[A_{Z_2} \right] + [D] \right) + \left[A_{\theta_2} \right] + [\bar{K}] \right\} \{r\} = \{F(s)\} \tag{A29}$$

where $s = i\omega$.

The baseline SAS can be included in the above equation by incorporating the transfer function defined from the SAS block diagram (see Figure 2 of the main text).

The different types of forcing function that could appear on the right-hand side of the above equation are given below in the frequency domain form.

Elevon generalized force description. -

$$\{F(s)\} = \left\{ A_{\delta_i} \right\} \delta_i(s) \qquad i = 1, 2 \tag{A30}$$

where $\delta_i(s)$ is the rotational coordinates for the elevons and may be a function of s.

Gust generalized force description. -

$$\{F(s)\} = \left[1 - \frac{s}{s + b_2 \frac{\bar{V}}{b_o}} \right] \left\{ A_{g_1} \right\} w_g(s) + \left\{ A_{g_2} \right\} w_g(s) \tag{A31}$$

Canard generalized force description. -

$$\{F(s)\} = q S_c C_{L_{\delta_3}} \{t_i\} \delta_3 = \{A_c\} \delta_3 \tag{A32}$$

where

t_i = element of the i^{th} row of the fourth column of $[T]^T$, i.e., displacement of the i^{th} mode at the location of the canard, FS 248

S_c = exposed area of one side of canard

$C_{L_{\delta_3}}$ = lift slope coefficient for canard, rad

Mass reaction device generalized force description. -

$$\{F(s)\} = s^2 M \{t_i\} \delta_m = s^2 \left\{A_{\delta_m}\right\} \delta_m \tag{A33}$$

where

M = mass of the mass-reaction device

δ_m = displacement of M

t_i = identical to t_i in the canard description

It should be noted that various combinations of the above forcing functions can be used, with the exception of the case involving both the canard and mass-reaction devices. These devices are considered mutually exclusive of one another.

Description of the Gust Model

The preliminary LAMS longitudinal gust model contains the wind filter, associated lift growth functions, and gust force coefficients. There are no penetration effects included in the present model. The input to the wind filter, η, is a unity rms "white noise" signal. The gust model is shown in Figure A3.

The wind filter is derived from the Press-Meadows power spectral density random gust model (ref. 7), as follows:

$$\Phi(\omega) = \sigma_u^2 \left(\frac{L}{V_o}\right)\left[\frac{1+3(L/V_o)^2\omega^2}{[1+(L/V_o)^2\omega^2]^2}\right]\left(\frac{ft^2/sec^2}{rad/sec}\right) \tag{A34}$$

where

σ_u^2 = mean-square gust velocity, ft^2/sec^2

L = scale of turbulence, ft

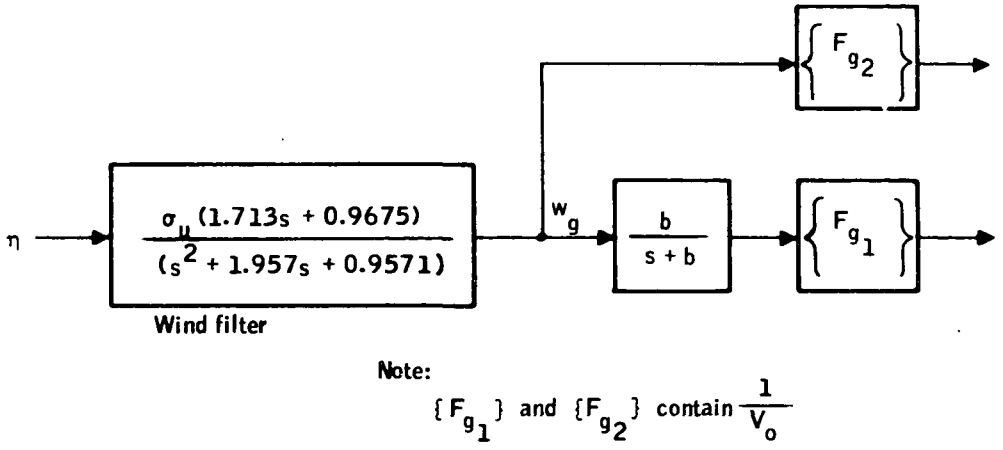

Figure A3. Preliminary Longitudinal Gust Model

V_o = velocity, ft/sec

ω = frequency, rad/sec

Using the fact that $\Phi(\omega)$, the Press-Meadows power spectral density model, is equal to $w_g(i\omega)^2$, a Laplace transfer function equivalent to Press-Meadows model can be developed. Note that

$$\Phi(\omega) = |w_g(i\omega)|^2 = w_g(i\omega)\, w_g^*(i\omega) \tag{A35}$$

where the asterisk denotes the complex conjugate. Factoring $\Phi(\omega)$ into appropriate terms and replacing $i\omega$ by s, the Laplace operator, it is found that

$$w_g(s) = \sigma_u \sqrt{\frac{3V_o}{L}} \; \frac{s + \frac{V_o}{\sqrt{3L}}}{\left(s + \frac{V_o}{L}\right)^2} \tag{A36}$$

or, substituting V_o = 978.33 ft/sec and L = 1000 ft,

$$w_g(s) = 1.713\, \sigma_u \left[\frac{s + 0.5648}{(s + 0.9783)^2}\right] \tag{A37}$$

Appendix A

Transformation of the Vehicle Equations of Motion

A change in the choice of generalized coordinates was made to eliminate zero eigenvalues from the unforced equations of motion, eq. (A29) with $\{F(s)\} = 0$. This change in variables was made by choosing $w_o = \dot{z}_o + V\theta_o$ and $\dot{\theta}_o$ as the first two generalized coordinates instead of z_o and θ_o as are used in eq. (A29).

Upon inspection of the components of eq. (A29), one notes that all of the aerodynamic forces and moments associated with the rigid-body motion (z_o, θ_o) are in fact only functions of the rigid-body downwash, w_o. Further examination of the system reveals that the aerodynamic terms are the only terms that involve z_o, θ_o and their time derivative except for the rigid-body equations which have terms involving $\ddot{z}_o$ and $\ddot{\theta}_o$. These acceleration terms can be easily represented in the new system by noting that $\ddot{z}_o = \dot{w}_o - V\dot{\theta}_o$.

Carrying out the above change in generalized coordinates and dividing each equation by the appropriate generalized mass, one can rewrite eq. (A29) as

$$\left\{ s^2 \left[\hat{M}\right] + \left[W(s)\right] \; s\left[\hat{A}_z\right] + \left[\hat{A}_{\theta_1}\right] + s\left[\hat{A}\right] + \left[\hat{B}\right] \right\} \{\hat{r}\} = \{\hat{F}(s)\} \quad \text{(A38)}$$

where

$$\left[\hat{M}\right] = \begin{bmatrix} 0 & \cdots & 0 \\ \vdots & 0 & 0 \\ \vdots & \vdots & \begin{bmatrix} & I & \end{bmatrix} \\ 0 & 0 & \end{bmatrix}$$

$$W(s) = \left[1 - \frac{a_1 s}{s + b_1 \left(\frac{V}{b_o}\right)} \right]$$

$$\hat{r} = \left[w_o, \dot{\theta}_o, r_3, \ldots, r_{16} \right]^T$$

$$\{\hat{F}(s)\} = \left\{\frac{F_i(s)}{m_u}\right\}$$

where $F(s)$ is defined in eqs. (A30) to (A33) and the symbol " ^ " denotes the transformed matrices as outlined above.

APPENDIX B
DESCRIPTION OF SYNTHESIS TECHNIQUES

This appendix describes two synthesis techniques applicable to the design of LAMS systems. These two techniques are referred to as the frequency response technique and the quadratic optimization technique. Both techniques have been thoroughly described in previous LAMS reports (see refs. 4 and 6). These descriptions are repeated in this appendix for the convenience of the reader. The description of quadratic optimization theory also includes the details of the theory peculiar to the YF-12A application.

An attempt was made in the LAMS YF-12A study to integrate the two techniques into a single unified procedure. It was the intent in performing this integration to capitalize on the strong point of each approach. The attempted integration of these techniques is discussed in this appendix following the discussion of the two individual techniques.

SYMBOLS

$\ddot{z}_c$	normal acceleration at an aircraft station where the acceleration is to be reduced, in./sec^2
$\ddot{z}_s$	aircraft motion measured by LAMS system, in./sec^2
w_g	gust velocity, ft/sec
δ	control surface deflection, rad
$K_c G(s)$	gains and filtering of LAMS system
Γ	desired attenuation of normal acceleration with LAMS system
$[\ ]$	rectangular or square matrix
$\lfloor\ \rceil$	diagonal matrix
$\{\ \}$	column matrix
$\lfloor\ \rfloor$	row matrix
$[\ ]^T$	matrix transpose

$*$ convolution operator e. g.

$$[a(t)]* \{b(t)\} = \left\{ \int_0^t a(t-t')\ b(t')\ dt' \right\}$$

r generalized coordinate vector

x state vector

u control vector

η white noise

$\hat{r}$ response vector

F state-transition matrix

G_1 control-input matrix

G_2 disturbance-input matrix

H state-response matrix

D control-response matrix

$\hat{M}$, $\hat{A}_{z_1}$, $\hat{A}_{\theta_1}$, $\hat{A}$, $\hat{B}$, $\hat{A}_{\delta_1}$, $\hat{A}_{\delta_2}$, $\hat{A}_{g_1}$, $\hat{A}_{g_2}$, $\hat{A}_c$, $\hat{A}_m$

(See Appendix A)

$\hat{C} = \hat{A} + \hat{A}_{z_1}$

$\hat{E} = \hat{A}_{\theta_1} + \hat{B}$

$\hat{T} = \hat{b}_1\ \hat{A}_{z_1} - \hat{A}_{\theta_1}$

$p = \lfloor p_1, \ldots, p_{18} \rfloor^T$ state variables associated with lift lag

p_{19} state variable associated with gust lag

p_{20} state variable associated with wind filter

p_{21}, p_{22}, p_{23}, p_{24}, p_{25} state variables associated with the baseline SAS

$w_o = \dot{z}_o + V_o\theta_o$, in./sec

θ_o pitch at vehicle reference point, rad

z_o plunge at vehicle reference point, in.

$r_3, \ldots, r_{18}$ generalized coordinates, in.

δ_1 inboard elevon deflection, rad

δ_2 outboard elevon deflection, rad

δ_3 canard deflection, rad

δ_m generalized coordinate associated with mass reaction device, rad

u_m control input to mass reaction device

L turbulence scale, ft

$K(t) = a_1 e^{-\hat{b}_1 t}$

$\psi(t) = \hat{b}_2 e^{-\hat{b}_2 t}$

$a_1, \hat{b}_1, \hat{b}_2$ coefficients of indicial lags $\hat{b} = b \frac{V_o}{b_o}$

V_o, V_o' velocity of vehicle

s Laplace operator

$\delta_{\dot{\theta}}$ scheduled gain

ϕ_j' slope of the j^{th} mode shape at the rate gyro location

ϕ_{i_j} deflection at station j of the i^{th} mode shape

Appendix B

FREQUENCY RESPONSE TECHNIQUE

This synthesis technique (ref. 6) is described by first presenting the general LAMS problem. The problem is presented in terms of the design objectives and design approach considerations which form a basis for the development of a LAMS system. Using this information, the formulas and conditions used in the synthesis procedure are established.

Design Objectives and Design Approach

The following design objectives should be used to form the basis for developing an effective LAMS system:

- Reduce response amplitudes of those modes (generally rigid-body and lower-frequency structural modes) that are significant in terms of their contributions to rms stress and acceleration levels at aircraft stations of interest
- Satisfy stability requirements
- Maintain adequate rigid-body dynamics in terms of good handling qualities
- Provide maximum tolerance to unpredicted variations in vehicle-system dynamics
- Minimize unfavorable coupling with structural modes above frequency range of significant structural modes
- Establish analytical design which permits economical and reliable hardware implementation

A necessary condition for load alleviation and mode suppression is the ability to sense the deflections, or a derivative of the deflections, of the significant modes and to apply control forces to these modes. The deflection rate and/or acceleration of the modes can be measured by conventional sensors (such as accelerometers or gyros) suitably located on the vehicle. A corrective control force can be applied through the deflection of one or more of the aerodynamic control surfaces. Hence, a design approach was assumed which would concentrate on the development of a system using conventional sensors to measure the modal deflection rates and/or accelerations and to command corrective action through the aerodynamic control surfaces.

Development of synthesis technique. - In general, the synthesis technique used to design a LAMS system should have the following properties:

- Facilitate design studies using a high-order mathematical model of the vehicle

- Enable use of this model in a frequency response form, thereby facilitating incorporation of unsteady aerodynamic effects in the frequency domain
- Capability to compute required controller characteristics directly from specification of meaningful design criteria
- Permit rapid and accurate evaluation of non-ideal controller characteristics

The synthesis technique described on the following pages is an attempt to provide a design procedure with these properties.

The technique consists of (1) specifying the control system filter, and (2) specifying the sensor configuration. The basic formula used in the synthesis technique specifies the control system filter (i. e., compensation) requirements in terms of a given sensor configuration and an allocated attenuation requirement on the rms stress or acceleration level at a given aircraft station (e. g., the pilot's station). For the sake of this discussion, only reductions in acceleration levels will be discussed. Clearly, the same techniques can be used for reducing stress levels. Additional requirements are specified in terms of stability constraints and in terms of restrictions resulting from the use of practical (in terms of mechanization) linear filters. These additional requirements enable the designer to specify a sensor configuration. As a consequence, once a reduction in rms acceleration level has been established at the given stations, it is possible to specify a sensor-filter combination. The synthesis procedure requires the vehicle dynamics to be described in a frequency response format in which output variables of load accelerations are related to input variables of wind gust and control surface deflection. Specification of data in this form facilitates incorporation of unsteady aerodynamics in the frequency domain rather than in the time domain, a factor often not included in other techniques.

The approach to be taken toward performance specification for purposes of controller synthesis is to specify the desired reduction in acceleration at the resonant peaks of each of the significant modes. The frequencies of these peaks will be determined from a frequency response plot between accelerations and the wind gust input, thereby including all known coupling effects. The required percentage reduction in amplitude at each frequency will be estimated from power spectral density plots of acceleration due to turbulence at selected vehicle stations. Knowing the rms acceleration and identifying its source in terms of individual modes, a design goal for reduction of resonant amplitude can be allocated to each mode. An important part of this allocation is definition of modes which do not cause significant acceleration contribution, so that the required control action at those particular frequencies can be relaxed. The objective of this process is to produce an appropriate allocation of control effort.

With this information, the controller can be specified (as will be shown) and then evaluated at other aircraft stations, and stability margins can be established. If all constraints are not met, the allocation of required reduc-

tions in amplitudes at the resonant modes can be modified and the process repeated until all the constraints are satisfied. This results in an iterative process but with an orderly and systematic means of attack. Relating peak accelerations to rms accelerations and specifying reductions required in terms of acceleration at a particular aircraft station are useful methods for expediting the control synthesis process. The final measures of control effectiveness are the actual rms accelerations at the various aircraft stations.

To establish the basic formulas, consider a general block diagram of the control system/vehicle dynamics as shown in Figure B1. This diagram illustrates the relationship (in transfer function form) between the acceleration level measured at a sensitive aircraft station, $\ddot{z}_c$, and the wind input, w_g. Clearly, the diagram could be expanded to include all the aircraft stations, but this is not necessary for the following discussion. The $\ddot{z}_s$ term is the quantity to be measured by a sensor located at some vehicle station. The $K_c G(s)$ term is the filter to be designed for the LAMS system. Thus, it is the task of the synthesis process to determine what quantity will be sensed ($\ddot{z}_s$) and to define a filter $[K_c G(s)]$ that will result in a specified reduction in acceleration ($\ddot{z}_c$) in response to the turbulence input, w_g. The aircraft model must be known in a frequency response form relating output variables of acceleration to input variables of wind turbulence, w_g, and control surface deflections, δ. Actuation system dynamics can either be included in the aircraft model or be left to be specified as part of the filter $[K_c G(s)]$.

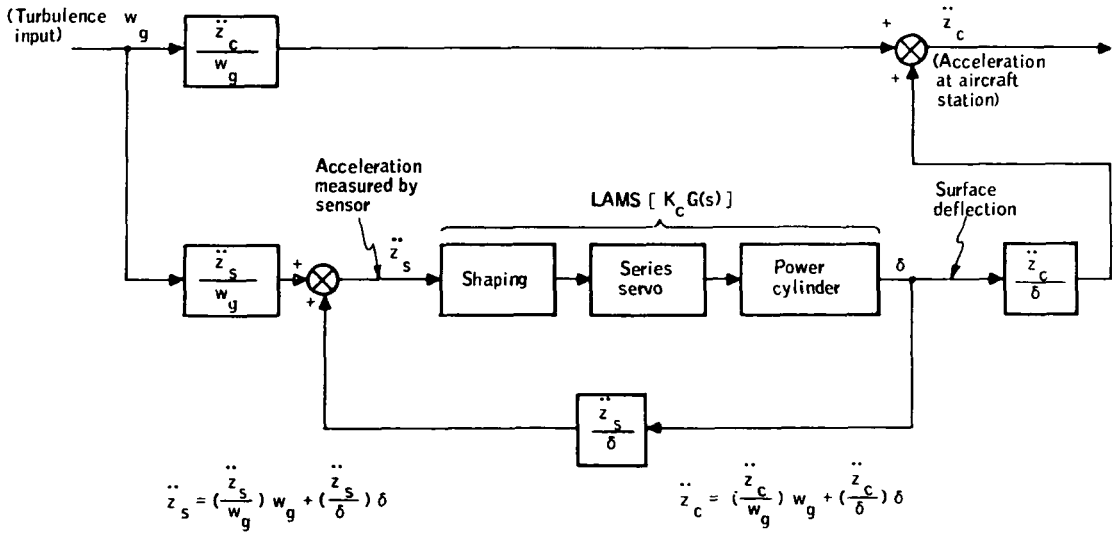

Figure B1. Vehicle/System Model General Block Diagram

With the design goals in terms of a reduction in acceleration at a selected station with augmentation to that without augmentation, one can derive an expression for the required filter characteristics $[K_c G(s)]$. Let Γ equal the ratio of acceleration at a particular station with augmentation to that without augmentation. Acceleration occurring at this station $(\ddot{z}_c)$ without augmentation is

$$\left(\ddot{z}_c\right)_{\substack{\text{no}\\ \text{Aug}}} = \left(\frac{\ddot{z}_c}{w_g}\right) w_g \tag{B1}$$

Acceleration at the sensitive station with augmentation is

$$\left(\ddot{z}_c\right)_{\substack{\text{with}\\ \text{Aug}}} = \left\{\frac{\ddot{z}_c}{w_g} + \left(\frac{\ddot{z}_s}{w_g}\right)\left[\frac{K_c G(s)}{1 - \left(\frac{\ddot{z}_s}{\delta}\right) K_c G(s)}\right]\left(\frac{\ddot{z}_c}{\delta}\right)\right\} w_g \tag{B2}$$

Thus, by definition of Γ we obtain:

$$\Gamma = \left\{\left(\frac{\ddot{z}_s}{w_g}\right)\left[\frac{K_c G(s)}{1 - \left(\frac{\ddot{z}_s}{\delta}\right) K_c G(s)}\right]\frac{\left(\frac{\ddot{z}_c}{\delta}\right)}{\left(\frac{\ddot{z}_c}{w_g}\right)} + 1\right\} \tag{B3}$$

This definition of Γ implies that Γ can be a complex number. The designer is free to pick any Γ, real or complex, within certain limits. Clearly, if the control is to reduce the amplitude of the acceleration at the discrete frequency points, then the absolute magnitude of Γ chosen must be less than one (i.e., $0 \le \Gamma < 1$). Selecting real values for Γ will result in lower gain values for the filter $[K_c G(s)]$ than will the selection of complex values. Low gain values for the filter are desirable from the standpoint of minimizing coupling with high-frequency structural modes.

We can solve eq. (B3) for $K_c G(s)$ to yield:

$$K_c G(s) = \frac{1}{\frac{\ddot{z}_s}{\delta}}\left[\frac{1}{1 - \frac{1}{1-\Gamma}\left(\frac{\ddot{z}_c/\delta}{\ddot{z}_c/w_g}\right)\left(\frac{\ddot{z}_s/w_g}{\ddot{z}_s/\delta}\right)}\right] \tag{B4}$$

This equation defines the filter characteristics $[K_c G(s)]$ in a frequency response form. It implies that if one picks the quantity to be measured $(\ddot{z}_s)$, and a value of Y at discrete frequency points (e.g., Γ_1, Γ_2, Γ_3 corresponding to the first three structural mode resonant frequencies), then a gain and phase requirement can be computed for $K_c G(s)$ at these discrete frequencies. If a filter can be designed to exhibit these gain and phase

characteristics, then the acceleration ($\ddot{z}_c$) will be attenuated by the values of Γ chosen at these frequency points. It is sufficient to specify a filter requirement at only the resonant frequencies. Thus, the resulting filter will be simpler than the inverse of the vehicle transfer function which would probably be obtained if the accelerations were to be reduced by only a cancellation technique.

The remaining task is to establish a procedure for defining the quantity to be measured ($\ddot{z}_s$). The objective is to specify the relative modal components of $\ddot{z}_s$ and not the type of sensor nor the combination of sensors required to actually provide $\ddot{z}_s$. The sensor combinations can be established by examining the properties of $\ddot{z}_s$ and comparing them with the mode shapes. The term $\ddot{z}_s$ is considered to be an acceleration quantity having the following form:

$$\ddot{z}_s = \ddot{z}_o + K_{\ddot{\theta}} \ddot{\theta}_o + \sum_{i=1}^{n} K_i \ddot{r}_{i+2} \qquad \text{(B5)}$$

where

$\ddot{z}_o$ = rigid-body plunging mode

$\ddot{\theta}_o$ = rigid-body rotation mode

$\ddot{r}_i$ = structural modes

In the discussion that follows, $\ddot{z}_s$ is referred to as the sensor complement. Thus, to define $\ddot{z}_s$ corresponds to defining the relative values of the modal deflections (K_i). To do this, we examine the following constraints:

1. A stability constraint is imposed on the system by the stability limits of the feedback loop shown below (see Figure B1):

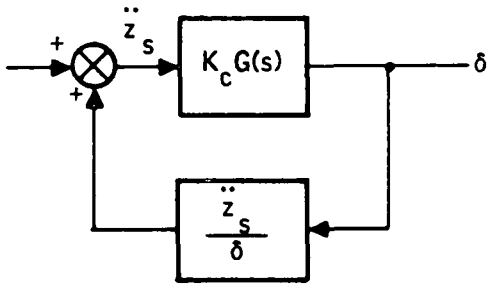

Figure B1. Vehicle/System Model General Block Diagram

This loop has the closed-loop transfer function given by:

$$H(s) = \frac{K_c G(s)}{1 - (\ddot{z}_s/\delta) K_c G(s)} \tag{B6}$$

The term H(s) is unstable whenever the roots of its demoninator lie in the right-half plane of a root locus diagram. The denominator will be unstable at the frequency at which

$$\phi_{s\delta} + \phi_g = 0 \text{ deg} \tag{B7}$$

and

$$\left| \left(\frac{\ddot{z}_s}{\delta} \right) K_c G(s) \right| \geq 1 \tag{B8}$$

where

$\phi_{s\delta}$ = phase angle of transfer function $(\ddot{z}_s/\delta)$

ϕ_g = phase angle of filter $[K_c G(s)]$

Since one cannot reduce the amplitude of the structural mode accelerations by gain stabilization, it is necessary to provide phase stabilization by proper selection of $\phi_{s\delta} + \phi_g$. Because of uncertainties in the mathematical model, it is necessary to require that over the range of frequencies where gain stabilization is not attainable nor desirable, a phase margin constraint is applied. For example, if it is desired to have minimum phase margins of 90 deg, the constraint becomes:

$$90 \text{ deg} \leq \phi_{s\delta} + \phi_g \leq 270 \text{ deg} \tag{B9}$$

At frequencies above the modes of interest (i. e., above frequencies where augmentation is to be applied) it is desirable to provide gain stabilization to eliminate this constraint on the phase angle.

With the above constraint on the phase angle of the sensor/filter combination, the problem is to find a solution which, over the frequency range of interest, will simultaneously satisfy this constraint and the phase constraint imposed by the filter equation [eq. (B4)]. These two constraints are repeated here for reference:

$$K_c G(s) = \frac{1}{\ddot{z}_s/\delta} \left[\frac{1}{1 - \frac{1}{1-\Gamma} \left(\frac{\ddot{z}_c/\delta}{\ddot{z}_c/w_g} \right) \left(\frac{\ddot{z}_s/w_g}{\ddot{z}_s/\delta} \right)} \right] \tag{B10}$$

$$90 \text{ deg} \leq \phi_{s\delta} + \phi_g \leq 270 \text{ deg} \tag{B10}$$

To impose the constraints defined by eq. (B10), we observe that

$$\phi_{s\delta} + \phi_g = \text{phase angle of} \left[\frac{1}{1 - \frac{1}{1-\Gamma} \left(\frac{\ddot{z}_c/\delta}{\ddot{z}_c/w_g} \right) \left(\frac{\ddot{z}_s/w_g}{\ddot{z}_s/\delta} \right)} \right] \tag{B11}$$

Defining

$$N = \frac{\left|\ddot{z}_c/\delta\right|}{\left|\ddot{Z}_c/w_g\right|}$$

$$V = \frac{\left|\ddot{z}_s/w_g\right|}{\left|\ddot{z}_s/\delta\right|}$$

$$\phi_1 = [\text{phase of } (\ddot{z}_c/\delta) - \text{phase of } (\ddot{z}_c/w_g)]$$

$$\phi_2 = [\text{phase of } (\ddot{z}_s/w_g) - \text{phase of } (\ddot{z}_s/\delta)]$$

and restricting $\phi_{s\delta} + \phi_g$ according to eq. (B9), we obtain a minimum attainable value on Γ, the attenuation factor:

$$\Gamma \geq 1 - VN \cos(\phi_1 + \phi_2) \tag{B12}$$

At any flight condition, N and ϕ_1 are defined for a given vehicle station. Thus, if we pick a quantity to be measured $(\ddot{z}_s)$, we can determine the lower bound on Γ (defined as Γ_{min}) in order to assure that the stability constraint, eq. (B10), is satisfied. That is:

$$\Gamma \geq \Gamma_{min} = 1 - VN \cos(\phi_1 + \phi_2) \tag{B13}$$

If we assign a value to Γ, say Γ_i, at a given frequency (ω_i), then we must find a quantity to be measured $(\ddot{z}_s)$, such that

$$\Gamma_i \geq \Gamma_{min}(\omega_i) \tag{B14}$$

or else we cannot simultaneously satisfy the stability constraint and provide the attenuation, $\Gamma = \Gamma_i$. The above condition is a necessary condition for specifying $\ddot{z}_s$, but it is not a sufficient condition.

2. To further specify the requirements for the quantity to be measured ($\ddot{z}_s$), it is necessary to examine other design objectives and analyze the practical constraints imposed on the filter $[K_c G(s)]$. The following design objective imposes a severe constraint on the type of filters and on $\ddot{z}_s$:

> Minimize unfavorable coupling with structural modes which lie above the frequency range of the modes to be controlled. To assure this objective is met, we impose the condition
>
> $$\left|\frac{\ddot{z}_s}{\delta}\right| \left| K_c G(s) \right| < 0.5$$
>
> at modal frequencies above the highest significant mode.

3. It is assumed the filter $[K_c G(s)]$ will be a linear filter made up of first- or second-order elements and that the poles of the filter will be stable. Thus, the design objective of high-frequency gain stabilization, for practical purposes, imposes an additional constraint on $K_c G(s)$. To meet this objective, the gain of the filter will be decreasing with increasing frequency at a rate of at least 6 dB per octave over the frequency range of the significant modes (for this argument assume the significant modes are the first three modes). From this, it becomes evident that if the same amount of attenuation (or more) is required at the second or third mode than as is required at the first mode frequency, then we impose

$$|K_i| \geq \left(\frac{f_i}{f_1}\right) |K_1| \quad \text{for } i = 2, 3$$

(where K_i is the i^{th} mode deflection) to compensate for the loss in gain due to the filter $[K_c G(s)]$. For gain stabilization of the fourth and higher modes (assuming three significant modes), it is generally desirable to minimize K_i for $i = 4, 5, \ldots$

4. A further consideration is the amount of phase or gain change with frequency required of the filter $[K_c G(s)]$. Sensor configurations should, in general, be chosen to minimize large phase or gain change requirements with frequency for the filter to facilitate the hardware implementation.

5. In some applications it is an objective to minimize the coupling with the rigid-body mode. This can be done by placing the sensor in a position

where the accelerations due to flexibility are the largest with respect to those due to rigid-body motions. The coupling can be further reduced by minimizing the gain of the filter at the rigid-body frequencies.

All of the above considerations enable one to essentially define the desired sensor complement, $\ddot{z}_s$. To summarize, the sensor complement should be chosen to satisfy the following constraints:

1) $\Gamma_{min} \leq \Gamma_i$

2) $|K_i| \geq \left(\frac{f_i}{f_1}\right) |K_1|$ for i = 2, 3 (assuming 3 significant modes)

3) Minimize variation in gain and phase changes with frequency required of the filter $[K_c G(s)]$

4) Minimize gain of sensor-filter combination at frequencies beyond significant structural modes

Once the quantity to be measured ($\ddot{z}_s$) has been defined (according to the above rules), realistic sensor locations and combinations of sensors can be examined to find one which will best provide $\ddot{z}_s$. With the actual sensor configuration defined, the filter requirements can be computed for that sensor configuration through the use of eq. (B4). Using these filter requirements, a practical filter can be designed. Finally, with the filter designed, the problem can be worked in reverse to check the "goodness" of the entire system. Thus, compromises in filter design can be analyzed to determine their effect on performance. It must be kept in mind that eq. (B4) does not have to be satisfied at all frequencies nor is its solution the only solution to the problem. Once a solution has been obtained, variations can be made on it to yield a possible better solution.

QUADRATIC OPTIMIZATION TECHNIQUE

Quadratic optimization techniques are derived from the concepts of modern control theory. Quadratic optimization differs from the more conventional servomechanism analysis of feedback control in that it is a procedure which is applied in the time domain rather than in the frequency domain. Optimal control synthesis is based on the notion of minimizing an analytical expression used as a measure of system performance. In quadratic optimization this expression, called the cost function, is a linear summation of quadratic elements. Each element represents a performance parameter to be minimized such as pilot's acceleration. Minimizing the cost function yields a set of gains on a linear combination of feedbacks which makes up the controller. The feedbacks, in the ideal case, include all the state variables (e. g., pitch rate, normal acceleration, etc.).

To use optimal theory, it is necessary to rewrite the equations of motion as a set of first-order linear differential equations. This set of first-order equations is referred to as the standard form. Reducing the equations to standard form generally varies from application to application. Details of this reduction for the YF-12A are described in subsequent paragraphs following the general description of quadratic optimization. The LAMS problem is treated as being statistical in nature. Hence, the equations of motion and the response equations are recast in terms of covariance equations. The response equations are simply linear combinations of state variables such as the output of an accelerometer located at some station on the vehicle. The standard form for the equations of motion and the response equations is as follows:

$$\dot{x}(t) = F\,x(t) + G_1\,u(t) + G_2\,\eta(t) \tag{B15}$$

$$r(t) = H\,x(t) + D\,u(t) \tag{B16}$$

where $x(t)$ is the state vector, $u(t)$ is the control vector, $r(t)$ is the response vector, and $\eta(t)$ is the white noise disturbance input. The terms F, G_1, G_2, H, and D are matrices defined by the aircraft dynamics.

To treat the problem statistically, the expected mean square values (covariances) for $x(t)$ and $r(t)$ are derived from eqs. (B15) and (B16). The following notation will be used:

$$\tilde{X}(t) = E\{x(t),\ x(t)^T\} = \text{expected value of } x(t)$$

$$\tilde{R}(t) = E\{r(t),\ r(t)^T\} = \text{expected value of } r(t)$$

Then, the state vector expected value for the system with no control $[u(t) = 0]$ satisfies the expression

$$\dot{\tilde{X}}(t) = F\,X(t) + \tilde{X}(t)F^T + G_2\,N\,G_2^T \tag{B17}$$

where

$$E\{\eta(t),\ \eta(t)^T\} = N\,\delta(t - \tau)$$

(δ is the Dirac delta function); and the response vector mean squared value satisfies the expression

$$\tilde{R}(t) = H^T\,\tilde{X}(t)\,H \tag{B18}$$

The optimal controller for a linear system is a linear combination of states,

$$u(t) = K\,x(t) \tag{B19}$$

Appendix B

The optimal control problem is that of selecting the set of gains, K, such that performance measure J* (the cost function)

$$J^* = E\{r(t)^T Q\, r(t)\} \tag{B20}$$

is minimized where

$$r(t) = (H + DK)\, x(t) \tag{B21}$$

for the controlled system. The solution is subject to the constraint

$$\dot{\tilde{X}} = (F + G_1 K)\tilde{X} + \tilde{X}(F + G_1 K)^T + G_2 N G_2^T = 0 \tag{B22}$$

The weighting matrix Q in eq. (B20) is diagonal and assigns the control emphasis to the desired responses.

The solution to the problem expressed by eqs. (B20) and (B22) is given as the solution to the two equations:

$$K = -(D^T Q D)^{-1} (D^T Q H + G_1^T S) \tag{B23}$$

$$\dot{S} = (F + G_1 K)^T S + S(F + G_1 K) + (H + D K)^T Q(H + D K) \tag{B24}$$

where S is a matrix of Lagrange multipliers.

Taken together, these equations represent the matrix Riccati equation. For the LAMS program, eqs. (B23) and (B24) were solved by converting them to difference equations and then computing S and K iteratively until the gains converged to a steady-state value.

Reduction to Standard Form

The vehicle equations of motion described in Appendix A must be reduced to standard form in order to apply quadratic optimization. This procedure as it applies to the YF-12A is described in the following paragraphs.

The equations of motion without the baseline SAS, as given in Appendix A, eq. A29, are given below in the frequency domain as:

$$\left\{\hat{M}\, s^2 + \left[1 - \frac{a_1 s}{s + \hat{b}_1}\right]\left(\hat{A}_{Z_1} s + \hat{A}_{\theta_1}\right) + \hat{A}s + \hat{B}\right\}\left\{r(s)\right\}$$

$$= \left\{\hat{A}_{\delta_1}\right\}\delta_1 + \left\{\hat{A}_{\delta_2}\right\}\delta_2 + \left[1 - \frac{s}{s + \hat{b}_2}\right]\left\{\hat{A}_{g_1}\right\} W_g + \left\{\hat{A}_{g_2}\right\} W_g$$

$$+ \begin{cases} \left\{\hat{A}_c\right\}\delta_3 & \text{for canard controller} \\ \text{or} & \\ s^2\left\{\hat{A}_m\right\}\delta_m & \text{for mass reaction controller} \end{cases}$$

The above equation can be rewritten in the time domain as:

$$\hat{M}\,\ddot{r}(t) + \hat{C}\,\dot{r}(t) + \hat{E}\,r(t) - \hat{A}_{z_1} K(t)*\ddot{r}(t) - \hat{A}_{\theta_1} K(t)*\dot{r}(t)$$

$$= \hat{A}_{\delta_1}\delta_1(t) + \hat{A}_{\delta_2}\delta_2(t) + \hat{A}_{g_1}\psi(t)*\dot{w}_g + \hat{A}_{g_2} w_g \qquad \text{(B25)}$$

$$+ \begin{cases} \hat{A}_c\,\delta_3(t) & \text{for the canard controller} \\ \text{or} & \\ \hat{A}_m\,\ddot{\delta}_m(t) & \text{for mass reaction controller} \end{cases}$$

where

$$\hat{C} = \hat{A} + \hat{A}_{Z_1}$$

$$\hat{E} = \hat{A}_{\theta_1} + \hat{B}$$

$$K(t) = a_1 e^{-\hat{b}_1 t}$$

$$\psi(t) = e^{-\hat{b}_2 t}$$

* denotes the convolution operator

$$r^T = \lfloor w_o,\ \dot{\theta}_o,\ r_3,\ \ldots,\ r_{18} \rfloor$$

By the introduction of new state variables, eq. (B25) can be put into the required standard form. The state variable forms of the convolutions appearing in eq. (B25), as well as the transformation of the gust, elevon, canard, and mass reaction device transfer functions to the desired form, are outlined below.

State variable form of the convolutions. - Let $p = \lfloor p_1, \ldots, p_{18} \rfloor^T$ and p_{19} be new state variables defined as follows:

$$p = K(t)* \dot{r}(t) = \dot{K}(t) * r(t) = - a_1 \hat{b}_1 \int_0^t e^{-\hat{b}_1(t-\tau)} r(\tau)\, d\tau \tag{B26}$$

One can readily see that p is a solution of the first-order differential equation

$$\dot{p} = \hat{b}_1 p - a_1 \hat{b}_1 r \tag{B27}$$

Since $k(t)*\ddot{r}(t) = -\hat{b}_1 p$, the terms of eq. (B25) involving the convolutions $K(t)*\ddot{r}(t)$ and $K(t) * \dot{r}(t)$ can be written as

$$-\hat{A}_{z_1} K(t)*\ddot{r}(t) - \hat{A}_{\theta_1} K(t)*\dot{r}(t) = \left(\hat{A}_{z_1} - \hat{A}_{\theta_1}\right)_p = T_p \tag{B28}$$

In a similar manner, the state equation governing $\psi(t)*\dot{w}_g(t)$ is found to be

$$\dot{p}_{19} = \hat{b}_2 p_{19} - \hat{b}_2 w_g(t) \tag{B29}$$

where

$$p_{19} = \psi(t)*\dot{w}_g(t)$$

Thus

$$A_{g_1} \psi(t) * \dot{w}_g(t) = A_{g_1} p_{19} \tag{B30}$$

Eqs. (B27), (B28), (B29), and (B30) define the transformation of the convolutions in eq. (B25) into the desired form.

State variable form of the gust function. - The gust transfer function given in Appendix A, eq. (A36), has the form:

$$w_g(s) = \sqrt{\frac{3V_o}{L}} \; \frac{\left(s + \frac{V_o}{\sqrt{3}\,L}\right)}{\left(s + \frac{V_o}{L}\right)^2} \; \eta(s) \tag{B31}$$

One can easily verify that $w_g(s)$ is a solution of the following second-order differential equation:

$$\ddot{w}_g(t) + 2\left(\frac{V_o}{L}\right)\dot{w}_g(t) + \left(\frac{V_o}{L}\right)^2 w_g(t) = \sqrt{\frac{3V_o}{L}}\left[\dot{\eta}(t) + \frac{V_o}{\sqrt{3}\,L}\,\eta(t)\right] \tag{B32}$$

By introducing a new state variable, p_{20}, eq. (B32) can be placed in the desired standard form as:

$$\dot{w}_g(t) = -2\,\frac{V_o}{L}\,w_g(t) + p_{20} + \sqrt{\frac{3V_o}{L}}\,\eta(t) \tag{B33}$$

where p_{20} satisfies

$$\dot{p}_{20} = -\left(\frac{V_o}{L}\right)^2 w_g(t) + \frac{V_o}{L}\sqrt{\frac{V_o}{L}}\,\eta(t) \tag{B34}$$

State variable form of the elevon equations of motion. - The transfer function for the inboard elevon is shown in Figure B2. Upon inspection, one finds the governing differential equation for $\delta_1(t)$ to be:

$$\ddot{\delta}_1 = -50.5\,\dot{\delta}_1 - 1568\,\delta_1 + 1568\,u_1 + 1568\,(p_{21} + p_{24}) \tag{B35}$$

where u_1 is the control input to the inboard elevon and $(p_{21} + p_{24})$ is the SAS input to the inboard elevon.

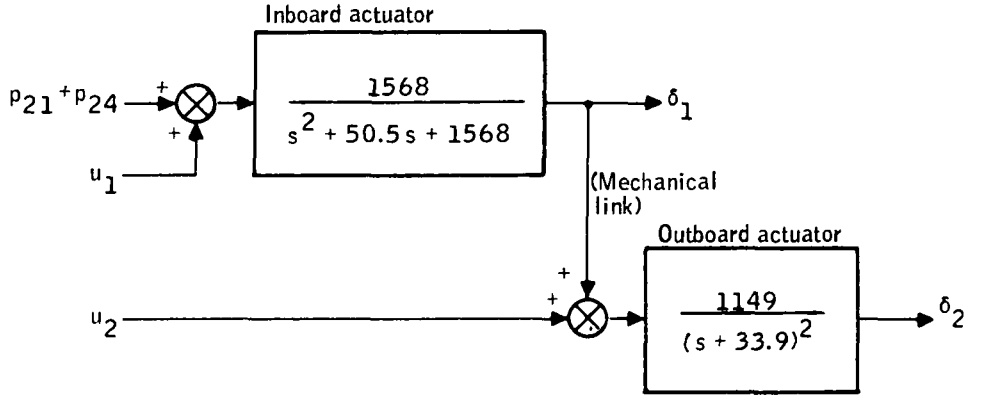

Figure B2. Inboard/Outboard Elevon Actuator Block Diagram

The governing differential equations for the outboard elevon system fall into two separate cases. The first case deals with the standard system with only an additional control input, u_3, to the outboard actuator. The governing differential equation for this case is readily determined from Figure B2 as:

$$\ddot{\delta}_2 = -67.8\,\dot{\delta}_2 - 1149\,\delta_2 + 1149\,\delta_1 + 1149\,u_2 \tag{B36}$$

The transfer function for the second case is shown in Figure B3. This system is designed to allow independent operation of the inboard and outboard elevon system by canceling the mechanical linkage input of δ_1 to the outboard actuator. The differential equation for $\delta_2(t)$ is found to be:

$$\begin{aligned} \ddot{\delta}_2 &= -67.8\,\dot{\delta}_2 - 1149\,\delta_2 + 1149\,p_{23} + 1149\,u_2 \\ \dot{p}_{23} &= p_{22} \\ \dot{p}_{22} &= -50.5\,p_{22} - 1568\,p_{23} + 1568\,(p_{21} + p_{24}) \end{aligned} \tag{B37}$$

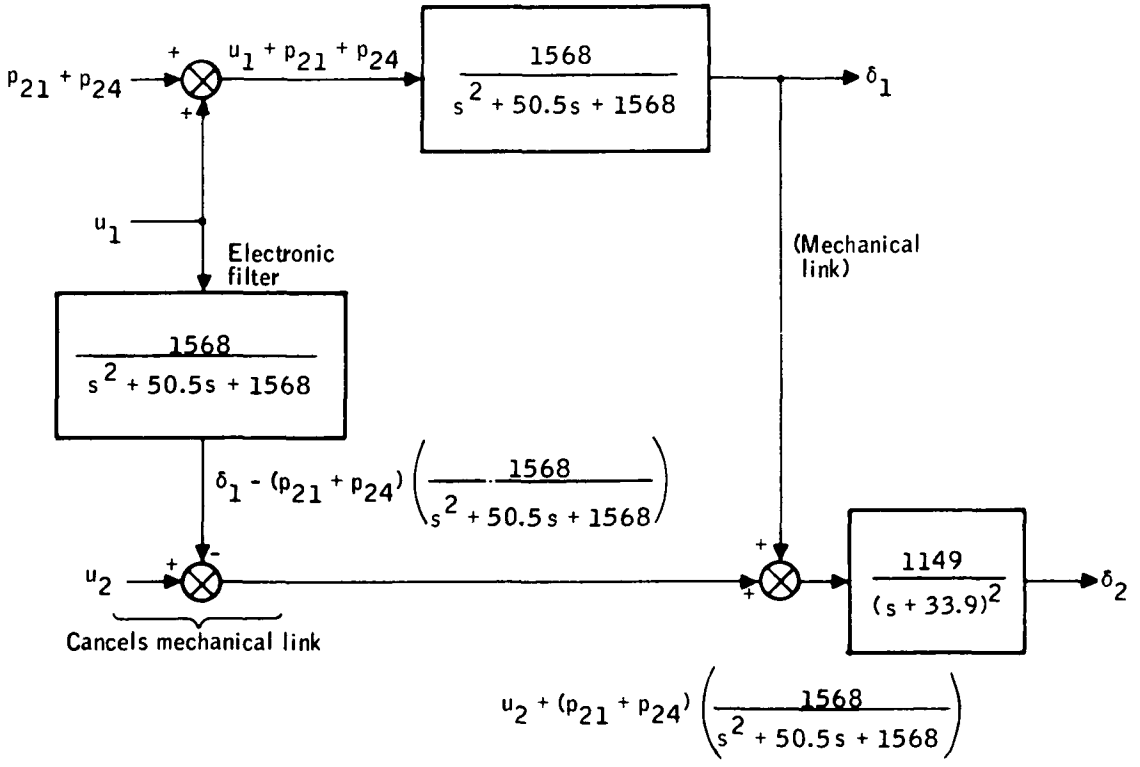

Figure B3. Electronic Cancellation of Mechanical Linkage

Canard and mass-reaction device state equations. - The canard actuator state equation for the optimal control studies was defined to be:

$$\dot{\delta}_3 = 30\,\delta_3 + 30\,u_3 \tag{B38}$$

where u_3 is the control input into the canard actuator.

The dynamics for the mass-reaction device were defined as:

$$\ddot{\delta}_m = -2\,\dot{\delta}_m - 4\,\delta_m - 4\,u_m \tag{B39}$$

where u_m is the control input to the actuator.

Baseline pitch SAS state equations. - The transfer function for the baseline pitch SAS is shown in Figure B4. For the frequency range of interest in this study, one can neglect the rate gyro and servo dynamics. For F/Cs 1, 1A, and 3, one has the following differential equation for the SAS output, p_{21}:

$$\dot{p}_{21} = 0.49\,\delta_{\dot{\theta}}\,\ddot{\theta}_o + 3.94\,\delta_{\dot{\theta}}\,\dot{\theta} + 0.49\,\delta_{\dot{\theta}} \sum_{j=1}^{16} \phi_j'(\ddot{r}_{j+2} + \dot{r}_{j+2}) - 3.94\,p_{21} \tag{B40}$$

where

$\delta_{\dot{\theta}}$ = scheduled gain

ϕ_j' = slope of j^{th} mode shape at the rate gyro location

r_j = j^{th} generalized coordinate in eq. (B25)

For the above flight conditions, $p_{24} \equiv 0$.

For F/C 2, the SAS output has an additional term, p_{24}, corresponding to the lagged pitch rate path in Figure B4. The governing state equations for p_{24} are:

$$\dot{p}_{25} = 4.006\,\ddot{\theta}_o + 4.006\,\dot{\theta}_o + 4.006 \sum_{j=1}^{16} \phi_j'(\ddot{r}_{j+2} + \dot{r}_{j+2}) - 10.49\,p_{25} - 0.8012\,p_{24} \tag{B41}$$

$$\dot{p}_{24} = p_{25}$$

where θ_o, ϕ_j' and r_j are defined as before.

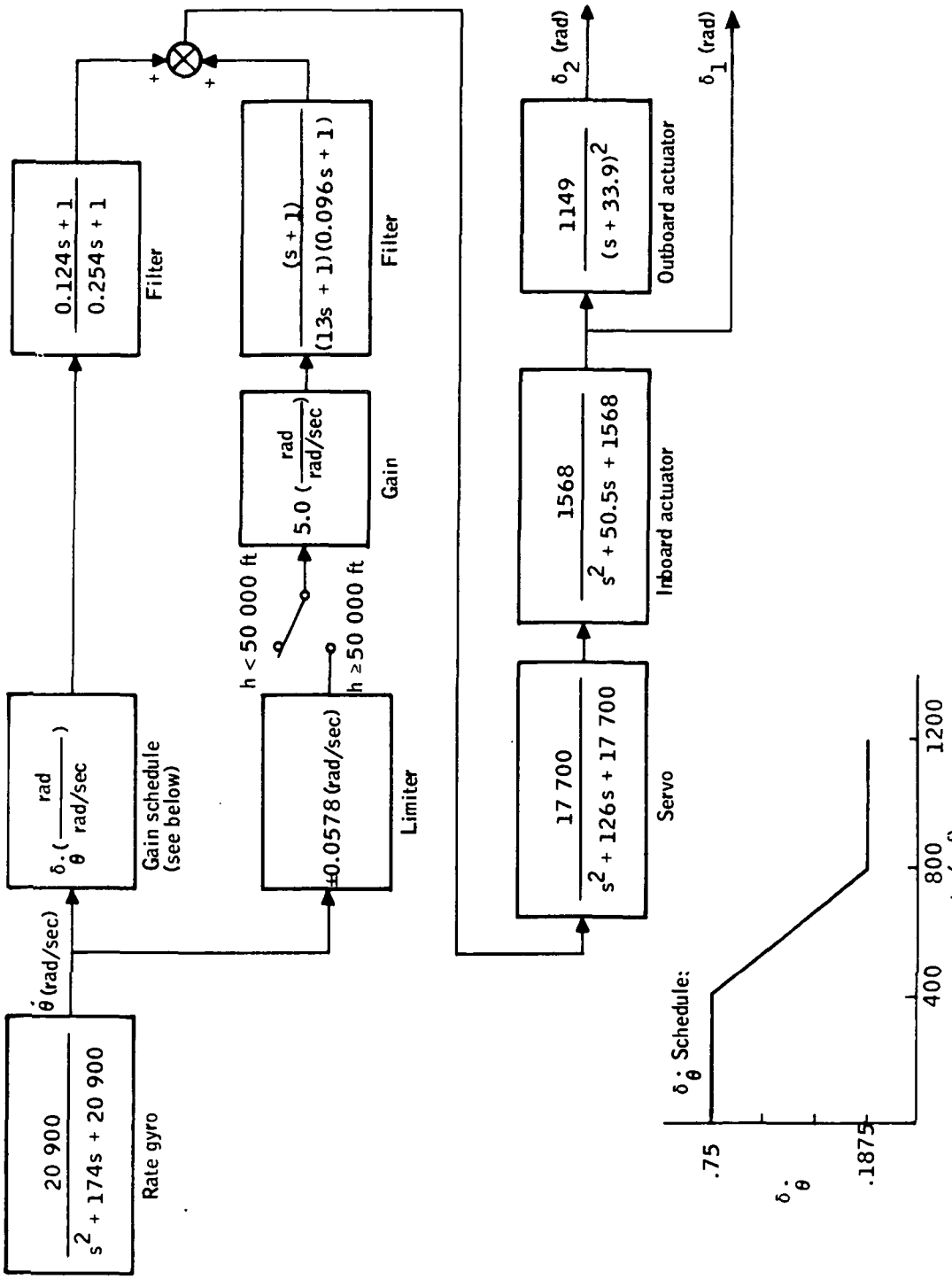

Figure B4. YF-12A Baseline SAS Block Diagram

Total state vector and state equations. - Using the new state variables and associated state equations defined in the preceding sections, eq. (B25) can be readily transformed into the required form using standard techniques. Thus, the form of the state equations becomes:

$$\dot{x} = Fx + G_1 u + G_2 \eta \tag{B42}$$

where $x^T = \lfloor w,\ \dot{\theta},\ \dot{r}_2, \ldots, \dot{r}_{18},\ r_2, \ldots, r_{18},\ p_1, \ldots, p_{20},\ w_g,$

$\dot{\delta}_1,\ \delta_1,\ \dot{\delta}_2,\ \delta_2,\ p_{22},\ p_{23},\ \delta_3,\ \dot{\delta}_m,\ \delta_m \rfloor$

$u^T = \lfloor u_1,\ u_2,\ u_3,\ u_m \rfloor$

η = white noise

One notes that in the above state vector, states p_{21}, p_{24}, and p_{25} are missing. These states are associated with the SAS and will be added after the feedback states have been transformed into accelerations and rates. Further observation shows that both the canard and mass-reaction state equations appear in eq. (B42). For any of the problems considered in this study, at most one of these devices will be used, and hence eq. (B42) must be modified to reflect this at the time of its use.

Transformation of the feedback states. - It is desired that the feedback states be velocities and accelerations rather than displacements and velocities. The following transformation will accomplish this objective but is different for the case of a mass-reaction control instead of a canard control. Thus, it is necessary to state two transformations, and hence we shall define two new state vectors and the associated state equations.

Let

$$\left[x^{(1)}\right]^T = \lfloor \dot{\theta}_o,\ w_o,\ \dot{r}_3, \ldots, \dot{r}_{18},\ r_3, \ldots, r_{18},\ p_1, \ldots, p_{20},$$

$$w_g,\ \dot{\delta}_1,\ \delta_1,\ \dot{\delta}_2,\ \delta_2,\ p_{22},\ p_{23},\ \delta_3 \rfloor \tag{B43}$$

be the state vector without the mass-reaction control satisfying the equation

$$x^{(1)} = F^{(1)} x^{(1)} + G_1^{(1)} u^{(1)} + G_2^{(1)} \eta \tag{B44}$$

where $F^{(1)}$, $G_1^{(1)}$, $G_2^{(1)}$ are the same as F, G_1, G_2 with columns and rows 1 and 2 interchanged along with the removal of the states and equations associated with the mass-reaction device. The $\left[u^{(1)}\right]^T$ term in this case is just $\lfloor u_1,\ u_2,\ u_3 \rfloor$.

Similarly, let

$$[x^{(2)}]^T = \lfloor \dot{\theta}_o,\ w_o,\ \dot{r}_3, \ldots,\ \dot{r}_{18},\ r_3, \ldots,\ r_{18},\ p_1, \ldots,\ p_{20},$$
$$w_g,\ \dot{\delta}_1,\ \delta_1,\ \dot{\delta}_2,\ \delta_2,\ p_{23},\ p_{24},\ \dot{\delta}_m,\ \delta_m \rfloor \tag{B45}$$

be the state vector for the system without the canard but including the mass-reaction control satisfying the equation

$$\dot{x}^{(2)} = F^{(2)}\, x^{(2)} + G_1^{(2)} + G_2^{(2)}\, \eta \tag{B46}$$

where $F^{(2)}$, $G_1^{(2)}$, $G_2^{(2)}$ are the same as F, G_1, G_2 with rows and columns 1 and 2 interchanged along with the removal of the canard states and equations. The $[u^{(2)}]^T$ term thus becomes

$$[u^{(2)}]^T = \lfloor u_1,\ u_2,\ u_m \rfloor$$

The transformation for the system with a canard controller is developed by first partitioning the state vector $x^{(1)}$ as follows:

$$x^{(1)} = (X,\ Y,\ Z) \tag{B47}$$

where

$$X = \dot{\theta}_o$$
$$Y^T = \lfloor w_o,\ \dot{r}_3, \ldots,\ \dot{r}_{18},\ r_3, \ldots,\ r_{18} \rfloor$$
$$Z^T = \lfloor p_1, \ldots,\ p_{20},\ w_g,\ \dot{\delta}_1,\ \delta_1,\ \dot{\delta}_2,\ \delta_2,\ p_{22},\ p_{23},\ \delta_3 \rfloor \tag{B48}$$

Thus, the governing differential equation for this system can be written as:

$$\begin{Bmatrix} \dot{X} \\ \dot{Y} \\ \dot{Z} \end{Bmatrix} = \begin{bmatrix} F_{11} & F_{12} & F_{13} \\ F_{21} & F_{22} & F_{23} \\ F_{31} & F_{32} & F_{33} \end{bmatrix} \begin{Bmatrix} X \\ Y \\ Z \end{Bmatrix} + \begin{bmatrix} 0 \\ 0 \\ G_{13} \end{bmatrix} \{u^{(1)}\} + \begin{Bmatrix} 0 \\ 0 \\ G_{23} \end{Bmatrix} \eta \tag{B49}$$

Now

$$\begin{Bmatrix} X \\ \dot{Y} \\ Z \end{Bmatrix} = \begin{bmatrix} I & O & O \\ F_{21}^{(1)} & F_{22}^{(1)} & F_{23}^{(1)} \\ O & O & I \end{bmatrix} \begin{Bmatrix} X \\ Y \\ Z \end{Bmatrix} = \begin{bmatrix} \\ TF^{(1)} \\ \\ \end{bmatrix} \begin{Bmatrix} X \\ Y \\ Z \end{Bmatrix} \tag{B50}$$

and

$$\begin{Bmatrix} \dot{X} \\ \ddot{Y} \\ \dot{Z} \end{Bmatrix} = \begin{bmatrix} \\ TF^{(1)} \\ \\ \end{bmatrix} \begin{Bmatrix} \dot{X} \\ \dot{Y} \\ \dot{Z} \end{Bmatrix}$$

$$= \begin{bmatrix} \\ TF^{(1)} \\ \\ \end{bmatrix} \begin{bmatrix} \\ F^{(1)} \\ \\ \end{bmatrix} \begin{bmatrix} \\ TF^{(1)} \\ \\ \end{bmatrix}^{-1} \begin{Bmatrix} X \\ \dot{Y} \\ Z \end{Bmatrix} + \begin{bmatrix} O & \\ F_{23}^{(1)} & G_{13} \\ & G_{13} \end{bmatrix} \{u^{(1)}\} + \begin{Bmatrix} O & \\ F_{23}^{(1)} & G_{23} \\ & G_{23} \end{Bmatrix} \eta \tag{B51}$$

or

$$\dot{x}_{new}^{(1)} = F_{new}^{(1)} x_{new}^{(1)} + G1_{new}^{(1)} u^{(1)} + G2_{new}^{(1)} \eta \tag{B52}$$

where

$$\left[x_{new}^{(1)}\right]^T = \lfloor \dot{\theta}_o,\ \dot{w}_o,\ \ddot{r}_3, \ldots,\ \ddot{r}_{18},\ \dot{r}_3, \ldots,\ \dot{r}_{18},\ p_1, \ldots,\ p_{20},$$
$$w_g,\ \dot{\delta}_1,\ \delta_1,\ \dot{\delta}_2,\ \delta_2,\ p_{22},\ p_{23},\ \delta_3 \rfloor \tag{B53}$$

and $F_{new}^{(1)}$, $G1_{new}^{(1)}$, $G2_{new}^{(1)}$ are defined by eqs. (B51) and (B52).

The transformation for the system with a mass-reaction controller is achieved by first partitioning the state vector $x^{(2)}$ as follows, where:

$$X = \dot{\theta}$$

$$Y^T = \lfloor w_o,\ \dot{r}_3, \ldots,\ \dot{r}_{18},\ r_3, \ldots,\ r_{18} \rfloor \tag{B54}$$

$$Z^T = \lfloor p_1, \ldots, p_{20},\ w_g,\ \dot{\delta}_1,\ \delta_1,\ \dot{\delta}_2,\ \delta_2,\ p_{22},\ p_{23},\ \dot{\delta}_m,\ \delta_m \rfloor$$

One notes that when the mass-reaction control is used in the system, the matrix $G_1^{(2)}$ contains elements in the first 18 rows that do not appear in $G_1^{(1)}$.

Thus, we now write:

$$G_1^{(2)} = \begin{matrix} \\ \\ \\ \end{matrix} \begin{matrix} u_1, u_2 \\ \\ \\ \end{matrix} \begin{bmatrix} O & G_{11m}^{(2)} \\ O & G_{12m}^{(2)} \\ G_{13}^{(2)} & G_{13m}^{(2)} \end{bmatrix} \begin{matrix} \\ \\ \\ \end{matrix} \begin{matrix} u_m \\ \\ \\ \end{matrix} = \left[\begin{array}{c:c} \hat{G}_1^{(2)} & \begin{matrix} G_{1m}^{(2)} \\ \\ \end{matrix} \end{array}\right] \tag{B55}$$

Thus, the state equation becomes:

$$\begin{Bmatrix} \dot{X} \\ \dot{Y} \\ \dot{Z} \end{Bmatrix} = \begin{bmatrix} F_{11}^{(2)} & F_{12}^{(2)} & F_{13}^{(2)} \\ F_{21}^{(2)} & F_{22}^{(2)} & F_{23}^{(2)} \\ F_{31}^{(2)} & F_{32}^{(2)} & F_{33}^{(2)} \end{bmatrix} \begin{Bmatrix} X \\ Y \\ Z \end{Bmatrix} + \left[\begin{array}{c:c:c} \hat{G}_1^{(2)} & \begin{matrix} G_{11m} \\ G_{12m} \\ \end{matrix} & \begin{matrix} \\ \\ G_{13m} \end{matrix} \end{array}\right] \begin{Bmatrix} \begin{Bmatrix} u_1 \\ u_2 \end{Bmatrix} \\ u_m \end{Bmatrix} + \begin{Bmatrix} O \\ O \\ G_{23}^{(2)} \end{Bmatrix} \eta \tag{B56}$$

One now solves for $\begin{Bmatrix} X \\ Y \\ Z \end{Bmatrix}$ and obtains

$$\begin{Bmatrix} X \\ Y \\ Z \end{Bmatrix} = \begin{bmatrix} I & O & O \\ F_{21}^{(2)} & F_{22}^{(2)} & F_{23}^{(2)} \\ O & O & I \end{bmatrix}^{-1} \begin{Bmatrix} X \\ \dot{Y} \\ Z \end{Bmatrix} + \begin{bmatrix} I & O & O \\ F_{21}^{(2)} & F_{22}^{(2)} & F_{23}^{(2)} \\ O & O & I \end{bmatrix}^{-1} \begin{bmatrix} O \\ G_{12m} \\ O \end{bmatrix} u_m \tag{B57}$$

Let

$$TF^{(2)} = \begin{bmatrix} I & O & O \\ F_{21}^{(2)} & F_{22}^{(2)} & F_{23}^{(2)} \\ O & O & I \end{bmatrix} \tag{B58}$$

Thus:

$$\begin{Bmatrix} \dot{X} \\ \ddot{Y} \\ \dot{Z} \end{Bmatrix} = \begin{bmatrix} TF^{(2)} \end{bmatrix} \begin{bmatrix} F^{(2)} \end{bmatrix} \begin{bmatrix} TF^{(2)} \end{bmatrix}^{-1} \begin{Bmatrix} X \\ \dot{Y} \\ Z \end{Bmatrix}$$

$$+ \begin{bmatrix} TF^{(2)} \end{bmatrix} \begin{bmatrix} F^{(2)} \end{bmatrix} \begin{bmatrix} TF^{(2)} \end{bmatrix}^{-1} \begin{Bmatrix} 0 \\ G_{12m} \\ 0 \end{Bmatrix} u_m \tag{B59}$$

$$+ \begin{bmatrix} TF^{(2)} \end{bmatrix} \begin{bmatrix} O \\ O \\ G_{13}^{(2)} \end{bmatrix} \begin{Bmatrix} u_1 \\ u_2 \end{Bmatrix} + \begin{bmatrix} TF^{(2)} \end{bmatrix} \begin{Bmatrix} G_{11m} \\ G_{12m} \\ G_{13m} \end{Bmatrix} u_m$$

$$+ \begin{bmatrix} TF^{(2)} \end{bmatrix} \begin{bmatrix} 0 \\ 0 \\ G_{23}^{(1)} \end{bmatrix} \begin{Bmatrix} u_1 \\ u_2 \end{Bmatrix} + \begin{Bmatrix} O \\ G_{12m} \\ O \end{Bmatrix} \dot{u}_m$$

The above state equation can be simplified by adding $\dot{u}_m$ as a state and letting $\dot{u}_m$ be a control. Thus, one obtains the following state equation:

$$\begin{Bmatrix} \dot{X} \\ \ddot{Y} \\ \dot{Z} \\ \dot{u}_m \end{Bmatrix} = \left[\begin{array}{c|cc} \hat{F} & \hat{F} \begin{Bmatrix} 0 \\ G_{12m} \\ 0 \end{Bmatrix} + \begin{bmatrix} TF^{(2)} \end{bmatrix} \begin{Bmatrix} G_{11m} \\ G_{12m} \\ G_{13m} \end{Bmatrix} \\ \hline 0 \ldots\ldots\ldots\ldots\ldots\ldots 0 \end{array}\right] \begin{Bmatrix} X \\ \dot{Y} \\ Z \\ u_m \end{Bmatrix}$$

$$+ \left[\begin{array}{cc|c} 0 & & 0 \\ F_{23}^{(2)} & G_{12}^{(2)} & G_{12m} \\ G_{13}^{(2)} & & 0 \\ \hline 0 & & 1 \end{array}\right] \left\{ \begin{Bmatrix} u_1 \\ u_2 \end{Bmatrix} \right\} + \begin{Bmatrix} 0 \\ F_{23}^{(2)} \\ G_{23}^{(2)} \end{Bmatrix} \begin{matrix} G_{23}^{(2)} \end{matrix} \eta \qquad \text{(B60)}$$

where

$$\hat{F} = \left[TF^{(2)}\right] \left[F^{(2)}\right] \left[TF^{(2)}\right]^{-1}$$

Thus, the new state equation becomes:

$$\dot{x}_{new}^{(2)} = F_{new}^{(2)} \; x_{new}^{(2)} + G_{1\,new}^{(2)} \; u_{new}^{(2)} + G_{2\,new} \eta \qquad \text{(B61)}$$

where

$$(x_{new}^{(2)})^T = \lfloor \dot{\theta}_o, \dot{w}_o, \ddot{r}_3, \ldots, \ddot{r}_{18}, \dot{r}_3, \ldots, \dot{r}_{18}, p_1, \ldots, p_{20},$$
$$w_g, \dot{\delta}_1, \delta_1, \dot{\delta}_2, \delta_2, p_{22}, p_{23}, \dot{\delta}_m, \delta_m, u_m \rfloor \qquad \text{(B62)}$$

and

$$(u_{new}^{(2)})^T = \lfloor u_1, u_2, \dot{u}_m \rfloor \qquad \text{(B63)}$$

Once the system has been transformed, the SAS states which are functions of $\ddot{\theta}_o$, $\ddot{r}_i$ and $\dddot{r}_i$ can easily be appended. The remaining task is to derive the response equations.

Appendix B

Description of the response equations. - The response equation used in the optimal control analysis is of the form

$$\hat{r} = Hx + Du \tag{B64}$$

where x is the state vector and u is the controller.

The desired responses, used in the study, are the vertical accelerations in g at FS 248, FS 738, and FS 1236 at WS32, along with the control vector. The vertical accelerations at the above points are given by:

$$n_{z_j} = \frac{1}{386}\left\{\dot{w}_o - V\dot{\theta}_o + \bar{x}_j\ddot{\theta} + \sum_{i=1}^{16}\phi_{i_j}\ddot{r}_{i+2}\right\} j = 4, 8, 16 \tag{B65}$$

where

$\bar{x}_j$ = distance in inches from the j^{th} station to the reference point, FS 900, and is negative for points forward of FS 900

ϕ_{i_j} = deflection at station j in the i^{th} elastic mode

The desired response vector is of the form:

$$(\hat{r})^T = \lfloor n_{z_4}, n_{z_8}, n_{z_{16}}, u_1, u_2, u_3 \text{ or } u_m \rfloor \tag{B66}$$

Hence, from the definition of r and n_{z_j}, one can form the matrix equation

$$\hat{r} = Hx + Du \tag{B67}$$

Optimal practicalization technique. - In previous LAMS applications the feedbacks specified in the optimal controllers included not just the mode feedbacks (including the rigid-body mode) but also the actuator states and the wind model states. Since the wind model states are not truly measurable, it was desirable to eliminate these feedbacks from the optimal controllers. Furthermore, it was desirable to generate optimal controllers which also did not contain some of the measurable feedbacks such as the rigid-body modes. To provide this increased flexibility in the optimization program, an additional optimization procedure was applied. This procedure is referred to as the practicalization procedure. It is used to drive the gains associated with the undesirable feedbacks to zero. A suboptimal controller is achieved by integrating a parameter, λ, from 1 to 0 in the equation:

$$K(\lambda) = K_1(\lambda) + \lambda K_2 \tag{B68}$$

while minimizing the cost J*. In the term $[K(\lambda)]$, $K_1(\lambda)$ includes the gains on those feedbacks to be retained, and K_2 includes those gains on the feedbacks

to be discarded. This is done by computing $dK_1/d\lambda$ using the implicit function theorem and numerical integration techniques. This practicalization scheme was used successfully in the Phase I study and is considered as a valuable tool.

Integration of synthesis techniques. -- Application of quadratic optimization techniques yields a controller which provides the required allocation of control effort among the force producers. To reiterate, however, the disadvantage of the technique is that the feedbacks are specified in terms of the state variables, rather than in terms of practical sensor outputs (e. g., accelerometer or rate gyro). The remaining task, then, is to make the transformation from state variable feedbacks to feedbacks from sensor outputs. The sensor output signals are simply linear combinations of the state variables and each combination is determined by the sensor location on the vehicle.

There are two schemes which can be used to make the transformation from state variable feedbacks to feedbacks from practical sensors. The first scheme consists of the following four steps:

1. Eliminate force producer crossfeed signals. For example, eliminate outboard elevon deflection and rate signals into the inboard elevon controller and vice versa. This is achieved by a simple matrix transformation which results in establishing filtering on each force producer input.

2. Eliminate insignificant state variable feedbacks. This is achieved by computing frequency responses of each feedback variable for a force producer input. The frequency responses are then compared with each other and with unity to determine their relative significance. This analysis is illustrated in Figure B5. The insignificant feedbacks are eliminated and stability is checked with the remaining feedbacks.

3. Reorganize remaining state variable feedbacks into groups so that each group is a linear combination of variables resembling a rate gyro or accelerometer output.

4. For each group in Step 3, find a sensor combination which will yield similar coefficients on the state variables. This is largely a trial and error procedure. One can always use as many sensors as there are state variables in each group and compute an ideal blend of the sensors. In most cases, however, this is not practical, especially when tolerance to parameter variations is taken into account.

The second scheme for transforming from state variable feedbacks to practical sensor feedbacks is to use the frequency response synthesis technique. In this scheme, the attenuation factors, Γ_i, required in the frequency

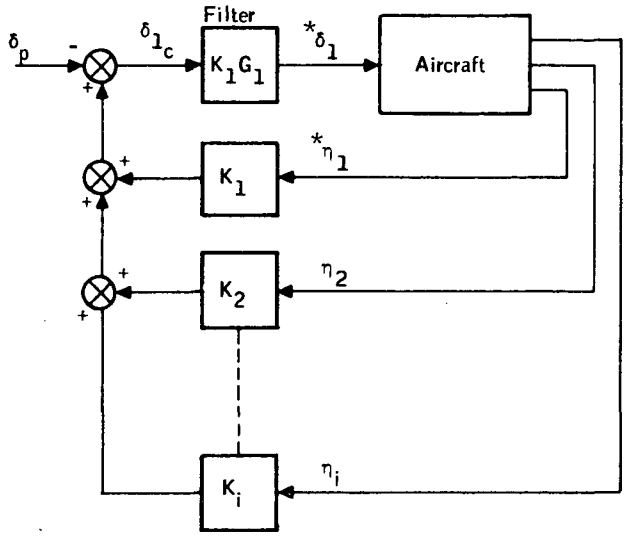

$*\delta_1$ = force producer deflection

$*\eta_i$ = state variable

$$\frac{\delta_{1_c}}{\delta_p} = \frac{1}{1 + [K_1(\frac{\eta_1}{\delta_1}) + K_2(\frac{\eta_2}{\delta_1}) + \cdots K_i(\frac{\eta_i}{\delta_1})]K_1G_1}$$

Figure B5. Elimination of State Variable Feedbacks

response technique are computed using the optimal control system. This, in essence, establishes the desired allocation of control effort which is lacking in the frequency response technique. Having computed the Γ_i's, the frequency response technique is applied to synthesize a control system. The force producer crossfeed signals in the optimal controller must be eliminated prior to computing the Γ_i's. The method used to compute the Γ_i's using the optimal controller is outlined in the following paragraphs.

In order to use the frequency response technique in the synthesis of optimal controller, it is necessary to make the appropriate transformations from the optimal controller transfer functions, (δ_i / w_g), all loops closed, to a form compatible with the frequency response technique as described in this appendix. Essentially, this means finding the appropriate Γ's at the frequencies of interest, such as the resonant peaks.

The inboard/outboard elevon controller of Figure B6 shows the corresponding terms of the optimal controller and the frequency response techniques where:

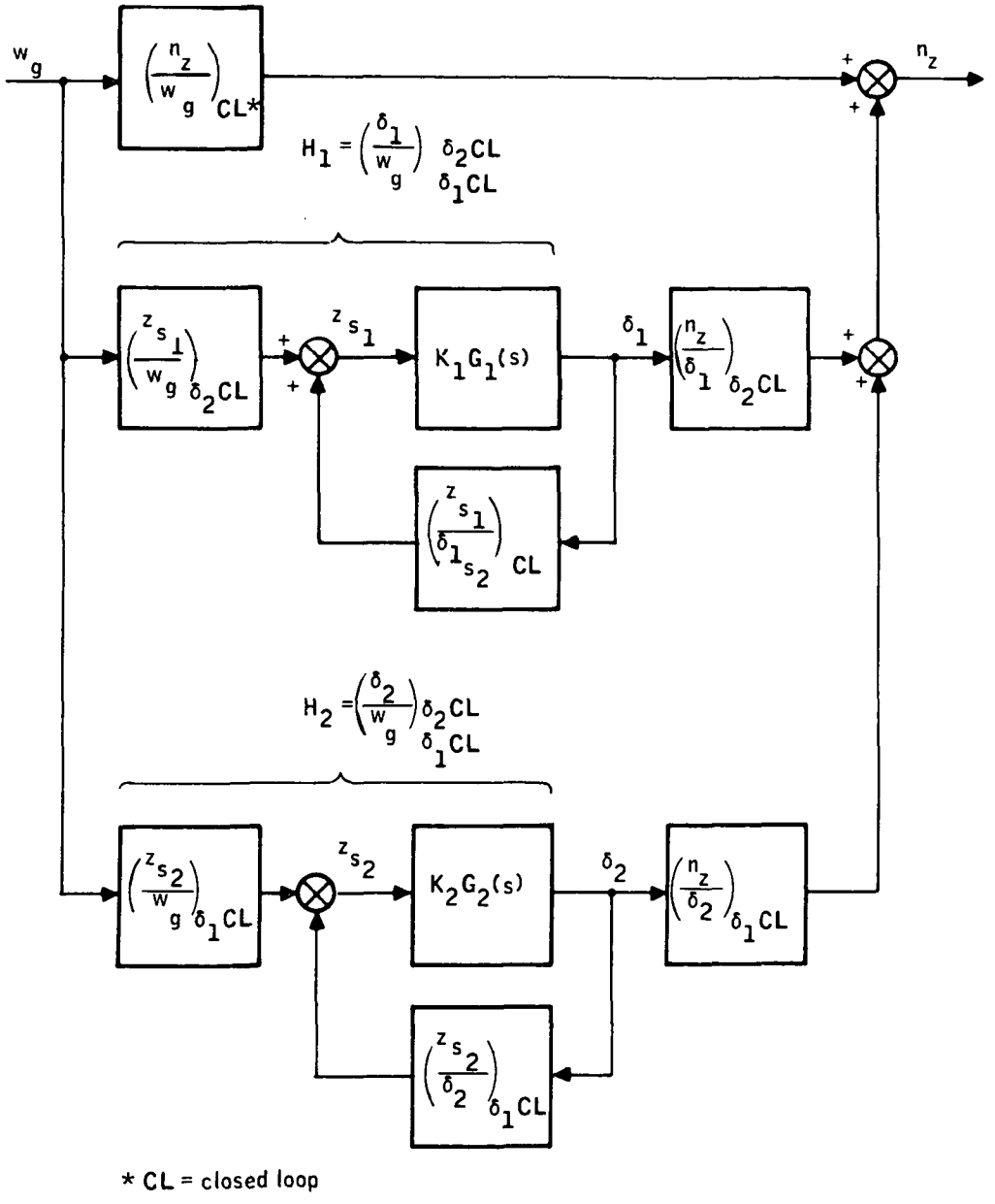

Figure B6. Inboard/Outboard Elevon Controller Dynamics General Block Diagram

- H_1 and H_2 are the transfer functions obtained from the optimization.
- G_1 and G_2 are the filters of the frequency response technique with their respective sensors, z_{s1} and z_{s2}.

The equations presented below are those for the δ_1 controller, but similar equations can be derived for the δ_2 loop.

From Figure B6, it can be seen that

$$H_1 = \left(\frac{z_{s1}}{w_g}\right)_{\delta_2 CL} \left[\frac{K_1 G_1(s)}{1 - K_1 G_1(s)\left(\frac{z_{s1}}{\delta_1}\right)_{\delta_2 CL}}\right] \tag{B69}$$

or by solving for $G_1(s)$

$$K_1 G_1(s) = \left(\frac{1}{z_{s1}/\delta_1}\right)_{\delta_2 CL} \left[\frac{1}{1 + \frac{1}{H_1}\left\{\frac{\left(z_{s1}/w_g\right)}{\left(z_{s1}/\delta_1\right)}\right\}_{\delta_2 CL}}\right] \tag{B70}$$

There is also a stability constraint on the above equation as evident from Figure B6. The stability of the δ_1 loop is determined by the following equations:

$$K_1 G_1(s)\left(\frac{z_{s1}}{\delta_1}\right)_{\delta_2 CL} = \left[\frac{1}{1 + \frac{1}{H_1}\left\{\frac{\left(z_{s1}/w_g\right)}{\left(z_{s1}/\delta_1\right)}\right\}_{\delta_2 CL}}\right] \tag{B71}$$

The Γ of the δ_1 controller can be determined at the frequencies of interest from eqs. (B4) and (B70):

$$\Gamma_1 = 1 + H_1 \left[\frac{\left(\ddot{z}_c/\delta_1\right)}{\left(\ddot{z}_c/w_g\right)}\right] \tag{B72}$$

From Eq. (B72) it can be seen that it is possible to compute Γ_1, knowing H_1 and the frequency responses of acceleration to gust and surface inputs at the vehicle station of interest. Knowing Γ_1, it is then possible by using the

frequency response technique to determine the necessary filter and sensor combination for the δ_1 loop. Substituting G_1 and Z_{s1} into the aircraft equations, one may then synthesize the δ_2 control loop by a similar procedure. Therefore, this method allows one to synthesize an optimal controller on a loop-by-loop basis.

Synthesis of Optimal Controllers

An attempt was made in the study to use both of the above schemes for transforming the state variable feedbacks to practical sensor outputs. Unfortunately, the optimal controller which was generated was not a reasonable system in terms of rigid-body handling qualities and stability constraints. There was not sufficient time nor justification in the study to warrant redefining the optimal controller. What is required is a handling quality constraint in the optimization cost function. The optimal controllers which were defined are described in the following paragraphs. None of these made use of a handling quality constraint, however. Instead, attempts were made to obtain reasonable handling qualities by trial and error adjustment of the quadratic weights in the cost function. This was not successful.

Optimal quadratic controllers were computed for various combinations of inboard and outboard elevons, and canard or mass-reaction force producers. These controllers were computed using selected quadratic weights at the high subsonic, heavyweight flight condition. Optimal controllers were also computed for a single set of quadratic weights for all four flight conditions using the inboard and outboard elevons.

Table B1 shows the ideal gains obtained with the inboard and outboard elevons at each of the four conditions. As is evident from this table, only five structural modes were included in F/Cs 1, 1A, and 3, but six modes were included at F/C 2. The p_{19}, p_{20}, and w_g terms represent wind model states which are usually eliminated by applying optimal practicalization procedure. The δ_1, δ_2 are inboard elevon position and outboard elevon position, respectively. Hence, each controller contains crossfeeds between the inboard and outboard elevons. These crossfeeds can be eliminated by a simple transformation. The p_{25}, p_{24}, and p_{21} terms represent states of the baseline SAS which are measurable. They also can be eliminated if so desired by the optimal practicalization procedure.

Table B2 shows the rms accelerations of these controllers at the four flight conditions. These results show substantial ride improvement is possible with these controllers at all four conditions. Figures B7, B8, and B9 show the PSD plots for the high subsonic, heavyweight flight condition. These responses show considerable rigid-body load alleviation in addition to good mode suppression performance.

TABLE B1. - IDEAL SENSING CONTROLLER GAINS FOR WEIGHTS 2, 1, 1, 1, 1

State	F/C 1		F/C 1A		F/C 2		F/C 3	
	u_1	u_2	u_1	u_2	u_1	u_2	u_1	u_2
$\dot{\theta}_o$	45.207	-0.71790	39.711	18.842	122.51	5.7964	8.5539	22.520
$\dot{w}_o$	-0.0033221	-0.00040836	-0.0026739	-0.0018892	-0.0030105	-0.0001216	-0.00023386	-0.0024749
$\ddot{\eta}_1$	0.00094	0.00042018	0.00084025	0.00061906	0.00081965	0.000046466	0.00034648	0.0011160
$\ddot{\eta}_2$	-0.00045194	0.00024351	-0.00079421	0.00024369	-0.00044964	0.00049179	-0.00087269	-0.00030006
$\ddot{\eta}_3$	0.00025797	-0.00067479	0.00041194	-0.00042184	-0.000013515	0.00049538	0.000087989	-0.00071031
$\ddot{\eta}_4$	-0.00024335	-0.00019197	0.000049181	-0.00020455	-0.00030133	0.000042567	0.000028412	-0.00023197
$\ddot{\eta}_5$	0.00039006	0.000090101	0.0016748	0.00066307	0.00071649	0.000026618	0.0013749	-0.0002721
$\ddot{\eta}_6$	----	----	----	----	-0.00064468	0.00017845	----	----
$\dot{\eta}_1$	0.014624	-0.0028574	0.014928	0.0022538	0.016328	0.00029741	0.0093611	0.0036768
$\dot{\eta}_2$	-0.0066318	-0.00085458	-0.012169	-0.0051413	-0.0051683	0.00041201	-0.0064863	-0.0038645
$\dot{\eta}_3$	-0.021495	-0.016805	-0.013674	-0.023736	0.026928	0.0022362	-0.0019221	-0.0025233
$\dot{\eta}_4$	-0.011032	0.0060302	-0.007858	0.0010212	-0.0040575	0.0042530	-0.0030088	0.0035285
$\dot{\eta}_5$	0.0060149	-0.001042	0.039133	-0.0054382	-0.0045837	0.0047784	-0.02773	-0.045513
$\dot{\eta}_6$	----	----	----	----	-0.034127	0.046477	----	----
p_{19}	-0.018618	0.0096170	-0.028544	0.0011272	-0.0055551	0.0017911	-0.018075	-0.0078788
p_{20}	0.0029791	-0.0032108	0.0039818	-0.0026941	0.00045155	-0.000050686	0.0047813	0.000067072
w_g	0.012085	-0.0025632	0.019988	0.0047427	-0.00031043	-0.0020109	0.010379	0.0077873
$\dot{\delta}_1$	-0.14251	-0.0012521	-0.21416	-0.0020801	-0.054402	0.0022507	-0.094655	0.0016246
δ_1	-15.253	8.8426	-23.022	5.4579	-1.9769	0.21183	-6.4765	-1.7888
$\dot{\delta}_2$	-0.0017085	-0.095865	-0.0028387	-0.10859	-0.0030714	-0.052896	0.0022170	-0.072008
δ_2	-8.5349	4.4437	-12.315	2.7646	-2.7057	-0.17278	-5.2813	-1.4291
p_{25}	----	----	----	----	-0.0072529	-0.0091372	----	----
p_{24}	----	----	----	----	-0.82188	-0.94710	----	----
p_{21}	-0.89063	-0.81179	-0.97235	-0.82043	-0.75324	-0.89906	-0.87981	-0.86170

TABLE B2. - RMS ACCELERATION PERFORMANCE WITH AN OPTIMAL CONTROL SYSTEM USING INBOARD AND OUTBOARD ELEVONS (QUADRATIC WEIGHTS = 2, 1, 1, 1, 1)

Fuselage station	F/C 1, high subsonic, heavyweight condition		F/C 1A, high subsonic, lightweight condition		F/C 2, cruise, heavyweight condition		F/C 3, low subsonic lightweight condition	
	SAS only	LAMS	SAS only	LAMS	SAS only	LAMS	SAS only	LAMS
248 (pilot)	0.0204g	0.008 g	0.0227g	0.0083 g	0.0095g	0.0036g	0.0085g	0.0033 g
738	0.0131	0.0052	0.0181	0.0065	0.0054	0.0035	0.0092	0.0035
1236 (aft fuselage)	0.0211	0.0060	0.0031	0.0080	0.0108	0.0038	0.0121	0.0052

At F/C 1 (i.e., the high subsonic, heavyweight condition) the optimal practicalization procedure was used to eliminate various feedbacks from the optimal control system. Of particular interest is the case where only the wind model states are eliminated.

Table B3 compares optimal gains with and without the wind states (p_{19}, p_{20}, w_g). Figures B7, B8 and B9 show the change in the mean square acceleration performance resulting from elimination of the wind states. Also shown are gains obtained with elimination of the baseline SAS signal (p_{21}) and the rigid-body feedbacks ($\dot{w}_o$, $\dot{\theta}_o$). To observe the effect of removing the wind states (which are not measurable by a sensor) it is best to examine the change in the closed-loop poles. Table B4 shows the roots of the rigid-body and structural modes for the optimal system with and without the wind states. The rms accelerations increased only slightly when the wind states were removed. But, as Table B4 shows, the short-period and the first structural mode roots changed significantly. The values of the roots shown indicate that the handling qualities of the airplane would be significantly affected by this controller. These results tend to substantiate the hypothesis that the cost function should be modified to include a handling qualities constraint such as model following. Additional practicalization of this optimal controller by eliminating the baseline SAS feedbacks to the system, and the rigid-body feedbacks failed to improve the character of these roots.

An effort was made to replace the idealized feedbacks with feedbacks from practical sensors for the optimal system without wind states. Beginning with the feedbacks shown in Table B1 for the system without wind states, the first step is to eliminate the actuator crossfeeds between the inboard

TABLE B3. - PRACTICAL CONTROLLER GAINS FOR WEIGHTS Q = 2, 1, 1, 1, 1, FLIGHT CONDITION 1

State	Perfect sensing		Without p_{19}, p_{20}, w_g		Without p_{19}, p_{20}, w_g, p_{21}		Without $\dot{\theta}_o$, $\dot{w}_o$, p_{19}, p_{20}, w_g, p_{21}	
	u_1	u_2	u_1	u_2	u_1	u_2	u_1	u_2
$\dot{\theta}_o$	45.207	-0.71790	34.722	35.145	33.845	34.654	----	----
$\dot{w}_o$	-0.0033221	-0.00040836	-0.0029137	-0.0030569	-0.0028578	-0.0030314	----	----
$\ddot{\eta}_1$	0.00094	0.00042018	0.00087768	0.00014212	0.00087386	0.00013519	0.00064348	0.00039713
$\ddot{\eta}_2$	-0.00045194	0.00024351	-0.00056177	0.00044281	-0.00056614	0.00044329	-0.00020769	0.0011607
$\ddot{\eta}_3$	0.00025797	-0.00067479	0.00025797	-0.00067479	0.00025797	-0.00067479	0.00025797	-0.00043554
$\ddot{\eta}_4$	-0.00024335	-0.00019197	-0.00024335	-0.00019197	-0.00024335	-0.00019197	-0.00030634	-0.00033471
$\ddot{\eta}_5$	0.00039006	0.000090101	0.00039006	0.000090101	0.00039006	0.000090101	0.00043508	0.000090101
$\dot{\eta}_1$	0.014624	-0.0028574	0.014624	-0.0028574	0.014624	-0.0028574	0.01657	-0.012665
$\dot{\eta}_2$	-0.0066318	-0.00085458	-0.0066318	-0.00085458	-0.0066318	-0.00085458	-0.019327	0.0070485
$\dot{\eta}_3$	-0.021495	-0.016805	-0.021495	-0.016805	-0.021495	-0.016805	-0.037581	-0.031195
$\dot{\eta}_4$	-0.011032	0.0060302	-0.011032	0.0060302	-0.011032	0.0060302	-0.0047142	0.010434
$\dot{\eta}_5$	0.0060149	-0.001042	0.0060149	-0.001042	0.0060149	-0.001042	0.0060149	-0.001042
p_{19}	-0.018618	0.0096170	----	----	----	----	----	----
p_{20}	0.0020791	-0.0032108	----	----	----	----	----	----
w_g	0.012085	-0.0025632	----	----	----	----	----	----
$\dot{\delta}_1$	-0.14251	-0.0012521	-0.14251	-0.0012521	-0.14251	-0.0012521	-0.14251	-0.0012521
δ_1	-15.253	8.8426	-11.827	-2.4550	-11.793	-2.5	-15.253	8.8426
$\dot{\delta}_2$	-0.0017087	-0.095865	-0.0017087	-0.095865	-0.0017087	-0.095865	-0.0017087	-0.095865
δ_2	-8.5349	4.4437	-7.3630	-1.2732	-7.3268	-1.29	-8.5349	4.4437
p_{21}	-0.89063	-0.81179	-0.89063	-0.81179	----	----	----	----

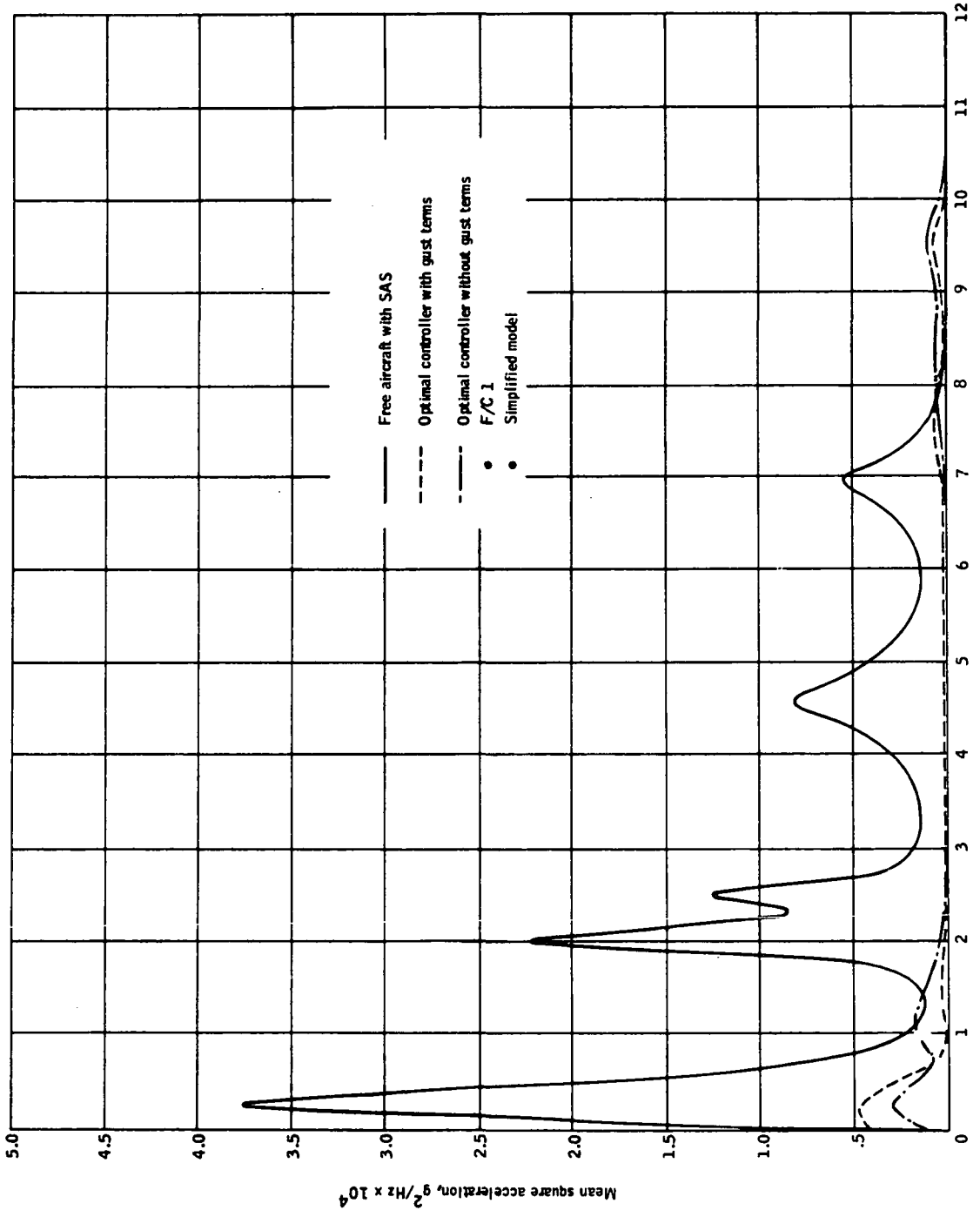

Figure B7. Mean Square Acceleration at FS 248 for a 1-ft/sec Turbulence Input With and Without Optimal Controllers -- F/C 1

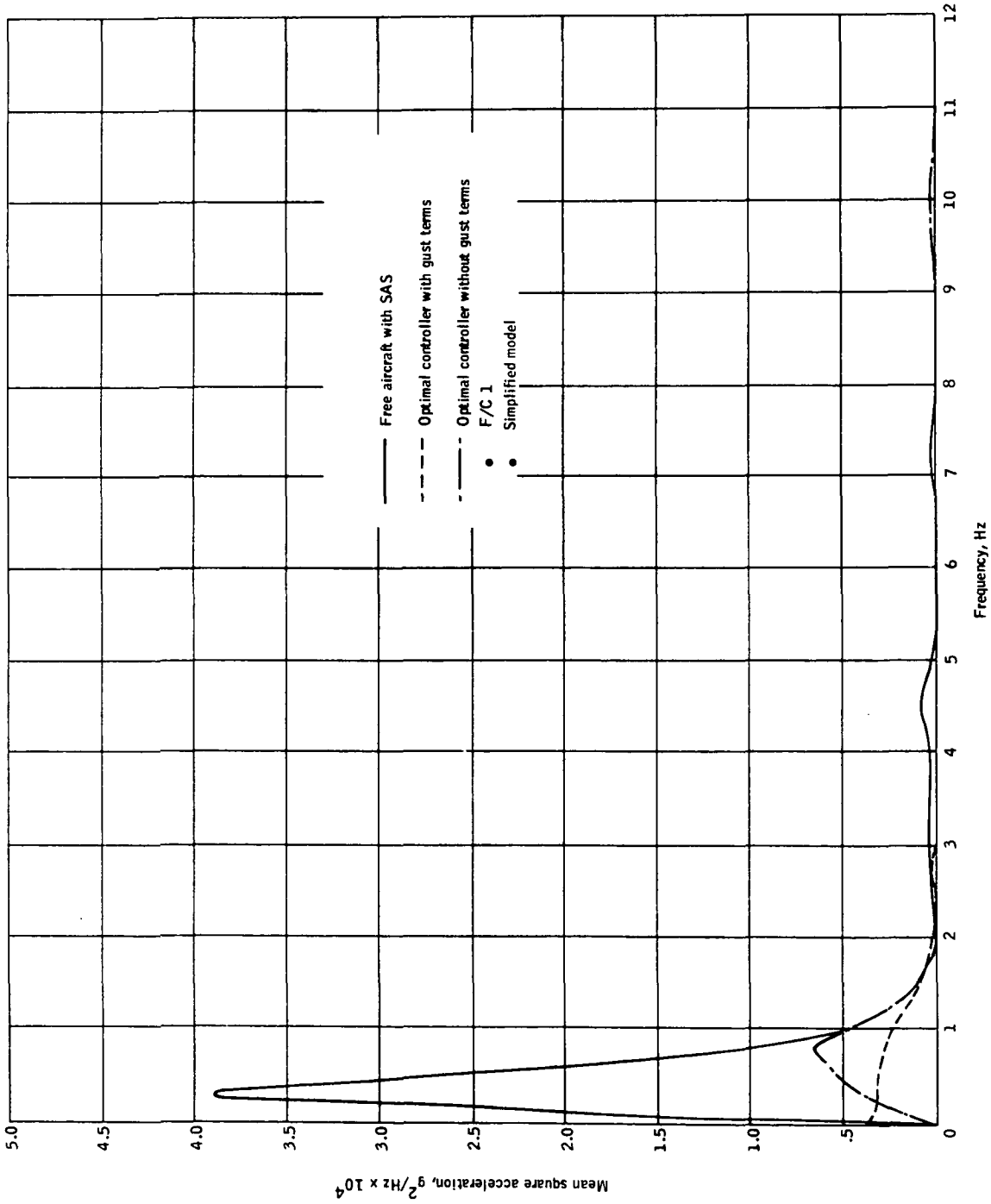

Figure B8. Mean Square Acceleration at FS 738 for a 1-ft/sec Turbulence Input With and Without Optimal Controllers -- F/C 1

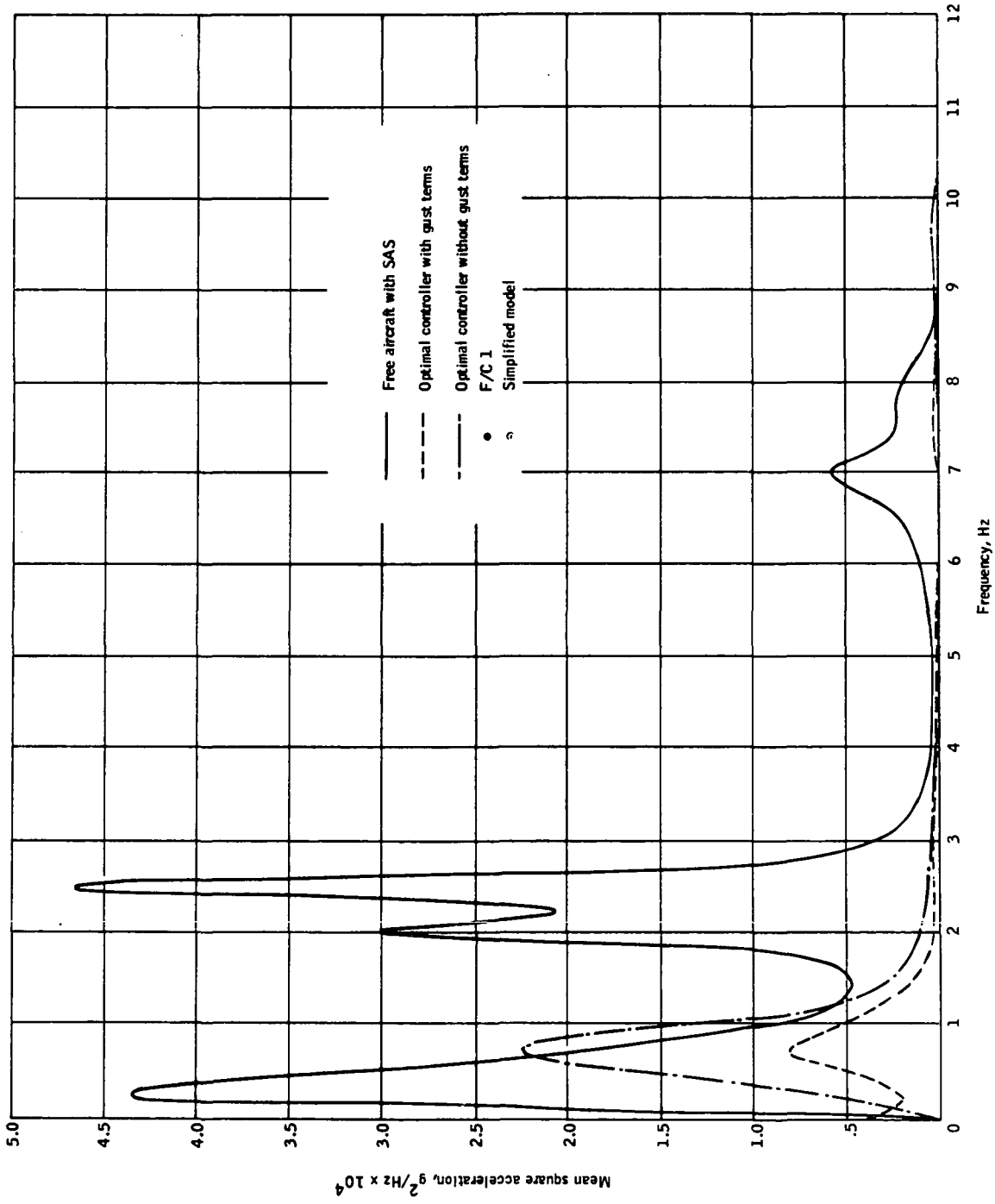

Figure B9. Mean Square Acceleration at FS 1236 for a 1-ft/sec Turbulence Input With and Without Optimal Controllers -- F/C 1

TABLE B4. - COMPARISON OF ROOTS FOR AN OPTIMAL SYSTEM WITH AND WITHOUT WIND STATES

Root description	Open-loop roots		Optimal system with wind states, closed-loop roots		Optimal system without wind states, closed-loop roots	
	Damping ratio	Frequency (rad/sec)	Damping ratio	Frequency (rad/sec)	Damping ratio	Frequency (rad/sec)
Rigid body	0.62	3.77	0.607	3.30	0.910	2.05
Mode 1	0.08	12.43	0.224	9.12	0.482	5.97
Mode 2	0.054	16.1	0.851	10.88	0.648	12.87
Mode 3	0.061	28.7	0.527	36.85	0.624	24.21
Mode 4	0.040	44.47	0.941	40.28	0.312	44.60
Mode 5	0.060	50.07	0.044	47.82	0.079	48.57

elevon and outboard elevons. This step, after some additional simplification, results in the system shown in Figure B10. The input signals z_{s1} and z_{s2} are defined as:

$$z_{s1} = -0.00291\,\ddot{z}_1 + 1\,\dot{\theta}_1 \tag{B73}$$

where

$$\ddot{z}_1 = \ddot{z}_o - 0.302\,\ddot{r}_3 + 0.143\,\ddot{r}_4 - 0.088\,\ddot{r}_5 + 0.0335\,\ddot{r}_6 - 0.134\,\ddot{r}_7$$

$$\dot{\theta}_1 = 0.515\,\dot{\theta}_o + 0.0146\,\dot{r}_3 - 0.0066\,\dot{r}_4 - 0.0215\,\dot{r}_5 - 0.011\,\dot{r}_6 + 0.006\,\dot{r}_7$$

and

$$z_{s2} = 0.00306\,z_2 + \dot{\theta}_2 \tag{B74}$$

where

$$\ddot{z}_2 = \ddot{z}_o - 0.046\,\ddot{r}_3 - 0.145\,\ddot{r}_4 + 0.220\,\ddot{r}_5 + 0.063\,\ddot{r}_6 - 0.029\,\ddot{r}_7$$

$$\dot{\theta}_2 = -0.743\,\dot{\theta}_o - 0.0028\,\dot{r}_3 - 0.0085\,\dot{r}_4 - 0.0168\,\dot{r}_5 + 0.006\,\dot{r}_6 - 0.001\,\dot{r}_7$$

The optimal feedbacks from the baseline SAS output, p_{21}, appear to negate the effects of the baseline SAS, at least on the inboard elevon. Subsequent analysis indicated, however, that these two p_{21} feedbacks in the

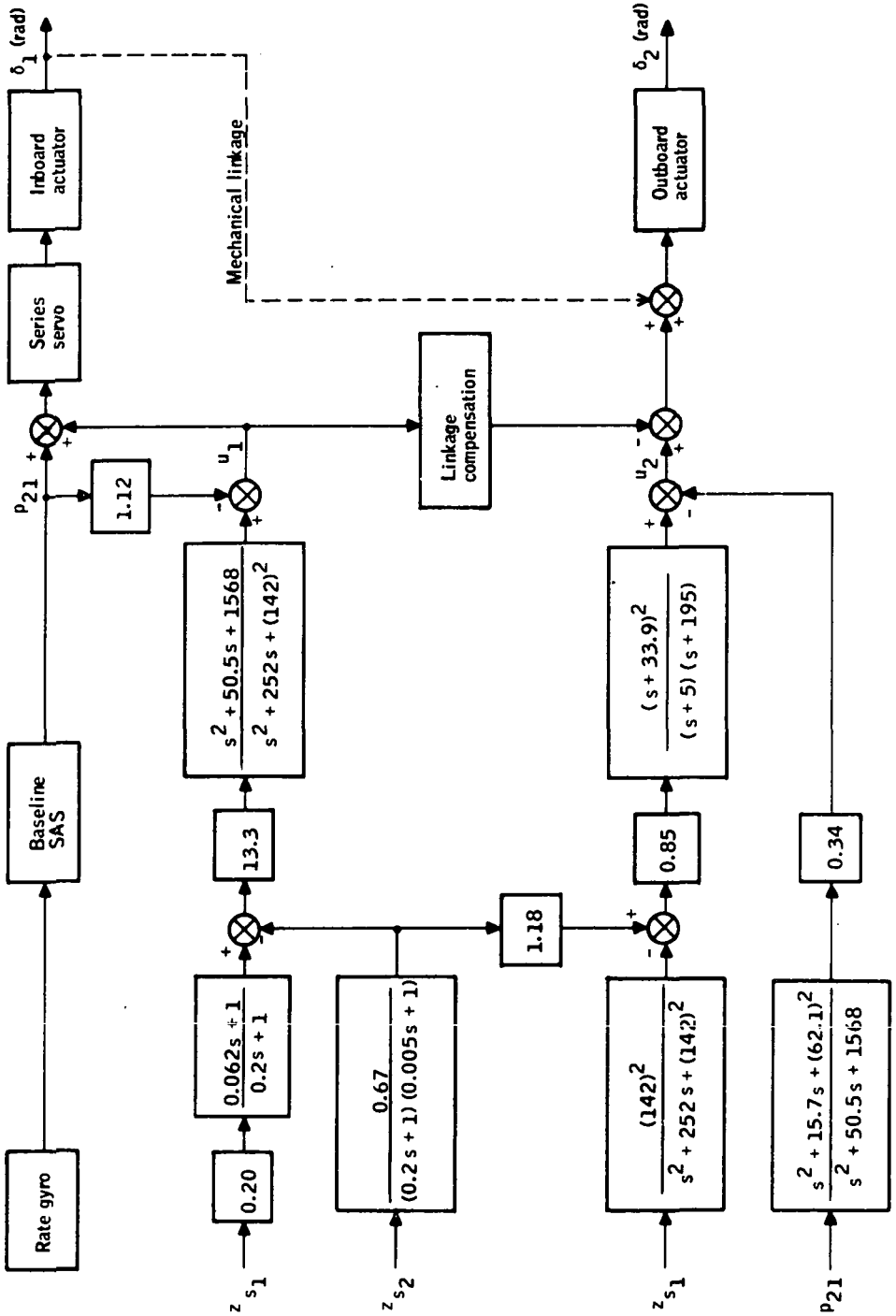

Figure B10. Transformed Optimal Control System

optimal system could be eliminated without a significant change in the ride quality performance. It is of interest to note that this optimal system contains compensation very similar to the compensation derived by frequency response analysis for the inboard/outboard elevon control system. The 0.2-sec first-order lag is predictable also from the application of North American's ILAF concept (see ref. 3).

As discussed previously, further attempts to reduce this controller to a system using practical sensors was not successful. The nature of the feasibility study did not warrant further analysis of this problem in the study.

Several optimal controllers were defined using either a canard or mass-reaction configuration plus the inboard and outboard elevons. However, in all cases the same problem was encountered. Reasonable handling qualities could not be assured. Regardless of the weighting factors selected, the rigid-body and first-mode frequencies were reduced to unacceptable values. Root-mean-square performance with either the mass-reaction configuration or the canard configuration was substantially better than that obtained with just the inboard and outboard elevons.

REFERENCES

1. Bender, M.A., Burris, P.M.: Aircraft Load Alleviation and Mode Stabilization (LAMS) Flight Demonstration Test Analysis; Air Force Report number AFFDL-TR-68-164, Air Force Flight Dynamics Laboratory, Wright-Patterson Air Force Base, Ohio, December 1969.

2. Kordes, E.E., Wykes, J.H.: Analytical Design and Flight Tests of a Model Suppression System on the XB-70 Airplane, presented at AGARD 34th Flight Mechanics Panel Meeting, Marseilles, France, April 21 - 24, 1969.

3. Wykes, John H., Nardi, Louis U., and Mori Alva S.: XB-70 Structural Mode Control System Design and Performance Analysis, NASA Contractor Report No. CR-1557, July 1970.

4. Bender, M.A., Burris, P.M.: Aircraft Load Alleviation and Mode Stabilization (LAMS) Air Force Report Number AFFDL-TR-68-158, Air Force Flight Dynamics Laboratory, Wright-Patterson Air Force Base, Ohio, April 1969.

5. Drischler, J.A.: Calculation and Compilation of the Unsteady-Lift Functions for a Rigid Wing Subjected to Sinusoidal Gusts and to Sinusoidal Sinking Oscillation, NACA TN 3748, 1956.

6. Edinger, L.D.: Design of Elastic Mode Suppression Systems for Ride Quality Improvement and Application to an SST, Paper No. 67-571, AIAA, 1967.

7. Press, H., Meadows, M.T., and Hadlock, I,: A Reevaluation of Data on Atmospheric Turbulence and Airplane Gust Loads for Application in Spectral Calculation, NACA TR 1272.

8. Dore, B.D.: The Unsteady Forces on Finite Wings in Transient Motion, Aeronautical Research Council Reports Memoranda, R&M No. 3456, 1966.

9. Watkins, C.E., Woolston, D.S., and Cunningham, H.J,: A Systematic Kernel Function Procedure for Determining Aerodynamic Forces on Oscillating or Steady Finite Wings At Sub-Sonic Speeds, NASA TR R-48, 1958.

10. Athans, M., Falb, P.L.: Optimal Control, McGraw-Hill, New York, New York, 1966.

"The aeronautical and space activities of the United States shall be conducted so as to contribute . . . to the expansion of human knowledge of phenomena in the atmosphere and space. The Administration shall provide for the widest practicable and appropriate dissemination of information concerning its activities and the results thereof."

—NATIONAL AERONAUTICS AND SPACE ACT OF 1958

NASA SCIENTIFIC AND TECHNICAL PUBLICATIONS

TECHNICAL REPORTS: Scientific and technical information considered important, complete, and a lasting contribution to existing knowledge.

TECHNICAL NOTES: Information less broad in scope but nevertheless of importance as a contribution to existing knowledge.

TECHNICAL MEMORANDUMS: Information receiving limited distribution because of preliminary data, security classification, or other reasons. Also includes conference proceedings with either limited or unlimited distribution.

CONTRACTOR REPORTS: Scientific and technical information generated under a NASA contract or grant and considered an important contribution to existing knowledge.

TECHNICAL TRANSLATIONS: Information published in a foreign language considered to merit NASA distribution in English.

SPECIAL PUBLICATIONS: Information derived from or of value to NASA activities. Publications include final reports of major projects, monographs, data compilations, handbooks, sourcebooks, and special bibliographies.

TECHNOLOGY UTILIZATION PUBLICATIONS: Information on technology used by NASA that may be of particular interest in commercial and other non-aerospace applications. Publications include Tech Briefs, Technology Utilization Reports and Technology Surveys.

Details on the availability of these publications may be obtained from:

SCIENTIFIC AND TECHNICAL INFORMATION OFFICE

NATIONAL AERONAUTICS AND SPACE ADMINISTRATION

Washington, D.C. 20546